Statistical Modeling and Analysis of Interference in Wireless Networks

Matthias Wildemeersch

Graduation committee:

Chairman and secretary:
    Prof.dr.ir. A.J. Mouthaan   University of Twente, EWI
Promotor:
    Prof.dr.ir. C. H. Slump   University of Twente, EWI
Referee:
    dr. A. Rabbachin   Massachusetts Institute of Technology, LIDS
Members:
    Prof.dr.ir. B. Nauta   University of Twente, EWI
    Prof.dr.ir. F. B. J. Leferink   University of Twente, EWI
    Prof.dr.ir. S. M. Heemstra de Groot TU Eindhoven
    Prof.dr. T. Q. S. Quek   Singapore University of Technology
                                           and Design, ISTD

STATISTICAL MODELING AND ANALYSIS OF INTERFERENCE
IN WIRELESS NETWORKS

DISSERTATION


to obtain
the degree of doctor at the University of Twente,
on the authority of the rector magnificus,
prof. dr. H. Brinksma,
on account of the decision of the graduation committee,
to be publicly defended
on November 14th, 2013, at 16:45h

by

Matthias Wildemeersch
born on August 11th, 1980
in Ghent, Belgium

This dissertation has been approved by:

Prof.dr.ir. C.H. Slump

To my parents

Abstract

In current wireless networks, interference is the main performance-limiting factor. The quality of a wireless link depends on the signal and interference power, which is strongly related to the spatial distribution of the concurrently transmitting network nodes, shortly denominated as the network geometry. Motivated by the ongoing revision of wireless network design, this dissertation aims to describe the relation between geometry and network performance.

Given the exponential growth of wireless devices, it is meaningful to evaluate how network interference affects signal detection. We propose a unified statistical approach based on the characteristic function of the decision variable to describe the detection performance, accounting for single and multiple interference, as well as different detection schemes and architectures. The proposed framework is able to capture the deployment density of the interferers, transmission power, and fading distribution of the interferers and the signal of interest. In addition, we establish a fundamental limit of the interferer node density beyond which robust energy detection is impossible. This work highlights the crucial role of spatial statistics in the evaluation of signal detection.

The capacity gain obtained through the densification of the network architecture comes at the expense of an increase in energy consumption. Although small cell access points consume little energy in comparison with the macrocell base stations, the massive deployment of these additional small cell base stations entails a significant increase in energy consumption. We extend the capacity analysis of small cell networks to include the energy consumption of the small cell tier. Considering a distributed sleep mode strategy for the small cell access points, we cast the trade-off between energy consumption and capacity as a set of optimization problems. We develop an analytical framework, which can be used in practice to correctly set sensing time and sensing probability whilst guaranteeing user quality of service. Furthermore, the analytical tool accounts for the network load and predicts the achievable energy reduction of the small cell tier by means of distributed sleep mode strategies as a function of the user density.

Finally, given that current networks are interference-limited, we study

how signal processing can improve the signal quality. We present a probabilistic framework to describe the performance gain of successive interference cancellation and show that the benefit is modest when users connect to the base station that provides the highest average signal-to-interference ratio. We extend the analysis to include novel ways to associate users to their access points and demonstrate that the benefits of successive interference cancellation are substantial for these operational scenarios.

By systematically incorporating the spatial statistics in the performance analysis, this dissertation presents a methodology and analytical toolset useful to enhance the understanding of the design, operation, and evaluation of future wireless networks.

Samenvatting

Interferentie is de belangrijkste prestatiebeperkende factor in huidige draadloze netwerken. De kwaliteit van een draadloze verbinding wordt bepaald door het signaal- en interferentievermogen, die allebei sterk gerelateerd zijn met de ruimtelijke verdeling van de actieve netwerk nodes, kortweg de netwerk geometrie. Aangespoord door de huidige herziening van het ontwerp van draadloze netwerken, beoogt dit proefschrift om het verband te beschrijven tussen de geometrie en de prestaties van het netwerk.

Door de exponentiële toename van draadloze toestellen is het zinvol na te gaan hoe netwerk interferentie de signaaldetectie kan beïnvloeden. We leggen een enkelvoudige statistische aanpak voor om de detectieprestaties te beschrijven, gebaseerd op de karakteristieke functie van de detectieveranderlijke. Hierbij houden we niet enkel rekening met enkelvoudige of meervoudige interferentie, maar ook met verschillende detectiestrategieën en architecturen. Het voorgestelde raamwerk is in staat om het effect weer te geven van de dichtheid van de interferentiebronnen, het transmissievermogen, en de fading verdeling van de storingsbronnen en het gewenste signaal. Bovendien leggen we een fundamentele limiet vast van de dichtheid van storingsbronnen waarna robuuste energiedetectie onmogelijk wordt. Dit werk verduidelijkt de cruciale rol van ruimtelijke statistiek voor de evaluatie van signaaldetectie.

De capaciteitswinst door de verdichting van het netwerk is ten koste van een toename van het energieverbruik. Hoewel 'small cell' basisstations weinig energie verbruiken in vergelijking met de macrocell basisstations, brengt het massaal inzetten van 'small cell' basisstations een aanzienlijke stijging van het energieverbruik met zich mee. We breiden de capaciteitsanalyse voor 'small cell' netwerken uit en houden rekening met het energieverbruik van het 'small cell' netwerk. We beschouwen een gedistribueerde slaap strategie voor 'small cell' basisstations en formuleren de wisselwerking tussen capaciteit en energieconsumptie als een reeks optimalisatieproblemen. We ontwikkelen een analytisch kader dat in de praktijk kan toegepast worden voor het correct afstellen van de sensing tijd en sensing probabiliteit, onderhevig aan kwaliteitsgaranties voor de

gebruiker. Deze analytische tool houdt bovendien rekening met de belasting van het netwerk en geeft de haalbare energiereductie van het 'small cell' netwerk aan dankzij slaapstrategieën in functie van de gebruikersdichtheid.

Aangezien huidige netwerken gedetermineerd worden door interferentie, analyseren we tenslotte hoe signaalverwerking de signaalkwaliteit kan verbeteren. We stellen een probabilistisch raamwerk voor om de prestaties te beschrijven van 'successive interference cancellation' en we tonen aan dat de verbetering bescheiden is indien de gebruiker zich associeert met het basisstation die de hoogste gemiddelde SIR levert. We breiden de analyse verder uit voor nieuwe associatiestrategieën en we tonen aan dat voor deze scenario's 'successive interference cancellation' de prestaties substantieel verbetert.

Door systematisch rekening te houden met de ruimtelijke probabiliteit, stelt dit proefschrift een methodologie en een reeks tools voor die nuttig zijn om het inzicht te verdiepen in het ontwerp, de werking, en de evaluatie van toekomstige draadloze netwerken.

Contents

List of Figures

Chapter 1

Introduction

1.1 Background and motivation

Interference is the most important capacity-limiting factor in current wireless networks. Since the groundbreaking work of Shannon [1] and prior to considering interference, the metric of interest to determine the link quality was the signal-to-noise ratio (SNR). The capacity, which is defined as the maximum data rate that can be transmitted reliably over a Gaussian channel, is upper bounded by the Shannon-Hartley theorem and is a simple function of the SNR and the bandwidth. The received signal power depends on the transmission power, the path loss, and the properties of the wireless propagation channel. In the single link model, the most important element to describe the link quality is the geometry, which is determined by the distance between the transmitter and the receiver. Today, due to spectrum shortage and the massive use of wireless devices, frequency and time resources are reused and concurrent transmissions are merely separated in space. In networks with multiple concurrent transmissions, network interference is the performance-limiting factor. Network interference is defined as the combined effect of all interfering transmissions at the receiver node and is largely governed by the geometry of the interferers [2]. Considering the critical role of interference to evaluate network performance, the metric of interest is the signal-to-interference-and-noise ratio (SINR) or the signal-to-interference ratio (SIR) in case the network is interference-limited. The characterization of the capacity in the information theoretical sense for networks with multiple concurrent transmissions is still an open problem. Nevertheless, the statistical characterization of interference and the SINR is an essential ingredient to deepen the understanding of the performance of wireless networks.

The location of the interferers can be modeled either deterministically by means of hexagonal lattices or stochastically by means of point processes [3].

Whereas the lattice structure is rigid, highly idealized, and mostly requires system-level simulations, the stochastic counterpart often leads, surprisingly, to tractable solutions. Furthermore, as spatial configurations can vary over an infinite number of realizations, it is also more relevant to consider statistical spatial models to describe the location of the network nodes. Therefore, to accurately assess the performance of wireless networks, there is a distinct need for probabilistic models that describe the randomness of the network nodes. In this work, we adhere to the stochastic modeling of the spatial distribution of network nodes based on the rich mathematical toolset of stochastic geometry, which allows us to capture realistic distributions of mobile users as well as deployment scenarios for access points. Stochastic geometry is intrinsically related to the theory of point processes and allows us to study and predict the performance of large-scale networks. The theory was initially applied in diverse fields such as astronomy, cell biology, and material sciences. Since two decades, stochastic geometry has found widespread application in wireless communications, starting from the optimization of hierarchical network architectures [4, 5] to the performance assessment of wireless systems. A common assumption for the node distribution in wireless networks is to consider a homogeneous Poisson point process (PPP) with intensity λ, where the number of nodes in the region $\mathcal{A}$ is Poisson distributed with mean $\lambda|\mathcal{A}|$ and where the number of users in disjoint regions is independent. More general spatial models that go beyond the homogeneous PPP exist and can accommodate for repulsion (Matern process) or clustering (Poisson cluster process), where generality is usually at the expense of tractability.

Motivated by many possible applications of interference modeling, such as network performance evaluation, design of the medium access policy, and interference engineering techniques, many efforts can be found in literature to characterize the aggregate interference generated by a multitude of interferers. When the interference stems from the sum of a large number of transmitters without a dominating term, a common approach is to apply the central limit theorem (CLT) and model the aggregate network interference as a Gaussian random process. While the Gaussian approximation holds in certain cases [6, 7], it is definitely not accurate in general. Due to the presence of dominant interferers, the distribution of the aggregate network interference features a heavier tail than the normal distribution, which can be well captured by the class of stable distributions [8]. There is a vast amount of literature dealing with the statistical modeling of the aggregate network interference in a Poisson field of interferers [2, 9–11]. Furthermore, spatial models that account for an exclusion region in cognitive radio networks [12, 13] and medium access control (MAC) schemes have been studied more recently [3, 14]. Different metrics are in use to assess link

performance and network performance. For instance, to evaluate the link quality of a so-called typical user, stochastic geometry provides us with the SINR distribution building on the notion of typicality, which is formalized as location independence. Likewise, the characterization of the SINR distribution enables the evaluation of the network as a whole by considering the area spectral efficiency (ASE). As an example, the transmission capacity is a metric that expresses the ASE and that is defined as the number of successful transmissions taking place in the network per unit area subject to a constraint on the outage probability. However, the transmission capacity is mainly dedicated to large-scale ad hoc networks and usually considers all transmitter-receiver pairs at the same distance, limiting its usefulness for future wireless networks.

Due to the exponentially increasing demand for mobile data, operators are obliged to review the network architecture so as to increase the capacity. As advanced physical layer techniques offer merely logarithmic benefits, the capacity problem is typically addressed by increasing the spatial reuse and reducing the transmitter-receiver distance. However, the installation of additional macrocell base stations is prohibitive for reasons of cost and practical deployment issues. Therefore, the trend is to add low-cost, low-power access points of different types such as microcells, picocells, and femtocells, which are jointly denominated as small cells. Heterogeneous networks consist of different tiers, each of which is characterized by its deployment density, transmit power, coverage area, SINR target value, path loss exponent, and backhaul. The macro-cellular network provides coverage, while the higher tiers of the network are intended to obviate coverage dead zones and increase the capacity in hot spot areas. The network topology consists of planned, regularly spaced infrastructure, as well as unplanned user-deployed access points. Heterogeneous networks present many opportunities to solve the capacity problem. However, owing to the densification, the resulting networks are interference-limited and many challenging questions arise related to design, coexistence, and interference management.

Such fundamental changes of the network architecture require novel ways of modeling and evaluating the network performance. As to network modeling, stochastic geometry plays a key role owing to the surprisingly tractable expressions that result from analysis and the flexibility of the model to include relevant system design aspects such as the randomness of the deployment, multiple tiers, biasing techniques, association policies, clustering, and repulsion. As to the evaluation of these networks, classic performance metrics such as the SIR distribution reach their limits. In [15] for instance, the analysis illustrates that in interference-limited networks the reduction of the transmitter-receiver distance is balanced by the increase

of the interference, such that the SIR is independent of the base station density. This example illustrates that the SIR distribution does not capture the linear increase of the network capacity with the base station density. Instead, it is more relevant to relate the SIR distribution to the cell area and consider the area spectral efficiency. The densification of the network also affects the load of each base station, which is defined as the number of users connected to a base station. The network load experiences large variations over the tiers due to the differences between coverage areas of base stations belonging to different tiers. As the load has a significant effect on the user experience, the assessment of multi-tier networks needs to account for the load distribution. At last, although base stations belonging to the higher tiers consume less energy than macrocell base stations, a massive deployment of so-called small cell access points (SAPs) results in a severe increase in the overall energy consumption, which needs to be accounted for in the performance evaluation. In conclusion, the drastic proliferation of wireless devices together with fundamental changes of the network architecture require a precise characterization of the interference and a novel methodology to assess the network performance, embracing the ongoing evolution of the network and reflecting prevalent interests such as user experience and energy efficiency.

1.2 Research questions and contributions

In this dissertation, we develop a stochastic geometry framework to study detection and communication performance in networks with multiple concurrent transmissions. From detection theory and information theory, we know that the ratio of signal power and interference power defines the detection performance and the throughput that can be reliably transmitted over a wireless channel. As the interference is determined by the geometry of the network nodes, the key challenge is to characterize the relationship between network topology and performance, which can be related both to detection and communication. The contribution of the dissertation is mainly methodological by systematically incorporating the spatial statistics in the network evaluation. To this end, we present analytical tools that uncover the relation between network topology and different performance metrics such as detection performance, coverage probability, rate distribution, and energy efficiency. As such, this dissertation provides the instruments to obtain fundamental insights, performance limits, and design guidelines for future wireless systems.

Although there is an extensive body of literature related to stochastic geometry and wireless communications, there are still many aspects that are ill understood. In the following, we introduce the research problems and

network aspects that will be covered in the dissertation.

Signal detection

In the presence of interference, reliable signal detection is jeopardized. Detection performance is well studied for different types of single interference, covering narrow-band and wide-band profiles, Gaussian interference, pulsed interference, etc. Given the exponential growth of wireless devices, it is meaningful to evaluate how multiple interferers affect the detection performance. This leads to the following research questions. *Is it possible to characterize the impact of aggregate network interference on the detection performance? Are there detection schemes and receiver architectures that are more resilient with respect to network interference? Can we define a fundamental limit of the detection robustness regarding the interferer density?*

Energy efficiency

The relentless increase in mobile data demand has compelled mobile operators to introduce heterogeneous networks with densely deployed base stations. Previously, cellular networks were designed and optimized with respect to metrics that reflect the quality of service (QoS) such as the sum throughput that can be brought to the users. Considerations akin to energy consumption were typically related to the mobile equipment in cellular and wireless sensor networks. Given the current densification of the wireless network and the corresponding increase in energy consumption, the environmental and financial cost to operate the network increase at fast pace. Therefore, the following research questions arise. *Is it possible to include energy efficiency in the design of future heterogeneous networks? Can we propose strategies to reduce the overall energy consumption of the network infrastructure, guaranteeing the QoS of the users?*

Interference management

As the densification of the network infrastructure results in interference-limited networks, there is an explicit incentive to study interference mitigation and coordination techniques. The SIR distribution, which depends on many factors including the path loss law, the spatial distribution of the active network nodes, and the characteristics of the wireless propagation channel, can be altered by using advanced interference cancellation (IC) techniques. Furthermore, the trend towards heterogeneity in future networks has also repercussions on the operation and evaluation of these networks. For instance, due to the substantial differences in coverage area between tiers, users can be diverted to access points based on

association policies that favor the higher tiers. In heterogeneous networks, the load varies largely over tiers and therefore, it can be beneficial to redirect users to access points with lower load. Unlike the analysis of the coverage probability, it is more relevant in those scenarios that account for network load to consider the rate distribution of a typical user who shares the network resources with other users. These revisions in the design, operation, and evaluation of the network lead to several challenging research problems. *Can we predict how advanced signal processing can improve coverage probability or QoS for mobile users? Can we provide an analytical tool for network performance assessment that embraces the fundamental changes in design, operation, and evaluation of future heterogeneous networks?*

1.3   Outline of the dissertation

The main contributions of this dissertation are a methodological approach to include spatial statistics into the performance analysis of wireless systems and an analytical framework to describe a set of system performance metrics, accounting for the design aspects of future networks. The dissertation is organized as follows.

- Chapter 2 reviews the mathematical concepts of stable distributions and stochastic geometry that will be useful for the remainder of the dissertation.

- In Chapter 3, we analyze the detection performance of a non-coherent receiver in terms of the detection and false alarm probability, accounting for different detection strategies. The detection of code division multiple access (CDMA) signals is resilient with respect to narrowband interference, as the contribution of the interference is negligible after despreading in the receiver. Starting from the impact analysis of a single interferer on the detection performance, we analyze how the performance of the non-coherent receiver is affected by the presence of a Poisson field of interferers.

- In Chapter 4, we evaluate how sleep mode strategies for small cell access points (SAPs) can reduce the energy consumption of the small cell tier. A distributed strategy is proposed that requires cognitive capabilities of the SAPs. We characterize the detection performance of an energy detector with respect to a typical user of the small cell tier, including the effects of the wireless propagation channel and the aggregate network interference. Unlike previous work where the detection robustness is described with respect to the noise uncertainty, we derive a fundamental limit of the robustness confining a region of

allowable interferer densities. We formulate an energy consumption model of the SAPs located within a macrocell that accounts for the sleep mode strategy and the detection performance. After characterizing the traffic that can be offloaded from the macrocell, we formulate several optimization problems which reflect the trade-off between energy consumption and network performance. The presented framework is useful for the energy efficient design and operation of small cell networks.

- In Chapter 5, we develop a probabilistic framework to evaluate the performance benefits of successive interference cancellation (SIC) in multi-tier heterogeneous networks. We bring together concepts of order statistics and stochastic geometry to address novel performance metrics and deployment scenarios. Specifically, we evaluate the SIR and rate distribution when the association is based on minimum load, maximum instantaneous SIR, and range expansion. Furthermore, the analysis is presented both for uplink (UL) and downlink (DL) scenarios. We aim to illustrate the achievable gains offered by SIC in multi-tier heterogeneous networks.

- Chapter 6 reviews the research questions that are formulated in Section 1.2 and provides a discussion on possible extensions for future work. Proofs and derivations are provided in the Appendix.

Note that the detection performance is constrained to non-coherent detectors for CDMA signals in Chapter 3. Nonetheless, the network performance evaluation in Chapter 4 and 5 is presented at system level and is not restricted by specific implementation details of modulation scheme or protocol.

Chapter 2

Interference modeling: Mathematical preliminaries

Due to the properties of the wireless propagation channel and the spatial distribution of the network nodes, interference in wireless networks has a stochastic nature. To capture the spatial randomness of the network nodes, the main tool applied in this dissertation is stochastic geometry, which has as major asset the ability to capture the principal dependencies in wireless networks as a function of a small number of system parameters. In this chapter, we review several definitions, properties, and theorems related to stable distributions and stochastic geometry, which will serve as the main building blocks in the remainder of the dissertation.

2.1 Stable distributions

We will frequently resort to stable distributions to model aggregate interference. The theory of stable distributions is developed in the 1920s and the 1930s and is well documented in [8, 16, 17]. There are different ways to define a stable random variable (r.v.). For instance, a random variable X is said to be stable if the linear combination of independent copies of X has the same distribution. Furthermore, the stable distribution has a field of attraction, as the sum of independent and identically distributed (i.i.d.) r.v.'s converges in distribution to a stable distribution. This generalized central limit theorem illustrates that the normal distribution belongs to the family of stable distributions. A stable r.v. can be also defined by means of the characteristic function (CF).

Definition 1. *A random variable X is said to be stable if there exist parameters $0 < \alpha_I \leq 2$, $-1 \leq \beta \leq 1$, $\gamma \geq 0$, and μ such that the CF $\psi_X(j\omega) = \mathbb{E}\{\exp(j\omega X)\}$*

has the following form

$$\psi_X(j\omega) = \begin{cases} \exp\left\{-\gamma|\omega|^{\alpha_I}\left(1 - j\beta\mathrm{sign}(\omega)\tan\left(\frac{\pi\alpha_I}{2}\right)\right) + j\omega\mu\right\}, & \alpha_I \neq 1 \\ \exp\left\{-\gamma|\omega|\left(1 + j\frac{2}{\pi}\beta\mathrm{sign}(\omega)\ln|\omega|\right) + j\omega\mu\right\}, & \alpha_I = 1 \end{cases}$$

$$(2.1)$$

The parameter α_I is called the characteristic exponent and determines the heaviness of the tail. For $\alpha_I = 2$, we get the normal distribution $X \sim \mathcal{N}(\mu, 2\gamma)$. Furthermore, β represents the skewness, γ has a meaning similar to variance of the normal distribution, and μ represents the shift parameter. For $\beta = \mu = 0$, X is said to be symmetric stable. A real stable r.v. X with parameters α_I, β, γ, and μ is denoted as $X \sim \mathcal{S}(\alpha_I, \beta, \gamma, \mu)$. For $\mu = 0$, the notation is simplified to $X \sim \mathcal{S}(\alpha_I, \beta, \gamma)$. The probability density functions (PDFs) of α-stable r.v.'s exist and are continuous, but in general they are not known in closed form, except for the Gaussian distribution, the Cauchy distribution, and the Lévy distribution. In the rest of the dissertation, the decomposition property and the scaling property of the class of α-stable distributions will be used.

Property 1 (Decomposition property)**.** *Consider a symmetric stable distribution* $X \sim \mathcal{S}(\alpha_I, 0, \gamma)$, *then X can be decomposed as* $X = \sqrt{U}G$, *where* $U \sim \mathcal{S}(\alpha_I/2, 1, \cos(\pi\alpha_I/4))$ *and* $G \sim \mathcal{N}_c(0, 2\gamma^{2/\alpha_I})$, *with U and G independent r.v.'s .*

Property 2 (Scaling property)**.** *Let* $X \sim \mathcal{S}(\alpha_I, \beta, \gamma)$ *with $\alpha_I \neq 1$ and k a non-zero real constant, then* $kX \sim \mathcal{S}(\alpha_I, \mathrm{sign}(k)\beta, |k|^{\alpha_I}\gamma)$.

2.2 Stochastic geometry

In a wireless network, multiple transmitter-receiver pairs are actively communicating using a shared resource. Apart from the signal of interest, a receiver is affected by the sum of interfering transmissions, which can be represented as a shot noise process

$$I(x) = \sum_{X_i \in \Phi} P_i h_i g_\alpha(x - X_i) \tag{2.2}$$

where P_i is the signal power, h_i the fading power coefficient, and $g_\alpha(x) = \|x\|^{-\alpha}$ is the power path loss function. The study of shot noise processes started more than a century ago with seminal contributions from Campbell [18], who characterized the average and variance, and Schottky [19]. As the capacity of a wireless link is determined by the ratio of the desired signal and interference power, (2.2) illustrates that the geometry of the network nodes plays a key role to describe the quality of communication. Stochastic

geometry is a well developed branch of applied probability inherently related with the theory of point processes. Stochastic geometry provides necessary tools to describe network properties by averaging over all possible realizations of a point process, such that location-independent insight can be gained into link performance. Often, this tool is able to express performance metrics as a function of few parameters and reveal dependencies between the system design and performance.

A formal introduction in stochastic geometry can be found in [20], while the application of stochastic geometry to wireless communications is well documented in [3,21,22]. In the following, we list the definitions, properties, and theorems relevant for this dissertation.

2.2.1 Point processes

Point processes play a fundamental role in the description of the network geometry. Let $\mathbf{N}$ be the set of sequences Φ of points in the d-dimensional space $\mathbb{R}^d$ that are finite (i.e. with a finite number of points in any bounded subset) and simple (i.e. $x \neq y, \forall x, y \in \Phi$), then a point process can be defined as a random variable that takes values from $\mathbf{N}$.

Definition 2. *A point process Φ on $\mathbb{R}^d$ is a measurable mapping from a probability space $(\Omega, \mathcal{A}, \mathbb{P})$ to $(\mathbf{N}, \mathcal{N})$*

$$\Phi \quad : \quad \Omega \to \mathbf{N} \tag{2.3}$$

where $\mathcal{N}$ denotes the smallest sigma algebra for the set of point sequences $\mathbf{N}$.

An alternative representation for the point process Φ is based on the sum of Dirac measures

$$\Phi = \sum_{i=1}^{\infty} \delta_{x_i} \tag{2.4}$$

where δ_x is the Dirac measure $\delta_x(B) = \mathbb{1}_B(x)$ for $B \subset \mathbb{R}^d$.

Definition 3. *The intensity measure of a point process Φ is the average number of points in a set $B \subset \mathbb{R}^d$, which can be written as*

$$\Lambda(B) = \mathbb{E}\{\Phi(B)\}. \tag{2.5}$$

Definition 4. *A point process Φ is said to be stationary if its distribution is invariant under translation, i.e.*

$$\Pr\{\Phi \in Y\} = \Pr\{x + \Phi \in Y\}, \quad \forall x \in \mathbb{R}^d, \quad \forall Y \in \mathcal{N} \quad . \tag{2.6}$$

A point process Φ is said to be isotropic if its distribution is invariant under rotation, i.e.

$$\Pr\{\Phi \in Y\} = \Pr\{\mathbf{r}\Phi \in Y\} \tag{2.7}$$

for any rotation $\mathbf{r}$ around the origin. Point processes that hold both the property of stationarity and isotropy are said to be motion-invariant.

For a stationary point process, the intensity measure simplifies to $\Lambda(B) = \lambda|B|$, where $|B|$ represents the Lebesgue measure of B and λ is denoted as the density or intensity of Φ.

The point process most notable for its ease of analysis is the Poisson point process (PPP). A stationary PPP is characterized by the properties that (i) the number of points in disjoint sets are independent r.v.'s, and (ii) the number of points in a set $B \in \mathbb{R}^d$ is Poisson distributed $\Phi(B) \sim \text{Poi}(\lambda|B|)$. Some operations that preserve the Poisson law explain the attractiveness of the PPP.

Property 3 (Superposition property). *The superposition of Poisson point processes $\Phi = \sum_k \Phi_k$ with density λ_k is again a Poisson point processes with density $\lambda = \sum_k \lambda_k$.*

Property 4 (Thinning property). *The thinning of a Poisson point process with intensity measure Λ considering the retaining probability $p(x)$ results in a Poisson point process with intensity measure $\Lambda_t(B) = \int_B p(x)\Lambda(dx)$.*

Besides the Poisson point process, there are many other point processes with a broad field of application. For instance, Neyman-Scott processes are used to capture clustering, while Matern processes are used to model repulsion.

2.2.2 Functions of point processes

Considering the expression of the shot noise process in (2.2), the analysis of the aggregate interference originating from a field of interferers involves the sum of a function evaluated at the points of the point process [23].

Theorem (Campbell). *Consider a measurable function $f(x) : \mathbb{R}^d \to \mathbb{R}^+$. Then, we have*

$$\mathbb{E}\left\{\sum_{x \in \Phi} f(x)\right\} = \int_{\mathbb{R}^d} f(x)\Lambda(dx) \quad . \tag{2.8}$$

Campbell's theorem can be applied to calculate the mean aggregate interference observed at the origin.

Theorem (Probability generating functional (PGFL)). *Let $f(x) : \mathbb{R}^d \to \mathbb{R}^+$ be a measurable function. The probability generating functional $\mathbb{E}\{\prod_{x \in \Phi} f(x)\}$ for the Poisson point process Φ is given by*

$$\mathbb{E}\left\{\prod_{x \in \Phi} f(x)\right\} = \exp\left(-\int_{\mathbb{R}^d}(1 - f(x))\Lambda(dx)\right) \quad . \tag{2.9}$$

The calculation of the outage probability is based on the Laplace transform of the aggregate interference, for which the PGFL can be used.

Palm theory formalizes the notion of the conditional distribution for general point processes, given that the process has a point at a location $x \in \mathbb{R}^d$. This is useful for instance for the calculation of the outage probability, where it is required to condition on the location of either the receiver or the transmitter.

Theorem (Slivnyak-Mecke). *Given a point process Φ, the distribution $\mathbb{P}^{!x}(.)$ denotes the reduced Palm distribution of Φ given a point at x. Then, we have*

$$\mathbb{P}^{!x}(.) = \mathbb{P}\{\Phi \in .\} \tag{2.10}$$

i.e., the reduced Palm distribution of the Poisson point process equals the distribution of the PPP itself.

Informally, Slivnyak-Mecke's theorem states that adding a point at x does not change the distribution of the other points of the PPP.

Chapter 3

Acquisition of GNSS signals in urban interference environment

[1]In urban environment, Global Navigation Satellite System (GNSS) signals are impaired by strong fading and by the presence of several potential sources of interference that can severely affect the acquisition. This chapter evaluates the acquisition performance for the most common acquisition strategies in terms of receiver operating characteristics (ROC) and studies the impact of fading and interference on the acquisition performance. Two different interference scenarios are considered: a single interferer and a network of interferers. We present a framework to evaluate the GNSS acquisition performance with respect to all relevant system parameters that jointly considers the acquisition method, the effect of radio signal propagation conditions, and the spatial distribution of the interfering nodes.

3.1 Background

Spread Spectrum (SS) techniques have been first applied in the military domain because of their intrinsic characteristics, such as the possibility to hide the signal under the noise floor, the low probability of interception and its robustness against narrowband interference [27]. Other beneficial properties have lead to the widespread use of Direct Sequence Spread Spectrum (DSSS) in commercial applications. In particular, thanks to the large transmission bandwidth that allows precise ranging, DSSS has been applied for location and timing applications such as Global Navigation Satellite Systems (GNSS).

---

[1]This chapter has been accepted for publication in IEEE Transactions on Aerospace and Electronic Systems [24]. The material of this chapter has been presented in part at IEEE NAVITEC, Noordwijk, the Netherlands, December 2010 [25], and at the IEEE International Conference on Communications (ICC), Budapest, June 2013 [26].

For a correct signal reception, the alignment between the transmitted spreading code and the locally generated sequence is fundamental. Code synchronization in DSSS systems consists typically of two sequential parts: acquisition and tracking. The acquisition yields a coarse alignment and the subsequent tracking ensures a continuous fine alignment of the phases. The code acquisition is a binary detection problem, where the decision has to be made for each possible code phase and Doppler frequency. These two variables constitute a two-dimensional search space which is discretized into different cells. Every detection or estimation process is composed of an observation block and a decision or estimation block [28]. In the observation block the cells in the search space are computed by downconverting the incoming signal, followed by a correlation with the local replica of the spread spectrum sequence. The cell values depend on the implementation details for the computation of a single cell (e.g. integration time), the presence of the signal of interest (SoI), noise and interference, and the channel conditions. The cell values are hence random variables with their statistical distribution [29], which we will further call the cell statistics. In the decision block a decision variable is calculated based on single or multiple cells of the search space, which determines the presence or absence of the SoI. Different acquisition strategies received wide research interest in the past [30–34]. The most popular acquisition strategy consists in comparing the maximum value of the search space with a threshold value and is called the threshold crossing (MAX/TC) criterion [31]. Another common acquisition strategy for GNSS signals relates the maximum cell in the search space to the second maximum, which has as main advantage to maintain the probability of false alarm independent of the noise power density [35].

The acquisition performance is well described in the presence of additive white Gaussian noise (AWGN). Recent studies show that, in urban environment, the detection of the GNSS signal can be seriously challenged by sources of unwanted interference [25, 36–39], in addition to the channel fading inherent to environments with a large amount of obstacles. For DSSS systems, the impact of channel fading on the acquisition performance has been studied in [40–47]. However, the analysis is focused on the acquisition by mobile terminals in cellular networks. The acquisition of GNSS signals differentiates itself from the acquisition in Direct Sequence - Code Division Multiple Access (DS-CDMA) networks by the extremely low GNSS signal power and by the different fading distributions that affect the SoI and the interference. Hence, considering that GNSS is a critical infrastructure, it is relevant to study the impact of different sources of interference to assess its performance in urban environment [48]. For single interferers, the impact of narrowband interference has been studied in [36]. Further, [39] and [25] discuss the interference originating from Digital Video Broadcasting -

Terrestrial (DVB-T) transmissions. None of the transmission bands for DVB-T are active within the frequency bands allocated for GNSS signals. However, some of the harmonics of DVB-T signals transmitted in the UHF IV and UHF V bands coincide with the GPS L1 or Galileo E1 bands and therefore, these signals can be potential sources of unintentional interference. Due to the increasing number of mobile devices equipped with radio transmitters, we can expect a drastic proliferation of possible sources of interference [49]. Although legal policies are established to protect the GNSS bands, there exist future realistic scenarios such as multi-constellation GNSS [50], the deployment of pseudolites [51–53] and ultra wideband (UWB) transmitters [54, 55], where the interference can originate from multiple transmitters [56], and where literature specifically warns for the severe interference effects and the resulting performance degradation inflicted on GNSS receivers. Another possible threat for GNSS systems are cognitive radio (CR) networks, which have been proposed recently to alleviate the problem of inefficiently utilized spectrum by allowing cognitive devices to coexist with licensed users, given that the interference caused to the licensed users can be limited. The frequency bands used for DVB-T transmissions are a possible candidate for opportunistic spectrum access (OSA) [57], yet the harmonics created in that frequency band are known to coincide with the GPS L1 or Galileo E1 bands. As a consequence, cognitive devices which are allowed to transmit in the UHF IV band when the digital television (DTV) broadcasting system is inactive, might create harmful interference to GNSS systems due to amplifiers' non-linear behavior [58]. Although literature mentions different types of interference that can affect GNSS receivers, a theoretical framework that accounts for the effects of single and/or multiple sources of interference and for the channel fading affecting both SoI and interfering signals is still missing.

In this chapter, we develop a framework for the GNSS acquisition performance that accounts for a single interferer as well as for a network of interferers. The framework is flexible enough to jointly account for different channel conditions for the SoI and the interfering signals, as well as the spatial distribution and density of the interfering nodes. Moreover, the proposed framework provides the acquisition performance for different decision strategies. The acquisition performance is characterized by means of mathematical expressions of the probability of detection ($\mathbb{P}_d$) and the probability of false alarm ($\mathbb{P}_{fa}$). The resulting Receiver Operating Curves (ROC) have been supported and validated by simulations. The main contributions of this work can be listed as follows (i) the theoretical comparison of the most common acquisition methods, (ii) the definition of a framework that allows to validate the acquisition performance for different channel conditions for the SoI and the interference, and (iii) the adoption of

aggregate network interference in the theoretical framework. The analytical framework for the acquisition performance of GNSS signals presented in this chapter is of interest both for the correct setting of the detection threshold in realistic (future) signal conditions as for the definition of limit system parameters that guarantee a minimum required acquisition performance. Moreover, the framework can be used to plan where alternative localization systems should be deployed in order to achieve ubiquitous and accurate localization performance.

The remainder of the chapter is organized as follows. In Section 3.2 the signal and system model is presented, introducing the assumptions that have been made. The search space is defined and the different acquisition strategies that have been studied are introduced. Section 3.3 analyzes the acquisition performance in the presence of a single interferer, while in Section 3.4 the case of aggregate interference is discussed. Numerical results are presented in Section 4.7. In Section 3.6 the conclusions are drawn.

3.2 Signal and System Model

In this section, we introduce the signal and system model, as well as the decision strategies that will be evaluated in the remainder of the chapter.

3.2.1 Signal Model

After filtering and downconversion in the receiver front-end, the k-th sample of the received signal entering the acquisition block has the following form

$$s[k] = \sum_{l=1}^{N_{\text{sat}}} r_l[k] + i[k] + n[k] \tag{3.1}$$

where $s[k]$ is the sum of N_{sat} satellite signals $r_l[k]$, an interference term $i[k]$, and the noise term $n[k]$. We assume the noise samples to be independent and to follow a complex normal distribution $\mathcal{N}_{\text{c}}(0, N_0 f_{\text{s}}/2)$, with f_{s} is the sampling frequency and N_0 the noise spectral density. The k-th sample of the GNSS signal received from a single satellite can be represented as

$$r_l[k] = \sqrt{2P} H_l c_l[k - \tau_{\text{c},l}] d_l[k - \tau_{\text{c},l}] \cos[2\pi(f_{\text{IF}} + f_{\text{d},l})k + \phi_l] \tag{3.2}$$

where P is the GNSS received signal power, H_l represents the fading affecting the l-th satellite signal, c_l is the code with corresponding code phase $\tau_{\text{c},l}$, f_{IF} and $f_{\text{d},l}$ are the intermediate frequency and the Doppler frequency, and ϕ_l is the carrier phase error. For simplicity, we suppose the data bit d_l to be 1. The main objective of the acquisition is to determine the code phases $\tau_{\text{c},1}, \tau_{\text{c},2}, ..., \tau_{\text{c},N_{\text{sat}}}$ and Doppler frequencies $f_{\text{d},1}, f_{\text{d},2}, ..., f_{\text{d},N_{\text{sat}}}$ of the satellites in

$$s[k] = \sum_l r_l[k] + i[k] + n[k]$$

$$\exp[j2\pi(f_{IF} + f_d)k] \qquad c[k - \tau]$$
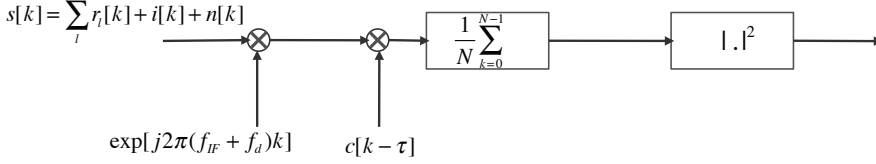
Figure 3.1: Schematic of the different processing steps for the calculation of the search space.

view. Since the GPS L1 and Galileo E1 are operating in protected spectrum, we consider as source of interference the harmonics or intermodulation products of emissions in the UHF IV and UHF V frequency bands.[2]

3.2.2 System Model

The acquisition of GNSS signals is a classical detection problem where a signal impaired by noise and interference has to be identified. Prior to the tracking of GNSS signals, the receiver identifies which satellites can be used to determine a position and time solution and provides a rough estimation of the code phases and the Doppler frequencies of the present satellite signals. In the receiver acquisition block, the signal as defined in (3.1) is first downconverted to baseband. Subsequently, the downconverted signal is correlated with a local replica of the code and the correlator output is integrated over an interval which is an integer a times longer than the code period length N. As shown in Fig. 3.1, the unknown phase of the incoming signal is finally removed by taking the squared absolute value of the complex variable.

The acquisition process is a binary decision problem with two hypothesis. The $\mathcal{H}_1$ hypothesis corresponds to the scenario where the signal is present and correctly aligned with the local replica at the receiver. The null-hypothesis $\mathcal{H}_0$ corresponds to the case where the SoI is not present, or present but incorrectly aligned with the local replica. The acquisition performance is measured in terms of the probability of detection and the probability of false alarm. The probability of detection $\mathbb{P}_d$ is the probability that the decision variable V surpasses the threshold ζ in the presence of the SoI and can be expressed as $\mathbb{P}_d(\zeta) = \Pr(V > \zeta | \mathcal{H}_1)$. The probability of false alarm $\mathbb{P}_{fa}$ is the probability that V surpasses ζ in absence of SoI or when the

---

[2]Our framework can be easily extended to the case of in-band (e.g. intentional) interference.

signal is not correctly aligned with the local replica, and can be expressed as $\mathbb{P}_{\text{fa}}(\zeta) = \text{Pr}(V > \zeta | \mathcal{H}_0)$.

In order to define the cell statistics, we characterize the different contributions to the cell values. The search space is discretized into different cells that correspond to possible values of the code phase and the Doppler frequency. The code phase $\tau_{\text{c},l}$ of the different satellites in view are chosen from a finite set $\{\tau_1, \tau_2, \ldots, \tau_{aN}\}$ with $\tau_p = (p-1)\Delta\tau$, where we choose $\Delta\tau$ equal to the chip time T_{c} to allow a tractable analysis. As for the Doppler frequency, the value is chosen from the finite set $\{f_1, f_2, \ldots, f_L\}$, with $f_q = f_{\min} + (q-1)\Delta f$, where the frequency resolution Δf and $f_{\min}$ are chosen according to the specifications of the application. Thus, we define the search space $\mathbf{X} \in \mathbb{R}^{aN \times L}$ where each cell $\mathbf{X}[p,q]$, $1 \leq p \leq aN$, $1 \leq q \leq L$ is given by

$$\mathbf{X}[p,q] =$$

$$= \left| \frac{1}{aN} \sum_{k=1}^{aN} \left[\sum_{l=1}^{N_{\text{sat}}} r_l[k] + i[k] + n[k] \right] c[k - \tau_p] e^{j2\pi(f_{\text{IF}} + f_q)k} \right|^2$$

$$= \left| \mathbf{X}_{\text{r}}[p,q] + \mathbf{X}_{\text{i}}[p,q] + \mathbf{X}_{\text{n}}[p,q] \right|^2 \tag{3.3}$$

with $\mathbf{X}_{\text{r}}[p,q]$, $\mathbf{X}_{\text{i}}[p,q]$, and $\mathbf{X}_{\text{n}}[p,q]$ the contributions of the satellite signals, the interference, and the noise, respectively.[3] The noise term $\mathbf{X}_{\text{n}}$ results from the downconversion and correlation with the local replica of the noise term in (3.1). The downconversion yields a complex Gaussian random variable (r.v.) with variance of the real and the imaginary parts equal to $N_0 f_{\text{s}}/4$. The correlation with the local replica yields the mean value of N zero-mean, complex Gaussian r.v.'s, and thus, $\mathbf{X}_{\text{n}} \sim \mathcal{N}_c(0, \sigma_{\text{n}}^2)$ with $\sigma_{\text{n}}^2 = N_0 f_{\text{s}}/(2N) = N_0/(2T_{\text{per}})$, where $T_{\text{per}} = NT_{\text{c}}$ is the code period. Note that, in order to have independent noise samples, the sampling rate is $1/T_{\text{c}}$. We consider the term that originates from a single interferer after downconversion and despreading to be a Gaussian process, such that $\mathbf{X}_{\text{i}} \sim \mathcal{N}_c(0, \sigma_{\text{i}}^2)$. It is widely accepted that the Gaussian distribution is a good approximation for the interference in DSSS systems [59, 60]. When the Gaussian approximation of the contribution to the decision variable produced by the despreading of the interfering signal is not accurate, the proposed framework yields a pessimistic performance analysis [61]. In order to account for the interaction between the interfering signal and the despreading sequence, the spectral separation coefficient (SSC) is commonly used [62]. Since the contribution of the interference to the decision variable can be modeled as a Gaussian r.v., and since the SSC values for complex white Gaussian noise are very similar for GPS C/A and Galileo BOC(1,1) coding [25], the proposed theoretical model holds for a generic GNSS signal.

---

[3]In order to reduce notational complexity, without loss of generality we assume $a = 1$.

In this work, we consider the Doppler frequency known and therefore, $\mathbf{X} \in \mathbb{R}^{aN \times L}$ reduces to a one-dimensional search space $\bar{X} \in \mathbb{R}^{aN}$ spanned over the set of code phase values. We refer to [63] for several acquisition techniques that include also the estimation of the Doppler frequency. For a known Doppler frequency, a cell of the search space $X[\tau] \in \bar{X}$ can be written as[4]

$$X[\tau] = \left| \sum_{l=1}^{N_{\text{sat}}} \sqrt{P} H_l R_l[\tau] e^{-j\phi_l} + X_{\text{i}}[\tau] + X_{\text{n}}[\tau] \right|^2 \tag{3.4}$$

where $R_l[\tau]$ is the cross-correlation function between the code under search and the code of the l-th satellite. The contribution of interference and noise for the different code phase values is represented by $X_{\text{i}} \in \mathbb{R}^{aN}$ and $X_{\text{n}} \in \mathbb{R}^{aN}$, respectively. We consider the set of $\{H_l\}$ as independent and identically distributed (i.i.d.), with a constant value over the integration time and average fading power $\mathbb{E}\{H_l^2\} = 1$. Without loss of generality, let satellite 1 be the satellite under search. The value of a search space cell can now be expressed as

$$X[\tau] = \left| \sqrt{P} H_1 R_1[\tau] e^{-j\phi_1} + \underbrace{\sum_{l=2}^{N_{\text{sat}}} \sqrt{P} H_l R_l[\tau] e^{-j\phi_l}}_{X_c[\tau]} + X_{\text{i}}[\tau] + X_{\text{n}}[\tau] \right|^2 \tag{3.5}$$

where $X_{\text{c}}[\tau]$ is the contribution of the cross-correlation noise to the value of a random search space cell. The distribution of $X_{\text{c}}[\tau]$ can be well approximated by a complex, zero-mean Gaussian distributed r.v. [25]. The variance of $X_{\text{c}}[\tau]$ can be written as

$$\sigma_{\text{c}}^2 = \left[\mathbb{E}\{H_l^2\}(N_{\text{sat}} - 1)P \right] \sigma_{\text{cross}}^2 / 2 \tag{3.6}$$

where σ_{cross}^2 is the variance of the cross-correlation originating from a single satellite.

3.2.3 Decision Strategies

The acquisition performance does not only depend on the cell statistics, but also on the acquisition strategy that has been adopted. Different decision variables are commonly used, often on a heuristic basis. In general, the goal of a decision strategy is to maximize the probability of detection and to minimize the probability of false alarm. In [28], the Generalized Likelihood Ratio Test (GLRT) is introduced. The GLRT leads to select the maximum of the search space defined as [31, 64]

$$V = \max\{\bar{X}\}. \tag{3.7}$$

---

[4]To reduce the complexity of notation, the index p is further discarded.

The decision is then taken by comparing V with a threshold. In the GLRT strategy, the Neyman-Pearson criterion is applied. For a selected probability of false alarm, a threshold that maximizes the probability of detection is chosen, such that the GLRT strategy is the optimal acquisition strategy when the signal conditions are perfectly known.

A second strategy to define a decision variable, called Maximum Ratio Test (MRT), uses the ratio between the first and the second maximum of the search space [35, 65]

$$V = \frac{X_{(1)}}{X_{(2)}} \tag{3.8}$$

where $X_{(1)} \geq X_{(2)} \geq ... \geq X_{(aN-1)}$ are order statistics of $\bar{X}$.

3.3 Single Interferer

In this section we consider the scenario where the interference stems from a single transmitter. We propose an analytical approach for the evaluation of the acquisition performance that is based on the characteristic function (CF) of the decision variable. To define the statistics of the decision variable for this scenario, we analyze the contribution of the interference to the search space cell values. Although the interfering signal does not necessarily feature a zero-mean Gaussian distribution, it can be shown that the contribution to the decision variable produced by the despreading of the interfering signal can be often approximated by a Gaussian random variable [59, 60]. As a case study, we consider a DVB-T base-station as a single transmitter and the third harmonic of the DVB-T signal as the interference in the GNSS E1/L1 bands [58]. However, our approach can be used for several single interferer scenarios where both SoI and interferer are affected by fading. The contribution of the third harmonic of DVB-T to the different cells of the search space has been discussed in [25], and can be expressed as $X_i \sim \mathcal{N}_c(0, \sigma_i^2)$. Therefore, the sum of the contributions stemming from the noise, the interference, and the cross-correlation can be merged to a single complex Gaussian r.v.

$$X_{\text{IN}} = X_c + X_i + X_n \sim \mathcal{N}_c(0, \sigma_{\text{tot}}^2) \tag{3.9}$$

with $\sigma_{\text{tot}}^2 = \sigma_c^2 + \sigma_i^2 + \sigma_n^2$.

This completes the definition of the cell statistics and we proceed with the discussion of acquisition performance of the GLRT and MRT decision strategies.

3.3.1 Generalized Likelihood Ratio Test

The probability of detection

$\mathbb{P}_d$ corresponds to the probability that the decision variable exceeds the threshold value in presence of the SoI. In the GLRT strategy, the maximum value of the entire search space is selected as the decision variable. Let X_1 denote the cell value corresponding to the correct code phase, assumed without loss of generality to be τ_1, and let $\bar{X}_- = \bar{X}\backslash\{X_1\}$ denote the search space excluding cell X_1. Considering a relatively strong satellite signal power, we suppose that $X_1 = \max\{\bar{X}\} = X_{(1)}$. The r.v. X_1 can be written as

$$X_1 = \left| \sqrt{P}H_1 e^{-j\phi_1} + X_c[\tau_1] + X_i[\tau_1] + X_n[\tau_1] \right|^2 \tag{3.10}$$

where we have considered the signal from satellite number 1 as the one under search[5]. When $X_1 = X_{(1)}$, the probability of detection can be found by applying the inversion theorem [66] and is given by

$$\begin{aligned} \mathbb{P}_d(\zeta|X_1 = X_{(1)}) &= \Pr\{X_1 > \zeta\} \\ &= \frac{1}{2} - \frac{1}{2\pi} \int_0^\infty \mathfrak{Re}\left\{ \frac{\psi_{X_1}(-j\omega)e^{j\omega\zeta} - \psi_{X_1}(j\omega)e^{-j\omega\zeta}}{j\omega} \right\} d\omega \end{aligned} \tag{3.11}$$

where $\psi_{X_1}(j\omega)$ is the CF of the decision variable X_1. Conditioning on H_1, the r.v. X_1 follows a non-central χ^2 distribution with 2 degrees of freedom and non-centrality parameter $\mu_{X_1} = H_1^2 P$. The CF of X_1 conditioned on H_1 can be expressed as

$$\begin{aligned} \psi_{X_1|H_1}(j\omega) &= \mathbb{E}\{e^{j\omega X_1|H_1}\} \\ &= \frac{1}{1 - 2j\omega\sigma_{\text{tot}}^2} \exp\left(\frac{j\omega H_1^2 P}{1 - 2j\omega\sigma_{\text{tot}}^2} \right). \end{aligned} \tag{3.12}$$

Taking the expectation over H_1, (3.12) yields

$$\psi_{X_1}(j\omega) = \frac{1}{1 - 2j\omega\sigma_{\text{tot}}^2} \psi_{H_1^2}\left(\frac{j\omega P}{1 - 2j\omega\sigma_{\text{tot}}^2} \right) \tag{3.13}$$

where $\psi_{H_1^2}$ is the CF of the fading power. In case of Ricean or Rayleigh fading, the fading power features a non-central chi-square and a central chi-square distribution, respectively. In both cases, the CF is known in closed form. The Ricean distribution is frequently used for modeling outdoor channels [67], while the Rayleigh fading channel is used for modeling indoor channel environments [68].

---

[5]We consider the maximum of the auto-correlation equal to 1.

To calculate $\mathbb{P}_d$ we supposed so far a strong signal power, which is made explicit in the conditions of (3.11). The signal missed-detection can however also occur when $X_1 \neq X_{(1)}$. In order to account for this case, we denote the maximum of the set of the incorrect code phase cell values as $X_2 = \max\{\bar{X}_-\}$, which follows a generalized exponential distribution [69].[6] The probability of detection is the result of the product of two probabilities, i.e. the detection probability of the cell corresponding to the correct code phase and the probability that the maximum of the rest of the search space is smaller than X_1 and therefore, $\mathbb{P}_d$ conditioned on H_1 can be expressed as

$$\mathbb{P}_d(\zeta|H_1) = \Pr(X_{1|H_1} > \zeta) \cdot \Pr(X_2 < X_{1|H_1}). \tag{3.14}$$

The two factors both are conditioned on the fading parameter h_1 and thus, they are not independent. The probability of detection conditioned on H_1 can now be written as

$$\begin{aligned}
\mathbb{P}_d(\zeta|H_1) &= \int_\zeta^{+\infty} \int_0^x f_{X_2}(y) f_{X_{1|H_1}}(x) \mathrm{d}y \mathrm{d}x \\
&= \int_\zeta^{+\infty} F_{X_2}(x) f_{X_{1|H_1}}(x) \mathrm{d}x
\end{aligned} \tag{3.15}$$

where $F_{X_2}(x)$ is the cumulative distribution function (CDF) of a generalized exponential function. The CDF of the generalized exponential distribution can be expressed as [69]

$$F_{X_2}(x; \varrho, \lambda_e) = (1 - e^{-\lambda_e x})^\varrho, \quad x > 0 \tag{3.16}$$

where $\varrho = N - 1$ and $\lambda_e = 1/2/\sigma_{\mathrm{tot}}^2$ are the scale and shape parameters, respectively. In order to take into account the effect of the fading, we propose a unified approach based on the CF of X_1. Using the inversion theorem for the calculation of the probability density function (PDF) of X_1, the probability of detection can be expressed as

$$\mathbb{P}_d(\zeta) = \frac{1}{\pi} \int_\zeta^{+\infty} F_{X_2}(x) \int_0^{+\infty} \Re\mathfrak{e}\{\Psi_{X_1}(j\omega) \exp(-j\omega x)\} \mathrm{d}\omega \mathrm{d}x. \tag{3.17}$$

By using the CF of X_1, we can easily include in the analysis the effect of fading on the SoI and on the interferer. The advantage of using the CF will become clear in the next section where we will show that a double numerical integration will likewise allow us to calculate the probability of detection including the effects of fading and the effects of multiple interference instead of a recursive solution of nested integrations.

---

[6]We do not consider the contribution of the autocorrelation of the SoI that is present in all cells of $\bar{X}_-$, since it is negligible. Instead, we use σ_{tot}^2 as defined in (3.9).

The probability of false alarm

$\mathbb{P}_{fa}$ corresponds to the probability that the decision variable exceeds the threshold value in absence of the signal. In this case, the entire search space is composed of i.i.d r.v.'s following an exponential distribution. The probability that the decision variable exceeds the threshold can thus be written as follows

$$\mathbb{P}_{fa}(\zeta) = 1 - F_{X_2}(\zeta; N, \lambda_e) = 1 - (1 - e^{-\lambda_e \zeta})^N. \qquad (3.18)$$

Remark: A third method proposed in [70] considers the decision variable defined as

$$V = \frac{X_{(1)}}{\sum_{X_k \in \bar{X} \setminus \{X_{(1)}\}} X_k / (N-1)}. \qquad (3.19)$$

Since for a given value of the signal-to-noise ratio (SNR) and the signal-to-interference ratio (SIR), the value by which $X_{(1)}$ is scaled is a constant, the performance of this method is identical to the GLRT acquisition strategy. However, this method is beneficial since it inherently includes an estimation of the noise power, which is necessary to correctly set the threshold.

3.3.2 Maximum Ratio Test

For the MRT, the decision variable is defined as the ratio of the highest correlation peak and the second highest correlation peak of the search space. This method is heuristic and has as main advantage that $\mathbb{P}_{fa}$ is independent of the noise power density. This approach allows to set a fixed threshold corresponding to a selected false alarm rate, which is independent of the noise power [35].

Probability of detection

As defined in Section 3.3.1, let X_1 be the cell value corresponding to the correct code phase, and $X_2 = \max\{\bar{X}_-\}$. We assume a relatively strong satellite signal, such that $X_{(1)} = X_1$ and $X_{(2)} = X_2$. We can now rewrite (3.8) as

$$\tilde{V} = X_1 - \zeta X_2. \qquad (3.20)$$

When the signal of interest is present, X_1 can be expressed as in (3.10) and follows a non-central chi-square distribution. Since the vector $\bar{X}_-$ is composed of i.i.d random variables that follow an exponential distribution, X_2 follows a generalized exponential distribution. In the presence of the SoI, the acquisition of the GNSS signal is successful if $\tilde{V} > 0$. Therefore, by using

the inversion theorem the probability of detection can be expressed as follows

$$\mathbb{P}_d(\zeta) = \Pr\left\{\tilde{V} > 0\right\}$$
$$= \frac{1}{2} - \frac{1}{2\pi}\int_0^\infty \mathfrak{Re}\left\{\frac{\psi_{\tilde{V}}(-j\omega) - \psi_{\tilde{V}}(j\omega)}{j\omega}\right\}d\omega \qquad (3.21)$$

where $\psi_{\tilde{V}}(j\omega)$ is the CF of the variable $\tilde{V}$. For a given threshold value ζ, the CF of the decision variable is given by

$$\psi_{\tilde{V}}(j\omega) = \mathbb{E}\left\{e^{j\omega\tilde{V}}\right\} = \mathbb{E}\left\{e^{j\omega(X_1 - \zeta X_2)}\right\}. \qquad (3.22)$$

Since X_1 and X_2 are independent r.v.'s, the CF of $\tilde{V}$ can be written as

$$\psi_{\tilde{V}}(j\omega) = \frac{1}{1 - 2j\omega\sigma_{\text{tot}}^2}\psi_{H_1^2}\left(\frac{j\omega P}{1 - 2j\omega\sigma_{\text{tot}}^2}\right)\psi_{X_2}(-j\omega\zeta). \qquad (3.23)$$

Since X_2 follows a generalized exponential distribution, the CF of X_2 can be written in closed form as [69]

$$\psi_{X_2}(j\omega) = \frac{\Gamma(N)\Gamma(1 - \frac{j\omega}{\lambda_e})}{\Gamma(N - \frac{j\omega}{\lambda_e})}. \qquad (3.24)$$

Unfortunately, the CF of X_2 is not in a convenient form for numerical integration, since the Gamma function diverges to infinity in the integration interval of (3.21). However, recently the generalized exponential function has been demonstrated to provide a good approximation of the Gamma distribution [71]. Therefore, we approximate the distribution of the generalized exponential r.v. with a Gamma distribution defined by the two paramters k and θ. In order to estimate the parameters of the Gamma distribution, we use the method of the moments by imposing the equivalence of the first two moments of the Gamma distribution with the first two moments of X_2. Since mean and variance of the Gamma distribution are expressed as

$$\mu_G = k\theta \text{ and } \sigma_G^2 = k\theta^2 \qquad (3.25)$$

and for X_2 we have

$$\mu_{X_2} = \frac{1}{\lambda_e}\left[\eta(N) - \eta(1)\right] \text{ and } \sigma_{X_2}^2 = \frac{1}{\lambda_e^2}\left[\eta\prime(1) - \eta\prime(N)\right] \qquad (3.26)$$

the parameters of the Gamma distribution can be expressed as

$$\theta = \frac{1}{\lambda_e}\frac{\eta\prime(1) - \eta\prime(N)}{\eta(N) - \eta(1)} \qquad (3.27)$$

and

$$k = \frac{[\eta(N) - \eta(1)]^2}{\eta\prime(1) - \eta\prime(N)} \tag{3.28}$$

where $\eta(x)$ and $\eta\prime(x)$ are the digamma and the polygamma function, respectively. Finally, the CF of the decision variable $\tilde{V}$ can be obtained by inserting the CF of the Gamma distributed r.v. X_2 in (3.23)

$$\psi_{\tilde{V}}(j\omega) = \frac{1}{1 - 2j\omega\sigma_{\text{tot}}^2}\psi_{H_1^2}\left(\frac{j\omega P}{1 - 2j\omega\sigma_{\text{tot}}^2}\right)(1 + j\omega\zeta\theta)^{-k}. \tag{3.29}$$

The probability of detection can be calculated by substituting (3.29) in (3.21). Note that in the GLRT strategy a second numerical integration is necessary to account for the probability that the cell corresponding to the correct code phase does not correspond to the maximum of the search space. Differently, the MRT strategy inherently accounts for this probability, i.e. the MRT strategy depends upon the probability distribution of the two independent r.v.'s X_1 and X_2 and therefore, contains the probability that X_2 exceeds X_1. Moreover, only a single numerical integration is needed.

The probability of false alarm

$\mathbb{P}_{\text{fa}}$ has been derived analytically in [72]. According to the theory of order statistics, $\mathbb{P}_{\text{fa}}$ can be written as

$$\mathbb{P}_{\text{fa}}(\zeta) = (N^2 - N)\mathcal{B}(N - 1, 1 + \zeta) \tag{3.30}$$

where $\mathcal{B}(a, b)$ represents the Beta function.

3.4 Aggregate Interference

The scenario where the interference stems from a network of interferers is of increasing importance, as reported in recent literature [2, 10, 13]. In this section, we consider multiple interferers scattered over the plane according to a homogeneous Poisson point process (PPP). It is known that for this scenario the approximation of the multiple interference by a Gaussian process is very poor. The aggregate network interference can rather be modeled as an α-stable process, where the characteristic exponent of the process is a function of the path-loss exponent, and the dispersion is affected by the channel randomness. We present a statistical model of aggregate interference that was proposed in [73] and [2], and we analyze the impact of this type of interference on the acquisition of the satellite signal for the GLRT acquisition strategy.

3.4.1 Interference Modeling

As discussed in Section 3.3, the correlation of a single interferer with the local replica of the code yields a complex Gaussian contribution to the decision variable. When we consider a network of interferers, we apply a stochastic geometry approach to capture the randomness of the topology and model the spatial distribution of the interferer locations according to a homogeneous Poisson point process [10]. The probability that k interferers lie inside region $\mathcal{R}$ depends on the spatial density of the interfering nodes λ and the area $A_{\mathcal{R}}$ of the region $\mathcal{R}$, and can be written as [74]

$$\Pr\{k \in \mathcal{R}\} = \frac{(\lambda A_{\mathcal{R}})^k}{k!} e^{-\lambda A_{\mathcal{R}}}. \tag{3.31}$$

Without loss of generality, we consider the receiver located at the origin of an infinite plane[7], and we express the aggregate interference measured at the origin as

$$X_{\mathrm{i}} = \sum_{m=1}^{\infty} I_m. \tag{3.32}$$

The m-th interfering signal in (3.32) can be written as

$$I_m = \frac{1}{R_m^{\nu}} G_m (I_{m,1} + j I_{m,2}) \tag{3.33}$$

where $I_{m,1}$ and $I_{m,2}$ are two i.i.d. Gaussian r.v.'s with zero mean and variance $\sigma_I^2/2$. The term σ_I^2 represents the interferer transmission power at a distance of 1 meter (far-field assumption) in the affected GNSS band. The r.v. G_m represent the fading that affects the m-th interferer. As in the far-field, the signal power decays with $1/R_m^{2\nu}$, where R_m is the distance of node m with respect to the victim receiver and ν is the amplitude path loss exponent. It is worth to notice that since $I_{m,1}$ and $I_{m,2}$ are two i.i.d Gaussian r.v.'s with mean equal to zero, I_m is circular symmetric (CS). We suppose that there is no coordination between the different transmitters and thus, they transmit asynchronously and independently. Under such conditions, it can be shown that X_{i} follows a symmetric stable distribution [2, 8, 10, 11, 74]

$$X_{\mathrm{i}} \sim \mathcal{S}_c(\alpha_I = 2/\nu, \beta = 0, \gamma = \pi \lambda C_{2/\nu}^{-1} \mathbb{E}\{|G_m I_{m,p}|^{2/\nu}\}) \tag{3.34}$$

with $C_x = \frac{1-x}{\Gamma(2-x)\cos(\pi x/2)}$. The characteristic exponent α_I depends on the path-loss exponent, while the dispersion γ is a function of the channel fading parameter, the interferer node density, and the interferer transmission power.

---

[7]Although the interferers are distributed over an infinite plane, only the nearest interferers have a substantial contribution to the aggregate interference.

3.4.2 Acquisition Performance in the Presence of Aggregate Interference

In the presence of aggregate interference, the decision variable can be expressed as

$$X_1 = |\underbrace{\sqrt{P}He^{-j\phi} + X_\mathrm{i}}_{M} + X_\mathrm{c} + X_\mathrm{n}|^2 \tag{3.35}$$

where M stands for the contribution to the decision variable of the SoI and the aggregate interference. The sum of the noise and cross-correlation noise is a Gaussian r.v. with variance $\sigma_\mathrm{nc}^2 = \sigma_\mathrm{n}^2 + \sigma_\mathrm{c}^2$. Conditioning on M, X_1 follows a non-central chi-square distribution with two degrees of freedom $X_1 \sim \chi_\mathrm{nc}^2(M^2, \sigma_\mathrm{nc}^2)$, where M^2 represents the non-centrality term. The CF of X_1 conditioned on M can be written as

$$\psi_{X_1|M}(j\omega) = \frac{1}{1 - 2j\omega\sigma_\mathrm{nc}^2} \exp\left(\frac{j\omega M^2}{1 - 2j\omega\sigma_\mathrm{nc}^2}\right). \tag{3.36}$$

By taking the expectation over M, the CF of X_1 can be expressed as

$$\psi_{X_1}(j\omega) = \frac{1}{1 - 2j\omega\sigma_\mathrm{nc}^2} \psi_{M^2}\left(\frac{j\omega}{1 - 2j\omega\sigma_\mathrm{nc}^2}\right). \tag{3.37}$$

Rayleigh fading for the signal of interest

We now consider the case of H distributed according to the Rayleigh distribution. Conditioning on X_i, M^2 follows a non-central chi-square distribution with two degrees of freedom $M_{|X_\mathrm{i}}^2 \sim \chi_\mathrm{nc}^2(X_\mathrm{i}^2, P\sigma_H^2)$. Therefore, the CF of M^2 conditioned on X_i can be written as

$$\psi_{M^2|X_\mathrm{i}}(j\omega) = \frac{1}{1 - 2j\omega P\sigma_H^2} \exp\left(\frac{j\omega X_\mathrm{i}^2}{1 - 2j\omega P\sigma_H^2}\right) \tag{3.38}$$

with $\sigma_H^2 = 1/2$. By inserting (3.38) in (3.37), the CF of X_1 conditioned on X_i can be expressed as follows

$$\psi_{X_1|X_\mathrm{i}}(j\omega) = \frac{1}{1 - 2j\omega(P/2 + \sigma_\mathrm{nc}^2)} \exp\left(\frac{j\omega X_\mathrm{i}^2}{1 - 2j\omega(P/2 + \sigma_\mathrm{nc}^2)}\right). \tag{3.39}$$

By taking the expectation over X_i, the CF of the decision variable can be expressed as

$$\psi_{X_1}(j\omega) = \frac{1}{1 - 2j\omega(P/2 + \sigma_\mathrm{nc}^2)} \psi_{X_\mathrm{i}^2}\left(\frac{j\omega}{1 - 2j\omega(P/2 + \sigma_\mathrm{nc}^2)}\right). \tag{3.40}$$

Consider a symmetric stable distribution $X \sim \mathcal{S}(\alpha_I, 0, \gamma)$, then X can be decomposed as $X = \sqrt{U}G$, where $U \sim \mathcal{S}(\alpha_I/2, 1, \cos(\pi\alpha_I/4))$ and

$G \sim \mathcal{N}_c(0, 2\gamma^{2/\alpha_I})$, with U and G independent r.v.'s [8]. By using the decomposition property of symmetric stable distributions, the aggregate interference term can be written as $X_i = \sqrt{U}G$. Therefore, the square of the aggregate interference can be expressed as:

$$X_i^2 = 2\gamma^\nu UC \qquad (3.41)$$

where C is a central chi-square random variable with two degrees of freedom. Conditioning on C and using the scaling property of a stable random variable[8], X_i^2 conditioned on C follows a stable distribution and therefore, the CF of X_i^2 conditioned on C is given by

$$\psi_{X_i^2|C}(j\omega) = \exp\left\{ -(2C)^{1/\nu}\gamma\cos\left(\frac{\pi}{2\nu}\right)|j\omega|^{1/\nu} \right.$$
$$\left. \times \left[1 - \text{sign}(j\omega)\tan\left(\frac{\pi}{2\nu}\right)\right] \right\}. \quad (3.42)$$

The r.v. $C^{1/\nu}$ can be approximated by a Gamma r.v. Z [11]. By taking the expectation over Z, we can express the CF of X_i^2 as

$$\psi_{X_i^2}(j\omega) = \left(1 + \theta_\nu 2^{1/\nu}\gamma\cos\left(\frac{\pi}{2\nu}\right)|j\omega|^{1/\nu} \right.$$
$$\left. \times \left[1 - \text{sign}(j\omega)\tan\left(\frac{\pi}{2\nu}\right)\right] \right)^{-k_\nu}. \quad (3.43)$$

Note that the first and second moment of $C^{1/\nu}$ can be expressed as $2^{1/\nu}\Gamma(\frac{N}{2} + \frac{1}{\nu})/\Gamma(\frac{N}{2})$ and $4^{1/\nu}\Gamma(\frac{N}{2} + \frac{2}{\nu})/\Gamma(\frac{N}{2})$. Similarly to what we have done in Section 3.3.2, the shape parameter k_ν and the scale parameter θ_ν of the Gamma r.v. Z can be found by applying the method of moments. By using (3.43) and (3.40), the closed form expression of the CF of X_1 can be written as

$$\psi_{X_1}(j\omega) = \frac{1}{1 - 2j\omega(P/2 + \sigma_{nc}^2)}\left\{ 1 + \theta_\nu 2^{1/\nu}\gamma\cos\left(\frac{\pi}{2\nu}\right) \right.$$

$$\times \left|\frac{j\omega}{1 - 2j\omega(P/2 + \sigma_{nc}^2)}\right|^{1/\nu}\left[1 - \text{sign}\left(\frac{j\omega}{1 - 2j\omega(P/2 + \sigma_{nc}^2)}\right)\tan\left(\frac{\pi}{2\nu}\right)\right] \right\}^{-k_\nu}.$$
$$(3.44)$$

Note that, when λ tends to zero (i.e. the dispersion γ tends to zero), (3.44) reduces to the scenario without interference where the SoI is subject to a Rayleigh fading channel. Inserting (3.44) in (3.17), $\mathbb{P}_d$ can be obtained. Note that for the scenario of aggregate interference the methodology to calculate $\mathbb{P}_d$ based on the CF requires a double integration, whereas the methodology based on the PDF requires a series of nested integrations in order to average over all random variables.

---

[8]If $X \sim \mathcal{S}(\alpha_I, \beta, \gamma)$, then $kX \sim \mathcal{S}(\alpha_I, \text{sign}(k)\beta, |k|^{\alpha_I}\gamma)$

Ricean fading for the signal of interest

For H that follows a Rician distribution, we cannot obtain a closed form expression of the CF. However, using the decomposition property for symmetric stable distributions, X_i can be expressed as $X_i = \sqrt{U}G$ with U and G defined as in Section 3.4.2. Therefore, conditioning on U, we find now that [10]

$$(X_i + X_n + X_n)_{|U} \sim \mathcal{N}_c(0, \sigma_{nc}^2 + U2\gamma^{2/\alpha_I}) \tag{3.45}$$

which is analogue to (3.9) where only one interferer is present. The framework reduces to the single interferer case and $\mathbb{P}_d$ conditioned on U can be found by (3.17). $\mathbb{P}_d$ can be derived by numerically averaging over a large set of realizations of U.

3.4.3 False Alarm Probability

A cell of the search space with no SoI can be expressed as $X[\tau] = |X_i[\tau] + X_c[\tau] + X_n[\tau]|^2$. The contribution of the aggregate interference to the search space can be represented by a vector $\bar{X}_i$ composed of aN elements. Since $\bar{X}_i$ is a multivariate symmetric stable r.v., the vector can be decomposed as

$$\bar{X}_i = \sqrt{U}\bar{G} \tag{3.46}$$

where $U \sim \mathcal{S}(\alpha_I/2, 1, \cos(\pi\alpha_I/4))$ and $\bar{G}$ is a aN-dimensional Gaussian random vector with $\bar{G} \sim \mathcal{N}_c(0, 2\gamma^{2/\alpha_I})$. Conditioning on U, for each cell of the search space where no SoI is present we have

$$X_i[\tau] \sim \mathcal{N}_c(0, U2\gamma^{2/\alpha_I}). \tag{3.47}$$

Therefore, the cell values of the search space have contributions from three Gaussian r.v.'s X_n, X_c, and $X_{i|U}$. Once again, the framework is equivalent to the scenario of a single interferer and the $\mathbb{P}_{fa}$ conditioned on U can be calculated using (3.18). The $\mathbb{P}_{fa}$ can be obtained by averaging over a large set of realizations of the stable distribution U.

Note on independence

The vector $\bar{X}_i$ is given by

$$\bar{X}_i = \sum_{m=1}^{\infty} \frac{G_m}{R_m^\nu} \bar{I}_m \tag{3.48}$$

where $\bar{I}_m$ is a vector of uncorrelated complex Gaussian r.v.'s. From (3.48), we can conclude that the components of $\bar{X}_i$ are identically distributed, yet mutually dependent. Bearing in mind that the elements of $\bar{X}_i$ are not independent, the search space cell that contains the SoI is not independent of

the rest of the search space. For the scenario of Rayleigh fading affecting the SoI, $\mathbb{P}_{fa}$ is calculated using a set of realizations of the aggregate interference, while $\mathbb{P}_d$ is calculated based on the closed form expression of the CF of the decision variable, thus neglecting the dependence of the search space cell containing the SoI and the rest of the search space. It can be shown through simulation that this approximation is accurate.

3.5   Numerical results

In this section, we evaluate the acquisition performance using the expressions developed in Section 3.3 and Section 3.4.

3.5.1   Single interferer

In order to test the validity of the analytical model for the GLRT detection strategy, we compare the ROC curves obtained using the analytical expressions given in (3.17) and (3.18) with the simulation result obtained with the Monte Carlo method. In the simulator environment, the signals are created in baseband where the acquisition is implemented according to Fig. 1. In each simulation we assume 8 random satellites to be in view, and we consider the same fading distributions as for the theoretical analysis. The DVB-T interference has been implemented as the third harmonic of a complex Gaussian signal. In the single interferer scenario 10^4 simulations are performed. The simulation parameters are summarized in Table 3.1.

Figure 3.2 shows the ROC curves of the GLRT for several values of the SIR.[9] Analytical results are indicated by lines, while markers represent the simulation results. The good agreement between the numerical and simulation results validates the proposed theoretical model for the GLRT. Figure 3.3 shows the ROC curves of the MRT detection strategy for several SIR values where the simulation results are indicated by markers. The figure shows a minor offset between the theoretical model and the simulation results, in particular for low values of the SIR. This effect is due to the approximation of the generalized exponential distribution using the Gamma distribution.

In Fig. 3.4, the performance of the GLRT and the MRT decision strategies are compared for the single interferer case in the absence of fading. Figure 3.4 reflects the optimality of GLRT in the absence of fading and under perfect synchronization.[10]   As illustrated in the figure, the proposed framework

---

[9]Note that we define both the SNR and the SIR for the decision variable, i.e. after the correlation with the local replica of the code.

[10]In such conditions the GLRT reduces to the Likelihood Ratio Test (LRT), which is optimal due to the Neyman-Pearson theorem [28].

Simulation Parameters	
Sampling frequency	1.023MHz
Intermediate frequency	0
Number of samples per chip	1
Code length	1023
Modulation	BPSK
SNR (post-correlation)	15 dB
SIR (post-correlation, single interferer)	15-30 dB
Number of simulations	10^4
INR (post-correlation)	0-15 dB
λ	$0.001 - 0.02 \text{m/s}^2$
realizations aggregate interference	10^6

Table 3.1:
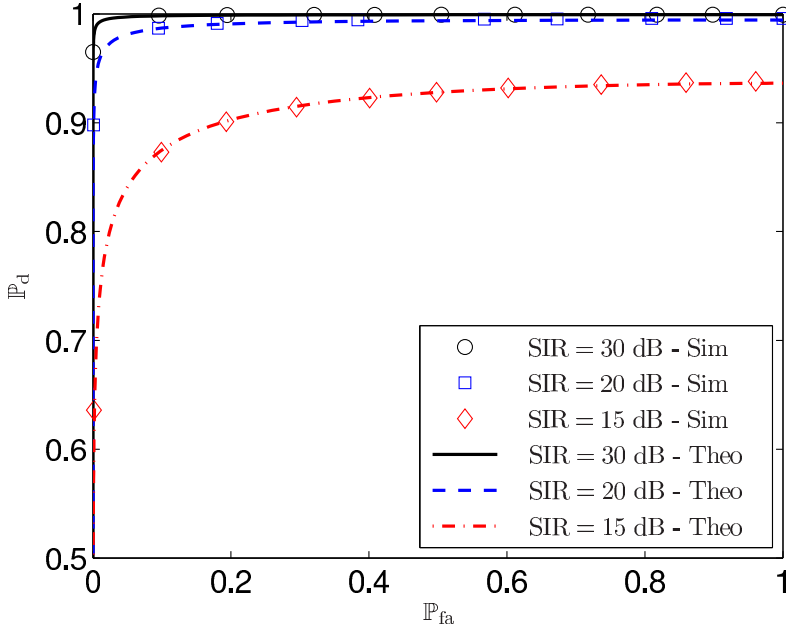
Figure 3.2: ROC curves for the GLRT acquisition strategy by simulation (markers) and theoretical analysis (lines) for SNR = 15 dB.

allows us to quantify how much the GLRT method outperforms the MRT strategy. Note that this justifies why in Section 3.4 only the GLRT method has been analysed.

Although this framework provides an analytical tool that allows us to include simultaneously the effect of fading on both SoI and interference, we only consider fading affecting either the SoI or the interference. We first
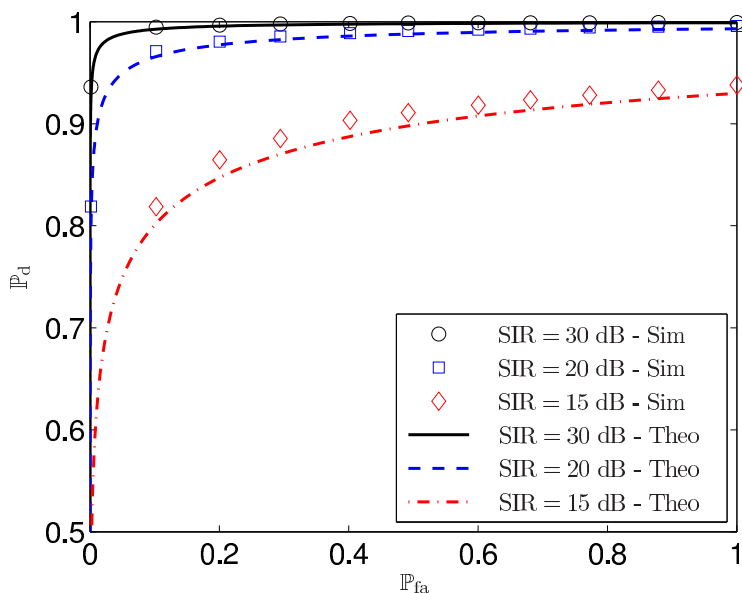
Figure 3.3: ROC curves for the GLRT acquisition strategy by simulation (markers) and theoretical analysis (lines) for SNR = 15 dB.
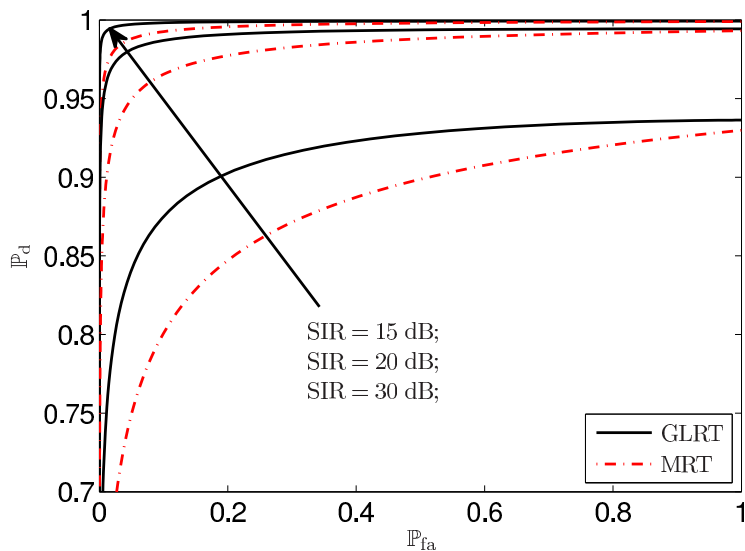
Figure 3.4: Analytical ROC curves for GLRT and MRT (SNR = 15 dB).

analyze the effect of Rician fading which is typical in urban environment. Rician fading is characterized by the parameter *K*, representing the ratio between the energy of the line-of-sight (LOS) component and the energy of the other multipath components. Figure 3.5 illustrates the effect on
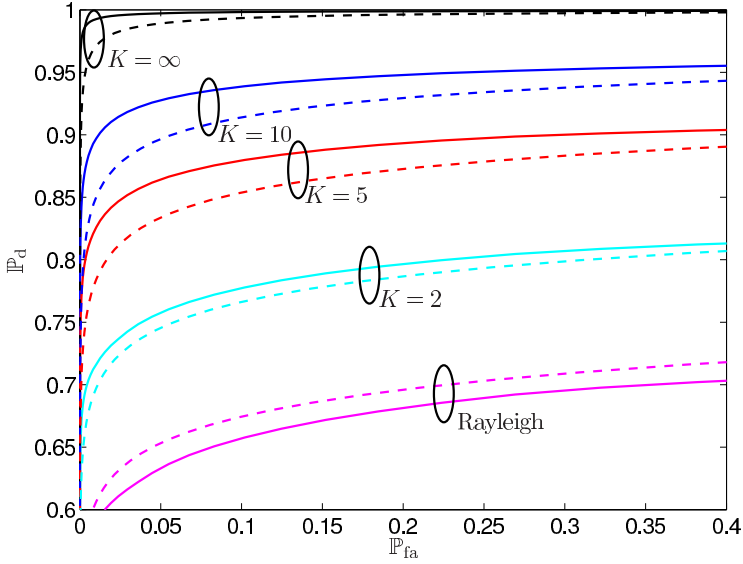
Figure 3.5: The impact of *K* on the ROC curves is represented, where fading is considered relative to the SoI for GLRT (solid lines) and MRT (dashed lines). SNR = 15 dB and SIR = 30 dB.

the acquisition performance of fading relative to the GNSS signal. From this figure we can notice that the acquisition performance decreases with decreasing values of *K*. Interestingly, the gap between the performance of GLRT and MRT diminishes with decreasing *K* until the point where MRT outperforms GLRT for *K* = 0. This is due to the fact that when fading affects the SoI, GLRT is not optimal anymore. From the numerical result presented in Fig. 3.5, we can conclude that MRT is more robust than GLRT in severe fading conditions. Figure 3.6 compares the acquisition performance of the GLRT and MRT acquisition strategies with different fading distributions relative to the interference. In order to better understand the effect of the interference, we select SIR = 15 dB which corresponds to a powerful interferer. While for high values of *K* GLRT outperforms MRT, we notice that MRT is clearly more robust than GLRT when the interference is subject to fading. Considering that for the MRT acquisition strategy both X_1 and X_2 contain contributions from the interference, it can be understood that the effect of the fading affecting the interference is partially cancelled by taking the ratio of X_1 and X_2.

3.5.2 Aggregate interference

In Section 3.4, we presented analytical and semi-analytical methods to determine the ROC curves corresponding to the GLRT acquisition strategy in the presence of aggregate interference. The obtained results include the
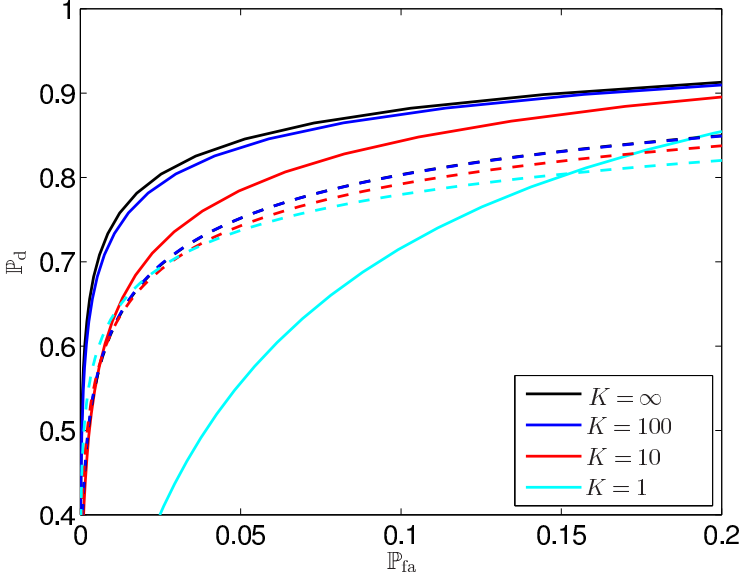
Figure 3.6: The impact on the ROC curves of Ricean fading relative to the interfering signal is represented as a function of the Rice factor *K* for the GLRT acquisition strategy (solid lines) and the MRT acquisition strategy (dashed lines). SNR = 15 dB and SIR = 15 dB.

effect of the spatial distribution of the interfering nodes and the transmission characteristics of both SoI and interference. In order to reduce the number of scenarios, we only consider Rayleigh fading for the interfering nodes which is realistic in challenging channel conditions, while for the SoI different fading distributions are considered. For simulation of the aggregate interference, 10^6 realizations of the stable r.v. have been generated.

Figure 3.7 illustrates the effect of the transmission power of the cognitive devices on the ROC curves for a constant value of *K*. For interference-to-noise ratio INR = 15 dB, the reduction of the acquisition performance is considerable. Figure 3.8 demonstrates the effect of different types of fading relative to the SoI. As expected, for higher values of *K* (stronger LOS), the ROC curve approaches the acquisition performance when there is no fading on the SoI. In Figure 3.9, we show the effect of the interferer density on the acquisition performance. We can notice that the performance deteriorates quickly with increasing interferer density.
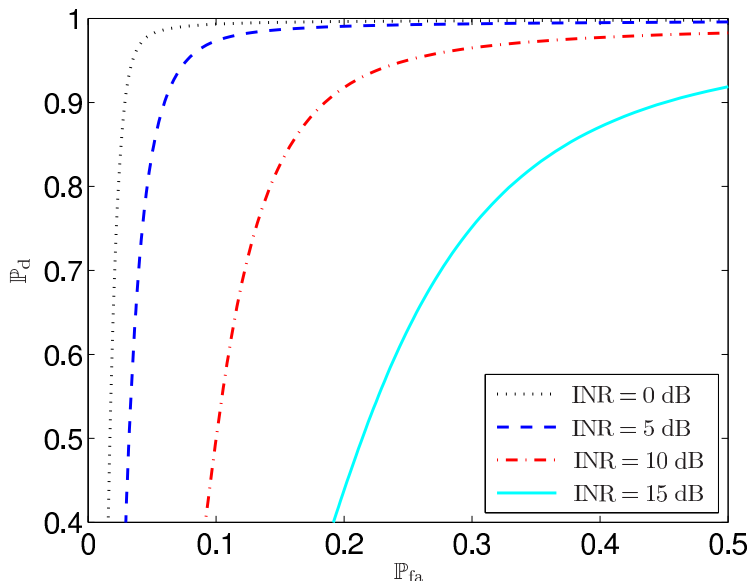
Figure 3.7: ROC curves for the GLRT method (SNR = 15 dB, $K = \infty$, and $\lambda = 0.01/m^2$) for varying values of INR.
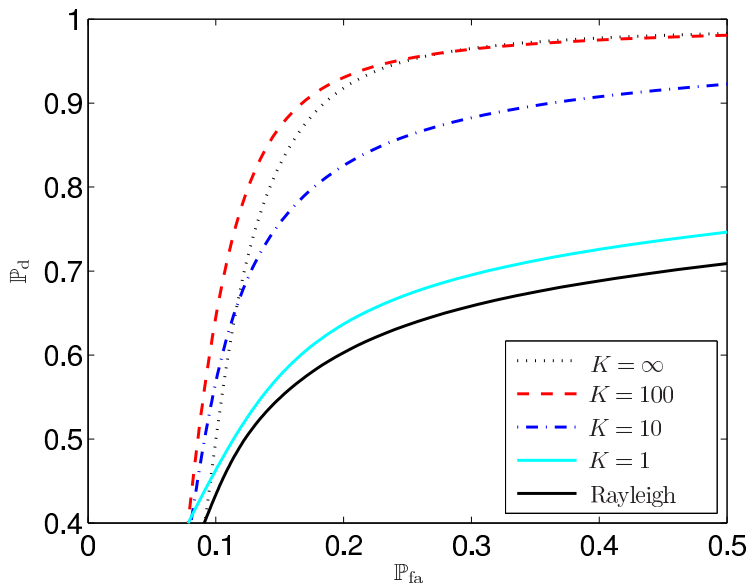
Figure 3.8: ROC curves for the GLRT method in the presence of a network of spatially distributed cognitive devices (SNR = 15 dB, INR = 5dB, $\lambda = 0.01/m^2$, and $\nu = 1.5$). The impact of the fading distribution (Ricean and Rayleigh) with regard to the SoI is considered.
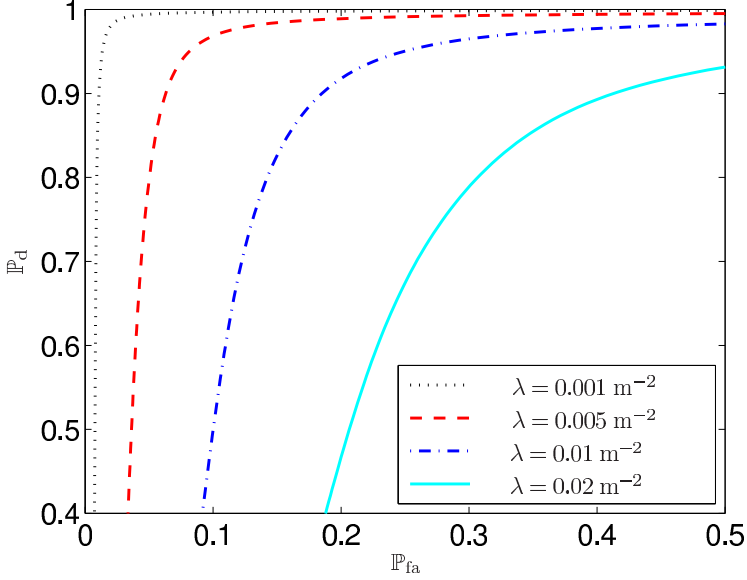
Figure 3.9: ROC curves for the GLRT method (SNR = 15 dB, $K = 10$, and INR = 10 dB), in a Ricean fading channel for varying λ.

3.6 Conclusions

In this chapter, we analyzed the acquisition performance of GNSS signals in realistic urban scenarios, challenged by the presence of interference. We derived analytical expressions of the detection and false alarm probability, that account for different acquisition strategies, single and multiple interferers, and different channel conditions. For the single interferer case, we analyzed both the GLRT and the MRT strategy and showed the effects of the channel fading on both the SoI and the interference. Further, we characterized the interference originating from spatially scattered interfering devices. For the multiple interference case, we analyzed the acquisition performance of the GLRT acquisition strategy. The expressions for the probability of detection and false alarm account for network parameters such as the interferer node density, the transmission power of the nodes and the fading distribution for the interference and the signal of interest. The analytical framework proposed in this chapter allows us to understand the effect of several environment related parameters on the acquisition performance of the GNSS signal. Therefore, the framework can be used both to determine threshold values for the discussed network parameters corresponding to a minimum acquisition performance, and to plan the deployment of alternative localization systems to guarantee ubiquitous and accurate positioning performance.

Chapter 4

Cognitive small cell networks: Energy efficiency and trade-offs

[1]Heterogeneous networks using a mix of macrocells and small cells are foreseen as one of the solutions to meet the ever increasing mobile traffic demand. Nevertheless, a massive deployment of small cell access points (SAPs) leads also to a considerable increase in energy consumption. Spurred by growing environmental awareness and the high price of energy, it is crucial to design energy efficient wireless systems for both macrocells and small cells. In this work, we evaluate a distributed sleep-mode strategy for cognitive SAPs and we analyze the trade-off between traffic offloading from the macrocell and the energy consumption of the small cells. Using tools from stochastic geometry, we define the user discovery performance of the SAP and derive the uplink capacity of the small cells located in the Voronoi cell of a macrocell base station, accounting for the uncertainties associated with random position, density, user activity, propagation channel, network interference generated by uncoordinated activity, and the sensing scheme. In addition, we define a fundamental limit on the interference density that allows robust detection and we elucidate the relation between energy efficiency and sensing time using large deviations theory. Through the formulation of several optimization problems, we propose a framework that yields design guidelines for energy efficient small cell networks.

---

[1]This chapter has been published in IEEE Transactions on Communications [75]. The material in this chapter has been presented in part at the IEEE Wireless Communications and Networking Conference (WCNC), Shanghai, China, April 2013 [76], and at the IEEE International Conference on Communications (ICC), Budapest, Hungary, June 2013 [77].

4.1 Background

Over the last years mobile data traffic has risen exponentially and along with this accruing mobile data demand, energy consumption has increased considerably [78–80]. Driven by growing environmental awareness and increasing electrical cost relative to the operation of mobile base stations (MBSs), green wireless communications has become an active field of research that tries to unite the opposing needs of growing mobile data activity and energy efficiency [81–83].

Conventional cellular networks based on the careful deployment of MBSs suffer from poor signal quality for indoor and cell edge users. Furthermore, the explosive surge in mobile data traffic accelerates the need for novel cellular architectures to meet such demands [80]. The LTE-Advanced or beyond standards propose heterogeneous networks (HetNet's) that consist of a macrocell network overlayed by small cells. The macro-tier guarantees the coverage, while the overlay network is a means to offload the data traffic from the macrocell network and to satisfy the local capacity demand. The small cells in this two-tier architecture can be micro-cells, pico-cells or femto-cells, where the distinction between the different types of small cells can be found in the size of the cells and the capability of auto-configuration and auto-optimization. Small cells can extend the network coverage and the reduced cell size leads to higher spatial frequency reuse and increased network capacity.

Although the introduction of heterogeneous networks can resolve the capacity demand issue [84, 85], the overall energy consumption is significantly increased by the installation of these additional base stations. Motivated by the high traffic demand fluctuations over space, time, and frequency, sleep mode techniques are a promising strategy to overcome this problem. For wireless sensor networks, the energy conservation by sleeping techniques for wireless devices running on battery power has been studied in [86]. The IEEE 802.16e and LTE standards support sleep mode strategies for mobile terminals and the trade-off between energy efficiency and response delay has been analyzed in [87]. Only some recent work is dedicated to sleep mode techniques for small cell access points (SAPs). In [88], the authors conclude that sleep mode operation is effective when the cell size is small and for light traffic conditions. Different sleep mode strategies for SAPs are introduced in [89], such that the wake-up mechanism can be driven by the SAP, the core network or the user equipment (UE). For WiFi access points, the UE driven approach has been studied in [90], but the reverse beaconing adds complexity to the hardware and assumes knowledge about the signal structure. In [91], the overall HetNet energy consumption is minimized based on sleep mode techniques for network-operated femtocells. This centralized sleep and wake-up mechanism assumes traffic load and user localization

awareness, and increases the signaling overhead. Therefore, it is attractive to investigate distributed sleep mode strategies, which do not involve an augmented UE complexity and require neither signaling nor user localization awareness.

To allow a distributed decision approach, the SAP needs cognitive capabilities to sense when a small cell user is active within the SAP coverage [89]. In future heterogeneous networks, cognitive capabilities will become essential not only for the energy efficient operation of the small cell tier, but also to overcome coexistence issues in multi-tier networks. Specifically, spectrum or carrier sensing by the cognitive SAPs enable interference avoidance and efficient spectrum allocation [92]. Hence, cognitive small cells allow the deployment of energy efficient and spectral efficient heterogeneous networks. Many ideas can be borrowed from the field of cognitive radio (CR). For cognitive radio networks (CRN), the trade-off between protection of the primary users (PU) and the throughput of the secondary users (SU) has been addressed in [93–95]. For SAP sleep mode techniques, this corresponds to the trade-off between traffic offload by means of a high detection probability and energy consumption, proportional to the false alarm rate. Although spectrum sensing and cognitive radio are intensely studied, there are still many issues that need to be addressed [96–99]. For instance, the cognitive capabilities are usually assessed for a deterministic (worst case) user location, while a random position of the user is of interest to determine energy consumption. The capacity and energy efficiency of base stations in heterogeneous networks has been studied in [100], but the impact of aggregate interference in dense network deployments has typically been neglected. Recent results show that it is fundamental to consider aggregate interference to accurately define the network performance [101–103].

In this chapter, we investigate how SAPs can be used to offload the traffic from the macrocell network and how they can exploit their sensing capabilities to enhance the energy efficiency. Specifically, these energy efficient SAPs can save power by entering into sleep mode when they are not serving any active small cell users. Considering open access control, the SAPs need to sense the transmissions from a macrocell user to an MBS, and switch on the pilot transmissions when user activity is detected within the SAP coverage. Due to the simplicity of passive sensing, we assume that all SAPs perform energy detection at the expense of being sensitive to noise and interference uncertainties. Furthermore, the transmissions from the macrocell user can be bursty, making the duty cycle of the sleeping mode at each SAP difficult to design to ensure a low probability of miss detection. Since the analysis of a deterministic (e.g. worst case) user location does not provide guidance for the definition of the SAP energy consumption, it is crucial to evaluate the typical user case, that is, to consider

a user with random location within the SAP coverage. Specifically, the main contributions of this chapter are listed as follows:

- We formulate an average network energy consumption model for the cognitive SAPs that are located within the Voronoi cell of an MBS accounting for the base station and user densities, detection performance, the sensing strategy, bursty macrocell user activity, and uncoordinated network interference uncertainties.

- We present a unified analytical framework that models the performance of passive sensing for a typical user within the SAP coverage, including the effects of propagation channel and aggregate network interference.

- We derive tractable expressions of the aggregate throughput and capacity that can be offloaded by the small cells within an the MBS Voronoi cell. This allows us to formulate the trade-off between energy consumption and throughput/capacity as a set of optimization problems.

- We define the interference wall, beyond which the target probability of detection and false alarm can not be obtained no matter how long the sensing time. This is a fundamental limit of the detection robustness, which confines the region of interferer densities enabling an energy efficient SAP design.

- Using techniques from large deviations theory, we determine how fast the false alarm rate converges to a stationary value as a function of the interferer density. The obtained rate function gives insight into how the detection performance affects the small cell energy consumption and traffic offload.

The remainder of the chapter is structured as follows. In Section 4.2, the system model is introduced. In Section 4.3, the energy consumption model and the sensing performance of the SAP are discussed. The traffic that can be offloaded from the macrocell is characterized in Section 4.4. In Section 4.5, the trade-off between traffic offload and energy consumption is discussed by means of several optimization problems. The limits of detection robustness and the implications on the energy efficiency are discussed in Section 4.6. Numerical results are shown in Section 4.7 and conclusions are drawn in Section 4.8.

4.2 System Model

4.2.1 Network topology

We consider a cellular network model that consists of a first tier of MBSs distributed according to a homogeneous Poisson point process (PPP) Θ with density λ_m, overlayed with a network of SAPs distributed according to a PPP Φ with density λ_s, where usually $\lambda_s > \lambda_m$. Modeling the locations of SAPs and the more regular MBSs by means of homogeneous PPPs is extensively discussed in literature and has been validated by numerical analysis and compared with actual base station deployments [15]. Moreover, recently theoretical evidence has been given for the accuracy of the PPP model [104]. The set of macrocells is known as the Poisson-Voronoi tessellation of $\mathbb{R}^2$ with respect to Θ. The Voronoi cell C_j corresponding to an MBS $x_{j,m}$ consists of those points in $\mathbb{R}^2$ which are closer to $x_{j,m}$ than to any other MBS and is defined as $C_j = \{y \in \mathbb{R}^2 \mid \|y - x_{j,m}\| \leq \|y - x_{i,m}\|, x_{i,m} \in \Theta \backslash \{x_{j,m}\}\}$. The SAPs that belong to C_j form the aggregate $A_j = \cup \{x_{i,s} \mid x_{i,s} \in \Phi \cap C_j\}$, and applying Campbell's theorem the mean number of SAPs within an MBS Voronoi cell is given by λ_s / λ_m [105]. The mobile users are scattered over $\mathbb{R}^2$ according to a PPP Ψ with density λ_u.[2] We consider universal spectrum allocation where both tiers can access the full spectrum and orthogonal frequency-division multiple access (OFDMA) or time-division multiple access (TDMA) as multiple access technique.[3] The SAPs operate in open access (OA) mode and are accessible for all users registered with the operator of the SAP. In order to enable a distributed sleep/wake-up scheme, the SAPs are foreseen of cognitive capabilities. When an SAP does not serve an active user call, it goes into sleep mode and senses periodically the macrocell uplink channel to detect user activity. The SAP applies passive sensing by means of an energy detector (ED) for reasons of low complexity and low power consumption [106]. The ED detection performance compared with other detection schemes has been studied exhaustively in literature [107, 108]. We limit our analysis to the ED since this scheme provides a lower detection bound. Once the SAP detects an active user in the macrocell uplink band within its coverage, the SAP switches on and starts the transmission of pilot signals. Subsequently, the UE reports the presence of the SAP to the MBS and the UE is handed over to the SAP. We assume that the uplink transmission power of the UE during the sensing period is constant and that after handover to the SAP, the UE adopts a lower and constant transmission power. It is well known that the ED has no capabilities to

---

[2]Note that Θ, Φ, and Ψ are independent point processes.

[3]The analysis can be extended to orthogonal spectrum allocation and affects the interferer densities, which is important for the performance detection and the offload analysis discussed in Section 4.3.2 and 4.4, respectively.
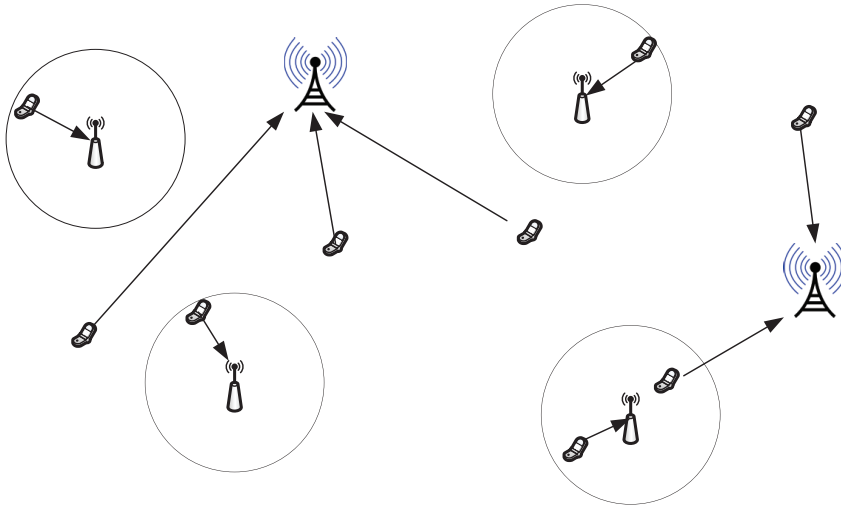
Figure 4.1: Spatial distribution of the MBSs, SAPs, and the UEs.

differentiate between the signal of interest (SoI) and interference or noise [106]. The measurements of the SAP under realistic conditions are corrupted by network interference, which can originate from macrocell users outside the SAP coverage, macrocell users within the SAP coverage that are not registered with the SAP operator, small cell users, cognitive devices using the same uplink band, and spurious emissions. As a result, we consider the case of the interfering nodes spatially distributed over the entire plane according to a homogeneous PPP Ω with density λ.[4] For a homogeneous PPP, the probability that k nodes reside within a region $\mathcal{R}$ depends on the density λ and the area $A_\mathcal{R}$ of the region $\mathcal{R}$, and can be expressed as [23]

$$\Pr[k \in \mathcal{R}] = \frac{(\lambda A_\mathcal{R})^k}{k!} e^{-\lambda A_\mathcal{R}}, \quad k = 0, 1, 2, ... \tag{4.1}$$

The spatial model consisting of a macrocell network overlayed with multiple small cells is illustrated in Fig. 4.1.

---

[4]Note that the model allows to include the presence of groups of interferers with different transmission power. The superposition of PPP's with densities $\lambda_1, \lambda_2, ...$ results in a PPP with density equal to a weighted sum of the densities, where the weighting factor depends on the transmission power P_i of the different PPPs and is given by $\lambda = \sum_i \lambda_i (P_i/P_u)^{2/\alpha}$, with P_u the transmit power of the UE, and α the path loss exponent.

4.2.2 Activity model

We define the activity of the UEs and SAPs using a time-slotted model as depicted in Fig. 4.2. Assuming a fixed slot duration T, the SAP senses the channel over a sensing time τ_s and is in active mode over $T - \tau_s$ when an active mobile user is detected[5]. Both the UE and the interfering nodes are assumed to have a bursty traffic mainly due to the mobility of the nodes, the switching between on and off states, and the switching between carriers in a multi-carrier system. Thus, the activity of an SAP, a UE and the interfering nodes in a given slot can be modeled as mutually independent Bernouilli processes with success probabilities p_s, p_u, and p_I, respectively. Moreover, the activity of the SAP, the UE, and the interfering nodes is assured to be independent across different slots. By the colouring theorem of PPPs, the active nodes that contribute to the interference form a PPP with density $p_I \lambda$ [23]. We will further refer to p_s as the sensing probability.
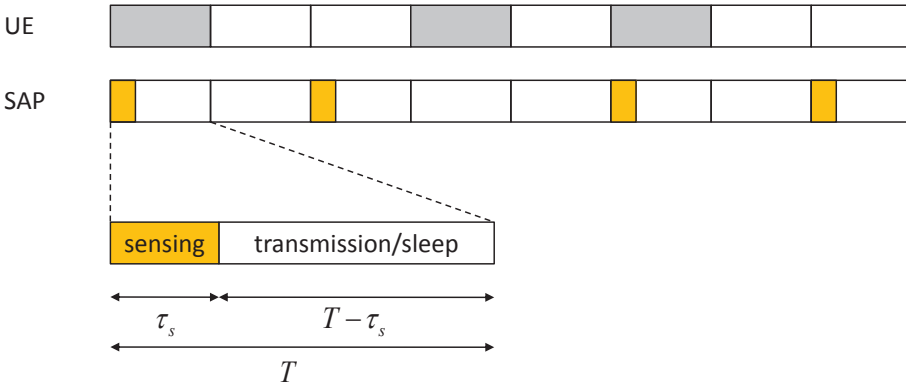
Figure 4.2: Time slotted model, representing the activity of UE and the SAP over time.

4.3 Cognitive SAP

In the following, we provide the average network energy consumption model for the SAPs and we characterize the relationship between the energy consumption and the detection performance of the cognitive SAP. The presented analysis is generic and accommodates for random locations of both the UE and the interfering nodes.

---

[5]Active mode consists of transmitting pilot signals, receiving signals, and signal processing. Note that we neglect the time related to the handover process for simplicity.

4.3.1 Energy consumption model

Three main contributions to the power consumption of cognitive SAPs can be identified: the power related to the circuit synchronization Ξ_c, the sensing power Ξ_s, and the processing power Ξ_t during active mode [109]. We consider the circuit synchronization is active over the entire time slot. The SAP senses the uplink channel according to a sensing scheme and the corresponding energy consumption is proportional to the sensing time. The UE signal detection is a binary hypothesis test problem. In the presence of a UE signal (hypothesis $\mathcal{H}_1$), the SAP starts the pilot transmissions when it senses the uplink channel and correctly detects the user activity. In the absence of the UE signal (hypothesis $\mathcal{H}_0$), the SAP starts the pilot transmissions when it incorrectly detects the presence of a user. The probability that there resides at least one active UE within the coverage of a typical SAP is given by $p_{UE} = 1 - \exp(-p_u \lambda_u \pi R^2)$. Therefore, the expected SAP energy consumption per cell can be modeled as

$$E_{\text{tot}} = \frac{\lambda_s}{\lambda_m} [\Xi_c T + p_{UE} \{p_s [\Xi_s \tau_s + \mathbb{P}_d \Xi_t (T - \tau_s)]\}$$
$$+ (1 - p_{UE}) \{p_s [\Xi_s \tau_s + \mathbb{P}_{fa} \Xi_t (T - \tau_s)]\}] \quad (4.2)$$

where $\mathbb{P}_d$ and $\mathbb{P}_{fa}$ are the probability of user activity detection and false alarm, respectively.

4.3.2 Non-coherent detection performance

Since the presence of multiple simultaneous UE transmissions in the macrocell uplink band eases the detection process, we consider the more challenging scenario with a single UE within the coverage of an SAP to define the detection performance. At the cognitive SAP, the received signal can be written as

$$\begin{aligned}
\mathcal{H}_0: \quad r(t) &= n(t) + i(t) \\
\mathcal{H}_1: \quad r(t) &= \frac{h(t)}{r_f^{\alpha/2}} s(t) + n(t) + i(t)
\end{aligned} \quad (4.3)$$

where $s(t)$, $n(t)$, and $i(t)$ represent the SoI, the additive white Gaussian noise and the aggregate network interference, respectively. The impulse response of the flat fading channel between the UE and SAP is represented by $h(t)$, r_f is the distance between the UE and the SAP, and α is the power path loss exponent. To facilitate the analysis, we consider that the typical SAP is at the origin of the Euclidean plane and the coverage of the SAP is a circular area around the origin with radius R. The energy of the SoI at the SAP can be written as $P_u r_f^{-\alpha} h^2$, where P_u is the transmit power of the UE. We

assume there is no power control in the macrocell network, and therefore, P_u is independent of the distance between the UE and the MBS.[6] The noise term has a zero-mean Gaussian distribution $n(t) \sim \mathcal{N}(0, \sigma_n^2)$. The interfering nodes consist of macrocell users, small cell users belonging to other SAPs, or (cognitive) devices which are active on the same band. Therefore, the aggregate network interference measured at the SAP can be written as

$$i(t) = \mathfrak{Re}\left\{\sum_{l=1}^{\infty} i_l(t)\right\} = \mathfrak{Re}\left\{\sum_{l=1}^{\infty} \frac{h_l \mathbf{X}_l^i}{r_{f,l}^{\alpha/2}}\right\} \qquad (4.4)$$

where we model the lth interferer amplitude $\mathbf{X}_l^i = X_{l,1}^i + jX_{l,2}^i$ as a zero-mean complex random variable (r.v.). Note that the r.v.'s $\mathbf{X}_l^i$ are circular symmetric, and independent and identically distributed (i.i.d.) in l since the interferers transmit independently. Therefore, with the interfering nodes scattered over $\mathbb{R}^2$ according to a PPP, the aggregate network interference follows a symmetric stable distribution [2, 10]

$$i \sim \mathcal{S}(\alpha_I = 4/\alpha, \beta = 0, \gamma = \pi\lambda C_{4/\alpha}^{-1} \mathbb{E}[|h_l X_{l,p}^i|^{4/\alpha}]) \qquad (4.5)$$

with C_x defined as

$$C_x \triangleq \begin{cases} \frac{(1-x)}{\Gamma(2-x)\cos(\pi x/2)}, & x \neq 1, \\ \frac{2}{\pi}, & x = 1. \end{cases} \qquad (4.6)$$

The decision variable V determines the presence or absence of the SoI. For the ED, V is defined as

$$V = \frac{1}{\tau_s} \int_0^{\tau_s} \left(\frac{h(t)}{r_f^{\alpha/2}} s(t) + n(t) + i(t)\right)^2 \mathrm{d}t. \qquad (4.7)$$

After sampling and considering block fading, the decision variable can be expressed as

$$V_{ED} = \frac{1}{N} \sum_{k=1}^{N} r^2[k] = \frac{1}{N} \sum_{k=1}^{N} \left(\frac{h}{r_f^{\alpha/2}} s[k] + i[k] + n[k]\right)^2 \qquad (4.8)$$

where $N = \lfloor \tau_s f_s \rfloor$ with f_s the sampling frequency equal to the Nyquist rate[7]. The probability of detection is defined as the probability that V_{ED} surpasses the threshold ζ in the presence of the SoI and is given by $\mathbb{P}_d = \Pr[V_{ED} > \zeta|\mathcal{H}_1]$. The probability of false alarm is defined as the probability that V_{ED}

---

[6]Since the users that benefit most from the deployment of small cells are located far away from the MBS, our model holds for the cell edge users who transmit at maximum power.

[7]For simplicity, we assume $N = \tau_s f_s$

surpasses the threshold in absence of the SoI and is given by $\mathbb{P}_{\text{fa}} = \Pr[V_{\text{ED}} > \zeta | \mathcal{H}_0]$. To calculate $\mathbb{P}_{\text{d}}$ and $\mathbb{P}_{\text{fa}}$, we propose a generic approach based on the characteristic function (CF) of the decision variable. Using the inversion theorem, the probability that the decision variable surpasses the threshold can be found as

$$\Pr[V_{\text{ED}} > \zeta] = \frac{1}{2} - \frac{1}{2\pi} \int_0^\infty \mathfrak{Re} \left\{ \frac{\psi_{V_{\text{ED}}}(-j\omega)e^{j\omega\zeta} - \psi_{V_{\text{ED}}}(j\omega)e^{-j\omega\zeta}}{j\omega} \right\} d\omega \quad (4.9)$$

where $\psi_{V_{\text{ED}}}$ represents the CF of V_{ED}. Under $\mathcal{H}_1$, $\psi_{V_{\text{ED}}}$ is provided in the following theorem for a typical user, i.e. a user with random location within the small cell coverage.

Theorem 1. *In the presence of Rayleigh block fading, the CF of the ED decision variable for a typical user in the presence of interference uncertainties is given by*

$$\psi_{V_{\text{ED}}|\mathcal{H}_1}(j\omega) = \frac{1}{\left(1 - 2j\omega\sigma_W^2\right)^{N/2}} \left[1 - {}_2F_1\left(1, \frac{2}{\alpha}; 1 + \frac{2}{\alpha}; \frac{R^\alpha(1 - 2j\omega\sigma_W^2)}{j\omega P_{\text{u}}}\right) \right]$$

$$\times \exp\left\{ -2^{2/\alpha}\gamma \cos(\pi/\alpha) \left| \frac{j\omega}{1 - 2j\omega\sigma_W^2} \right|^{2/\alpha} \left[1 - \text{sign}\left(\frac{j\omega}{1 - 2j\omega\sigma_W^2}\right) \tan(\pi/\alpha) \right] \right\}$$

$$(4.10)$$

where ${}_2F_1(.)$ is the Gaussian hypergeometric function.

Proof. See Appendix A.1. □

For the calculation of $\mathbb{P}_{\text{fa}}$ in the presence of aggregate interference, we apply the same methodology as in Appendix A.1, yet in absence of the SoI. The CF of the decision variable under $\mathcal{H}_0$ can be expressed as

$$\psi_{V_{\text{ED}}|\mathcal{H}_0}(j\omega) = \frac{1}{\left(1 - 2j\omega\sigma_W^2\right)^{N/2}}$$

$$\times \exp\left\{ -2^{2/\alpha}\gamma \cos(\pi/\alpha) \left| \frac{j\omega}{1 - 2j\omega\sigma_W^2} \right|^{2/\alpha} \left[1 - \text{sign}\left(\frac{j\omega}{1 - 2j\omega\sigma_W^2}\right) \tan(\pi/\alpha) \right] \right\}$$

$$(4.11)$$

and $\mathbb{P}_{\text{fa}}$ can be obtained applying the inversion theorem.

4.4 Traffic offload

In order to evaluate the trade-off between the energy consumption and the achievable traffic offload, we define the small cell aggregate offload

capacity and aggregate offload throughput which reflect the traffic that can be accommodated by the SAPs in a macrocell and also account for the sensing probability, the sensing time, and the sensing performance. We consider a saturated resource model, intending that each user always has a non-empty queue of data to be transmitted. The small cell capacity assumes adaptive modulation while the small cell throughput assumes a fixed transmission rate. Note that an exact analysis of the aggregate offload capacity and throughput requires an exact distribution of the area of the small cells which constitute a multiplicatively weighted Voronoi tessellation. The area distribution of a Voronoi tessellation is an open research problem for which an approximation has been proposed in [110]. Yet, in order to present a tractable analysis, we consider a distance based association policy with respect to the small cells. This relaxation of the original problem yields a unified framework that allows us to obtain both the detection performance and aggregate offload capacity and throughput.

4.4.1 Aggregate Offload Capacity

The aggregate capacity that can be offloaded per macrocell is given by the typical user uplink capacity in an SAP multiplied with the number of loaded and active SAPs within the macrocell coverage. Assuming OFDMA or TDMA, the typical user uplink capacity in an SAP equals the sum-capacity of N users sharing the same resource block. The expected number of SAPs per macrocell is given by λ_s/λ_m [105]. We assume a distance based access policy with respect to the SAPs, where access can be granted when the mobile user is within the coverage R of the SAP. For this access policy, the probability that an SAP has at least one active user within the SAP coverage can be found by the complement of the null probability of a Poisson r.v. in (4.1) and is given by $p_l = 1 - \exp(-p_u \lambda_u \pi R^2)$. Let $N_s^{(l)} = p_l \lambda_s/\lambda_m$ be the expected number of SAPs in a macrocell with active users, then we define the capacity that can be offloaded from an MBS that accounts for the sensing procedure as follows:

$$\xi_c(\tau_s) = N_s^{(l)} p_s \mathbb{P}_d \frac{T - \tau_s}{T} \bar{C}(\lambda, R, \alpha) \tag{4.12}$$

where $\bar{C} = \mathbb{E}[\ln(1 + \eta)]$ is the average channel capacity in uplink for a typical UE[8] and η is the signal-to-interference-and-noise ratio (SINR). The aggregate offload capacity is a function of the densities of MBSs, SAPs, and mobile users, where λ_u affects the offload capacity by changing the number of loaded small cells.[9] When the SoI and all the interfering signals are affected

---

[8]Note that we consider $X_{i,l}$ complex Gaussian and the interferers quasi-static.

[9]Note that we assume here that the coverage areas of different SAPs do not overlap, which is realistic considering a reduction of the coverage range with increasing small cell density.

by Rayleigh fading, we can derive the average channel capacity in the next theorem as a special case of [111].

Theorem 2. *A typical user is uniformly distributed over the coverage of the SAP, i.e. a circular area with radius R, while the interfering nodes are spatially scattered over the two-dimensional plane $\mathbb{R}^2$ according to a homogeneous PPP. The average channel capacity in the uplink of a typical user within the coverage of the associated SAP for a Rayleigh fading channel is given by*

$$
\bar{C}(\lambda, R, \alpha) = \frac{1}{R^2} \int_0^R \int_0^\infty \exp\left(-\frac{\sigma_n^2}{P_u}(e^x - 1)r_f^\alpha\right)
$$
$$
\times \exp\left(-\frac{2\pi^2}{\alpha}\csc\left(\frac{2\pi}{\alpha}\right)\lambda\left(\frac{P_i}{P_u}(e^x - 1)\right)^{2/\alpha}r_f^2\right)dx\,2r_f dr_f \quad (4.13)
$$

where P_u and P_i are the transmission power of the UE and of each interferer.

Proof. See Appendix A.2. □

Using Theorem 2, we formulate the following corollary for a special case.

Corollary 1. *For $\alpha = 4$, the average channel capacity of a typical user can be expressed as*

$$
\bar{C}(\lambda, R, 4) = \int_0^\infty \frac{1}{2R^2}\sqrt{\frac{\pi}{b(x)}}\exp\left(\frac{a^2(x)}{4b(x)}\right)
$$
$$
\times \left[\text{erfc}\left(\frac{a(x)}{2\sqrt{b(x)}}\right) - \text{erfc}\left(\frac{a(x) + 2b(x)R^2}{2\sqrt{b(x)}}\right)\right]dx \quad (4.14)
$$

where $a(x) = (\pi^2/2)\lambda\sqrt{(e^x - 1)P_i/P_u}$ and $b(x) = (\sigma_n^2/P_u)(e^x - 1)$.

Proof. The proof of the corollary follows straightforwardly from [15] with some simple mathematical manipulations. □

The expression of the average channel capacity when $\alpha = 4$ can be bounded using the bounds of the Q function $\exp(-x^2/2)/\sqrt{\pi}(x/\sqrt{2} + \sqrt{x^2/2 + 2}) < Q(x) < \exp(-x^2/2)/\sqrt{\pi}(x/\sqrt{2} + \sqrt{x^2/2 + 8/\pi})$.

4.4.2 Aggregate Offload Throughput

Assuming a constant transmission rate, the throughput that the small cell tier can accommodate and that accounts for the sensing strategy can be expressed as

$$
\xi_t(\tau_s, \eta_t) = N_s^{(l)} p_s \mathbb{P}_d \frac{T - \tau_s}{T}\rho \quad (4.15)
$$

where $\rho = \ln(1 + \eta_t)\mathbb{P}_s(\eta_t)$ is the throughput in uplink for a typical UE, η_t is the target SINR, and where the success probability is defined as $\mathbb{P}_s(\eta_t) = \mathbb{P}[\eta > \eta_t]$.

Theorem 3. *The success probability for a typical user in the coverage of an SAP and in the presence of network interference is given by*

$$\mathbb{P}_s(\eta_t) = \frac{1}{R^2} \int_0^{R^2} \exp\left(-\frac{\sigma_n^2}{P_u}\eta_t x^{\alpha/2}\right) \exp\left(-\frac{2\pi^2}{\alpha}\lambda\left(\frac{P_i\eta_t}{P_u}\right)^{2/\alpha} \csc\left(\frac{2\pi}{\alpha}\right) x\right) dx$$

(4.16)

Proof. See Appendix A.3. $\qquad\square$

For the interference limited case, (4.16) becomes

$$\mathbb{P}_s(\eta_t) = \frac{\exp(-\vartheta R^2) - 1}{\vartheta}$$

(4.17)

where $\vartheta = \pi\lambda(2\pi/\alpha)\csc(2\pi/\alpha)(P_i\eta_t/P_u)^{2/\alpha}$. For the special case of $\alpha = 4$, we formulate the following corollary.

Corollary 2. *For $\alpha = 4$, the success probability of a typical user can be expressed as*

$$\mathbb{P}_s(\eta_t) = \frac{1}{2R^2}\sqrt{\frac{\pi}{d}}\exp\left(\frac{c^2}{4d}\right)\left[\text{erfc}\left(\frac{c}{2\sqrt{d}}\right) - \text{erfc}\left(\frac{c + 2dR^2}{2\sqrt{d}}\right)\right]$$

(4.18)

where $c = \frac{\pi^2}{2}\lambda\csc\left(\frac{\pi}{2}\right)(\eta_t P_i/P_u)^{1/2}$ and $d = \sigma_n^2\eta_t/P_u$.

Proof. Similar to proof in [15]. $\qquad\square$

4.5 Traffic offload versus energy consumption trade-off

In this section, we show how the framework developed in Sections 4.3 and 4.4 can be useful for the design of energy efficient small cell networks by means of several optimization problems.

4.5.1 Optimization of energy consumption constrained by traffic offload

In the following, we first investigate the energy minimization with regard to the sensing time, and then optimize the energy consumption with respect to sensing time and sensing probability.

Optimization of sensing time

In this problem, the objective of the system design is to offload the traffic whenever there is an active user within the coverage of an SAP. Therefore, a constraint on $\mathbb{P}_d$ is imposed and the problem can be formulated as

$$\min_{\tau_s} \quad E_{\text{tot}}$$

$$\text{s.t.} \quad \mathbb{P}_d(\tau_s, \zeta) \geq \mathbb{P}_d^* \tag{4.19}$$

where $0 \leq \tau_s \leq T$ and $\mathbb{P}_d^*$ is the target probability of detection. For a given sensing time, a threshold ζ^* can be chosen as to satisfy the constraint $\mathbb{P}_d(\tau_s, \zeta^*) = \mathbb{P}_d^*$. Let $E_2(\mathbb{P}_d, \tau_s)$ and $E_3(\mathbb{P}_{\text{fa}}, \tau_s)$ denote the second and the third term of E_{tot} in (4.2), respectively. If we select a detection threshold $\zeta' < \zeta^*$ such that $\mathbb{P}_d(\tau_s, \zeta') > \mathbb{P}_d(\tau_s, \zeta^*)$ and $\mathbb{P}_{\text{fa}}(\tau_s, \zeta') > \mathbb{P}_{\text{fa}}(\tau_s, \zeta^*)$, then we also have $E_2(\mathbb{P}_d(\tau_s, \zeta'), \tau_s) > E_2(\mathbb{P}_d(\tau_s, \zeta^*), \tau_s)$ and $E_3(\mathbb{P}_{\text{fa}}(\tau_s, \zeta'), \tau_s) > E_3(\mathbb{P}_{\text{fa}}(\tau_s, \zeta^*), \tau_s)$. Therefore, the optimal solution is achieved under the equality constraint and the optimization problem can be reformulated as

$$\min_{\tau_s} \quad \lambda_s/\lambda_m[\Xi_c T + p_s \Xi_s \tau_s + p_{\text{UE}} p_s \mathbb{P}_d^* \Xi_t (T - \tau_s)$$

$$+ (1 - p_{\text{UE}}) p_s \mathbb{P}_{\text{fa}}(\tau_s, \zeta^*) \Xi_t (T - \tau_s)]. \tag{4.20}$$

For the special case of a user with fixed position and using the Gaussian approximation for the decision variable, the threshold value corresponding with $\mathbb{P}_d^*$ is given by [108]

$$\zeta^* = \sigma_n^2(1 + \eta)[1 + \mathcal{Q}^{-1}(\mathbb{P}_d^*)\sqrt{2/(\tau_s f_s)}] \tag{4.21}$$

and $\mathbb{P}_{\text{fa}}$ under the constraint of $\mathbb{P}_d$ is given by

$$\mathcal{Q}\left(\frac{(1 + \eta)[1 + \mathcal{Q}^{-1}(\mathbb{P}_d^*)\sqrt{2/(\tau_s f_s)}] - 1}{\sqrt{2/(\tau_s f_s)}}\right). \tag{4.22}$$

Under this scenario, we formulate the following proposition.

Proposition 1. *For a user with a fixed position and using the Gaussian approximation, the optimization problem as defined in* (4.20) *has a unique optimal solution* τ_s^*.

Proof. See Appendix A.4 $\qquad\qquad\qquad\qquad\qquad\qquad\qquad\qquad\qquad\qquad\qquad\square$

Joint optimization of sensing time and sensing probability

Since it is energetically inefficient to sense continuously, to reduce idle listening we optimize the energy consumption with respect to p_s and τ_s

subject to constraints on ξ_c and $\mathbb{P}_d$. The optimization problem can be formulated as

$$\min_{p_s, \tau_s} \quad E_{\text{tot}}$$
$$\text{s.t.} \quad \xi_c \geq \xi_c^*, \quad \mathbb{P}_d \geq \mathbb{P}_d^* \tag{4.23}$$

which can be solved applying a two-step approach. For every value of $\tau_s \in [0, T]$, the optimal sensing probability can be calculated reformulating the optimization problem as follows:

$$\min_{p_s} \quad E_{\text{tot}}$$
$$\text{s.t.} \quad \xi_c \geq \xi_c^*, \quad \mathbb{P}_d \geq \mathbb{P}_d^*. \tag{4.24}$$

For a fix value of τ_s, we follow the argumentation of Section 4.5.1 to conclude that the optimal sensing probability can be found under the equality constraint. The optimal sensing probability is given by

$$p_s^* = \frac{\xi_c^*}{N_s^{(l)} \mathbb{P}_d^* \frac{T - \tau_s}{T} \bar{C}}. \tag{4.25}$$

To present a tractable analysis, we consider a user at a fixed distance from the SAP and apply the Gaussian approximation for the decision variable. The minimal energy consumption can be found by inserting (4.25) into (4.2). With $\mathbb{P}_d = \mathbb{P}_d^*$, $\mathbb{P}_{\text{fa}} = \mathcal{Q}((\zeta^* - \sigma_n^2)/(\sqrt{2/(\tau_s f_s)}\sigma_n^2))$, and $\zeta^* = \mathcal{Q}^{-1}(\mathbb{P}_d^*)\sqrt{2/(\tau_s f_s)}\sigma_n^2(1 + \eta) + \sigma_n^2(1 + \eta)$, (4.23) can be rewritten as

$$\min_{\tau_s} \mathcal{K}(\tau_s) = \min_{\tau_s} \quad \frac{\zeta^* T}{N_s^{(l)} \mathbb{P}_d^* (T - \tau_s) \bar{C}} \Xi_s \tau_s$$
$$+ \frac{\zeta^* T \Xi_t}{N_s^{(l)} \mathbb{P}_d^* \bar{C}} (p_{\text{UE}} \mathbb{P}_d^* + (1 - p_{\text{UE}}) \mathbb{P}_{\text{fa}}(\tau_s, \zeta^*)) \tag{4.26}$$

where $\mathbb{P}_{\text{fa}}(\tau_s, \zeta^*) = \mathcal{Q}\left(\mathcal{Q}^{-1}(\mathbb{P}_d^*)(1 + \eta) + \eta\sqrt{\tau_s f_s/2}\right)$. Since $\mathcal{K}(\tau_s)$ is differentiable on $[0, T]$, and $\mathcal{K}'(\tau_s)$ is increasing on $[0, T]$, $\mathcal{K}(\tau_s)$ is convex and there exists an optimal τ_s^* for (4.26). For the limits of the sensing time interval, the first derivative of $\mathcal{K}$ is given by

$$\lim_{\tau_s \to T} \mathcal{K}'(\tau_s) = \infty$$
$$\lim_{\tau_s \to 0} \mathcal{K}'(\tau_s) = \frac{\zeta^* \Xi_s}{\mathbb{P}_d^* \bar{C}} + \frac{\zeta^* T \Xi_t}{\mathbb{P}_d^* \bar{C}} (1 - p_{\text{UE}}) \mathbb{P}'_{\text{fa}}(\tau_s, \zeta^*) \tag{4.27}$$

where the last expression is negative if $\mathbb{P}'_{\text{fa}}(0, \zeta^*) < -\Xi_s/(\Xi_t T(1 - p_{\text{UE}}))$. Under this condition, the optimal sensing time can be found in the range $[0, T]$ by applying the bisection algorithm with tolerable sensing time error ϵ. The two-step optimization is illustrated in the following algorithm.

Algorithm 1 Joint optimization of the sensing time and sensing probability

Initialise $\tau_{\min} \leftarrow 0, \quad \tau_{\max} \leftarrow T$
while $\tau_{\max} - \tau_{\min} > \epsilon$ **do**
    $\tau_s \leftarrow (\tau_{\min} + \tau_{\max})/2$
    $p_s^* \leftarrow \xi^* T / (\mathbb{P}_d^* (T - \tau_s) \bar{C})$
    if $\partial E_{\text{tot}}(p_s^*, \tau_s)/\partial \tau_s < 0$ **then**
        $\tau_{\min} \leftarrow \tau_s$
    else
        $\tau_{\max} \leftarrow \tau_s$
    end if
end while

4.5.2 Optimization of QoS under energy constraint

The system designer can decide to limit the energy consumption of a small cell. In this scenario, the optimization problem can be cast as

$$\max_{\tau_s} \quad \xi_c(\tau_s)$$
$$\text{s.t.} \quad \mathbb{P}_{\text{fa}} \leq \mathbb{P}_{\text{fa}}^*. \tag{4.28}$$

Following a similar reasoning as in Section 4.5.1, we can show that the optimal solution can be found under the equality constraint. If we consider network interference, the detection threshold ζ can be found numerically using (4.9) and (4.11). In the case when we apply the Gaussian approximation for the decision variable, the threshold satisfying the constraint is given by $\zeta^* = \sigma_n^2(1 + \sqrt{2/(\tau_s f_s)} \mathcal{Q}^{-1}(\mathbb{P}_{\text{fa}}^*))$. The optimization problem can now be reformulated as

$$\max_{\tau_s} \quad \mathcal{Q} \left(\frac{\zeta^* - \sigma_n^2(1+\eta)}{\sqrt{2/(\tau_s f_s)}\sigma_n^2(1+\eta)} \right) (T - \tau_s). \tag{4.29}$$

With a change of variable $(\zeta^* - \sigma_n^2(1+\eta))/(\sqrt{2/(\tau_s f_s)}\sigma_n^2(1+\eta)) \to u$, it can be shown that there exists an optimal sensing time that yields the optimal capacity. Specifically, the optimal sensing time can be found as follows

$$\frac{\partial \xi_c(\tau_s)}{\partial \tau_s} = N_s^{(l)} p_s \bar{C} \left[-\mathcal{Q}(u) + (T - \tau_s) \frac{e^{-u^2/2}}{\sqrt{2\pi}} \frac{du}{d\tau_s} \right] = 0 \tag{4.30}$$

where the optimal solution can be found numerically.

4.6 SAP performance limits

In the former section, we illustrated how the proposed framework can be used to design energy efficient SAPs. In this section, we focus on the limits

of the energy detector and obtain an expression of the $\mathbb{P}_{\text{fa}}$ decay rate as a function of the aggregate network interference. As such, in the context of green communications, this analysis confines a region of interferer densities where the cognitive SAP can be used advantageously in order to reduce the network wide energy consumption.

4.6.1 Interference wall

In [108,112], environment-dependent uncertainties are shown to be the cause of the so-called SNR wall, below which the detector is not robust regardless the sensing time. Noise uncertainty caused by the noise estimation has been discussed in [113]. An SAP with a UE within its coverage finds itself in a high-SNR environment, and therefore, the SNR-wall due to noise estimation is not relevant in this scenario. However, another source of uncertainty is the network interference. In the following, we derive an expression of the noise uncertainty due to the network interference.

Unbounded path-loss model

Under $\mathcal{H}_0$, the decision variable can be written as

$$V_{\text{ED}} = \frac{1}{N} \sum_{k=1}^{N} (i[k] + n[k])^2. \tag{4.31}$$

As discussed in Chapter 2, the network interference can be decomposed as $i[k] = \sqrt{U}G$, where U is a skewed stable distribution and G follows a normal distribution. Therefore, the received signal under $\mathcal{H}_0$ conditioned on U can be expressed as a normal r.v. $r[k]_{|\mathcal{H}_0,U} \sim \mathcal{N}(0, \sigma_n^2 + 2\gamma^{\alpha/2}U)$. With γ defined as in (4.5), the variance of $r[k]_{|\mathcal{H}_0,U}$ can be written as $\sigma_{\text{tot}}^2 = \sigma_n^2 + 2\gamma^{\alpha/2}U = \sigma_n^2(1 + 2\eta_i(\pi C_{4/\alpha}^{-1}\mathbb{E}[|h_l X_{l,p}^i|^{4/\alpha}])^{\alpha/2}\lambda^{\alpha/2}U)$, such that η_i is the interference-to-noise ratio (INR). Let $G = 2\eta_i(\pi C_{4/\alpha}^{-1}\mathbb{E}[|h_l X_{l,p}^i|^{4/\alpha}])^{\alpha/2}U$, then the total variance takes values in the interval $\sigma_{\text{tot}}^2 \in [\sigma_n^2, \sigma_n^2(1 + \lambda^{\alpha/2}G)]$ since the skewed stable distribution U only takes positive values. For high values of the sensing time, the central limit theorem can be applied and $\mathbb{P}_{\text{d}}$ and $\mathbb{P}_{\text{fa}}$ can be found in terms of Q-functions. In order to be robust with respect to the network interference, we get

$$\mathbb{P}_{\text{fa}} = Q\left(\frac{\zeta - (1 + \lambda^{\alpha/2}G)\sigma_n^2}{\sqrt{2/N}(1 + \lambda^{\alpha/2}G)\sigma_n^2}\right)$$

$$\mathbb{P}_{\text{d}} = Q\left(\frac{\zeta - (1 + \text{SNR})\sigma_n^2}{\sqrt{2/N}(1 + \text{SNR})\sigma_n^2}\right). \tag{4.32}$$

We define the sample complexity N^* as the sensing time needed to obtain the target $\mathbb{P}_d$ and $\mathbb{P}_{fa}$. Eliminating ζ from the equations in (4.32) and solving to N, the sample complexity can be written as

$$N^* = \frac{2(\mathcal{Q}^{-1}(\mathbb{P}_{fa})(1 + G\lambda^2) - \mathcal{Q}^{-1}(\mathbb{P}_d)(1 + \text{SNR}))^2}{(\text{SNR} - G\lambda^{\alpha/2})^2}. \tag{4.33}$$

It follows that as $\lambda \to (\text{SNR}/G)^{2/\alpha}$, we have $N^* \to \infty$. In other words, a target $\mathbb{P}_{fa}$ and $\mathbb{P}_d$ cannot be attained within a finite sensing time for some interfering node density approaching $(\text{SNR}/G)^{2/\alpha}$. We call this limit the interference wall $\lambda_{\text{wall,s}}$ and note that $\lambda_{\text{wall,s}}$ is a function of the SNR, INR, the power path loss exponent, and the fading. However, to calculate G, a percentile of the distribution has to be selected that corresponds to a worst case, due to the heavy tails of the stable distribution.

Bounded path-loss model

The heuristic approximation based on the stable distribution is computationally intensive and sensitive to the selection of the percentile. In order to find a solution with higher accuracy, we consider that the interferers are located in the annulus $\mathcal{A}$, defined by the radii $d_{\min}$ and $d_{\max}$. Under such conditions, it can be shown that $i[k]$ in (4.31) follows a truncated stable distribution [13]

$$i[k] \sim S_t(\gamma', \alpha_{\text{T}} = 4/\alpha, g) \tag{4.34}$$

where α_{T} corresponds to the characteristic exponent of the stable distribution, γ' corresponds to the dispersion, and g reflects the decaying of the tail of the truncated stable distribution. The coefficients γ' and g can be determined by the method of the cumulants, by imposing the equality of the second and fourth cumulant of the truncated stable distribution with the respective cumulants of the network interference. Applying the approach of Section 4.6.1, we further approximate the interference by a Gaussian r.v., such that the received signal follows a normal distribution $r[k]_{|\mathcal{H}_0} \sim \mathcal{N}(0, \sigma_n^2 + \sigma_i^2)$, where σ_i^2 represents the second order moment of the truncated stable distribution

$$\sigma_i^2 = \mathbb{E}[i^2[k]] = \frac{\partial^2 M_i(t, \lambda)}{\partial t^2}\Big|_{t=0} = \sigma_n^2 \mathcal{I}\lambda \tag{4.35}$$

where $M_i(t, \lambda)$ is the moment generating function (MGF) of the truncated stable distribution. After some manipulations, $\mathcal{I}$ can be expressed as

$$\mathcal{I} = \frac{2}{\alpha/2 - 1}(d_{\min}^{2-\alpha} - d_{\max}^{2-\alpha})$$

$$\times \left(\frac{(\alpha_{\text{T}} - 3)(\alpha_{\text{T}} - 2)(d_{\min}^{2-\alpha} - d_{\max}^{2-\alpha})(\alpha - 1)}{(d_{\min}^{2-2\alpha} - d_{\max}^{2-2\alpha})(\alpha/2 - 1)P_i\sigma_h^2} \right)^{\frac{2-\alpha_{\text{T}}}{2} + \frac{1}{2}(\alpha_{\text{T}} - 2)} \eta_i \pi \sigma_h^2. \tag{4.36}$$

Note that the variance of the network interference is linear in the interferer density λ and the parameter $\mathcal{I} = f(d_{\min}, d_{\max}, \alpha, \eta_i, \sigma_h^2)$. For $\alpha = 4$, the parameter $\mathcal{I}$ further simplifies to $2(d_{\min}^{-2} - d_{\max}^{-2})P_i\pi\sigma_h^2$. Eliminating ζ from the expressions of $\mathbb{P}_d$ and $\mathbb{P}_{fa}$, the sample complexity can now be expressed as

$$N^* = \frac{2(\mathcal{Q}^{-1}(\mathbb{P}_{fa})(1 + \mathcal{I}\lambda) - \mathcal{Q}^{-1}(\mathbb{P}_d)(1 + SNR))^2}{(SNR - \mathcal{I}\lambda)^2} \tag{4.37}$$

and the interference wall is given by $\lambda_{\text{wall,t}} = SNR/\mathcal{I}$.

4.6.2 False alarm decay

To express the relationship between energy consumption and interfering node density, we determine how fast $\mathbb{P}_{fa}$ converges to its target value. As such, we provide a tool to evaluate how increasing the sensing time affects the energy efficiency. A direct method to obtain the PDF of V_{ED} as a function of the sensing time is cumbersome[10]. Instead, we will use tools from large deviations theory to determine how fast the target $\mathbb{P}_{fa}$ can be reached. According to the Cramer theorem, we have for interference-limited networks

$$\mathbb{P}_{fa}(\zeta) = Pr[1/N \sum_N i^2[k] > \zeta] \le e^{-NI(\zeta)} \tag{4.38}$$

which decays exponentially with the sensing time and the decay rate is determined by the rate function $I(x)$. In order to have finite moments, we model the aggregate interference power $I_\Omega = \sum i^2[k]$ according to a truncated stable distribution. The CF of the truncated stable distribution is given by [114]

$$\psi_{I_\Omega}(j\omega) = \exp\left(\gamma'\Gamma(-\alpha')\left[(g - j\omega)^{\alpha'} - g^{\alpha'}\right]\right) \tag{4.39}$$

where α' is chosen equal to the characteristic exponent of the stable distribution in the unbounded path loss model. The parameters of the truncated stable distribution can be found using the method of the cumulants. From (4.39), the cumulants of the truncated stable distribution can be expressed as

$$\begin{aligned}
\kappa_I(n) &= \left.\frac{1}{j^n}\frac{d^n}{d\omega^n}\ln\psi_{I_\Omega}(j\omega)\right|_{\omega=0} \\
&= (-1)^n\gamma'\Gamma(-\alpha')g^{\alpha'-n}\Pi_{i=0}^{n-1}(\alpha' - i). \tag{4.40}
\end{aligned}$$

Building on Cambell's theorem [13], the cumulants of the aggregate interference can be expressed as

$$\kappa(n) = P_i^n\frac{2\pi\lambda}{2 - n\alpha}(d_{\max}^{2-n\alpha} - d_{\min}^{2-n\alpha})\mu_{h^2}(n). \tag{4.41}$$

---

[10]Note that we expressed the CF of V_{ED} in Section 4.3.2

Using (4.40) and (4.41), the parameters γ' and g can be written as a function of the first two cumulants as follows

$$
\begin{aligned}
\gamma' &= \frac{-\kappa(1)}{\Gamma(-\alpha')\alpha'\left(\frac{\kappa(1)(1-\alpha')}{\kappa(2)}\right)^{\alpha'-1}} \\
g &= \frac{\kappa(1)(1-\alpha')}{\kappa(2)}.
\end{aligned}
\tag{4.42}
$$

Since $i^2[k]$ are assumed to be i.i.d., the Cramer theorem can be applied and we can express the rate function as the Legendre-Fenchel transform of the logarithmic MGF

$$
I(x) = \sup_\theta \left(\theta x - \gamma'\Gamma(-\alpha')[(g-\theta)^{\alpha'} - g^{\alpha'}] \right).
\tag{4.43}
$$

For $\theta < g$, let the first derivative be equal to zero and solving to θ for $\alpha = 4$, we have

$$
\theta = g - \left(\frac{-\gamma'\Gamma(-\alpha')}{2x}\right)^2.
\tag{4.44}
$$

Substituting θ in (4.43), the expression of the rate function is given by

$$
I(x) = gx + \sqrt{g}\gamma'\Gamma(-\alpha') + \frac{(\gamma'\Gamma(-\alpha'))^2}{4x}.
\tag{4.45}
$$

4.7 Numerical Resuls

In this section, we present some numerical results that provide insight into the trade-off between energy consumption and traffic offload of the SAPs within a MBS Voronoi cell.

4.7.1 Traffic offload

Figure 4.3 depicts the success probability for a typical user within the coverage of an SAP. With the interferers distributed according to a PPP, this figure illustrates that the success probability decreases drastically with increasing interfering node density. Figure 4.4 shows $\mathbb{P}_d\bar{C}$ (the uplink capacity of a typical user in the SAP coverage corrected for the detection probability) as a function of the interferer density. The figure illustrates the combined effect of the increasing detection performance and the decreasing average channel capacity with λ.
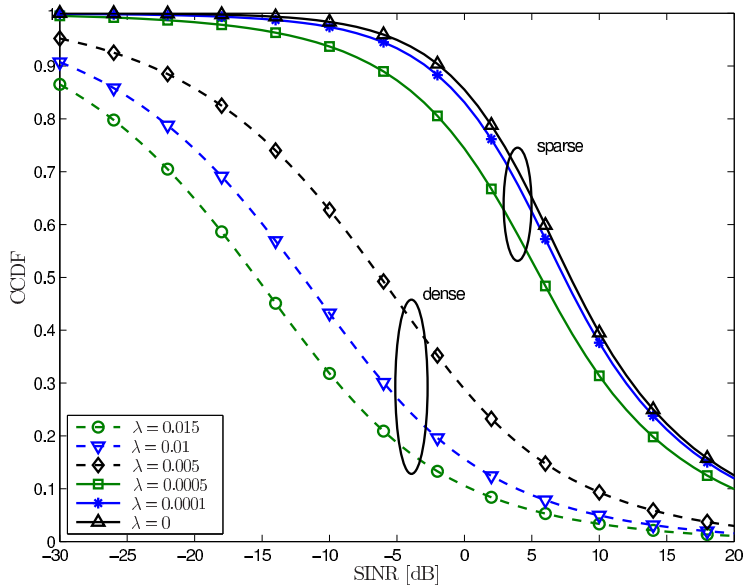
Figure 4.3: The success probability in the presence of sparse and dense interferers.
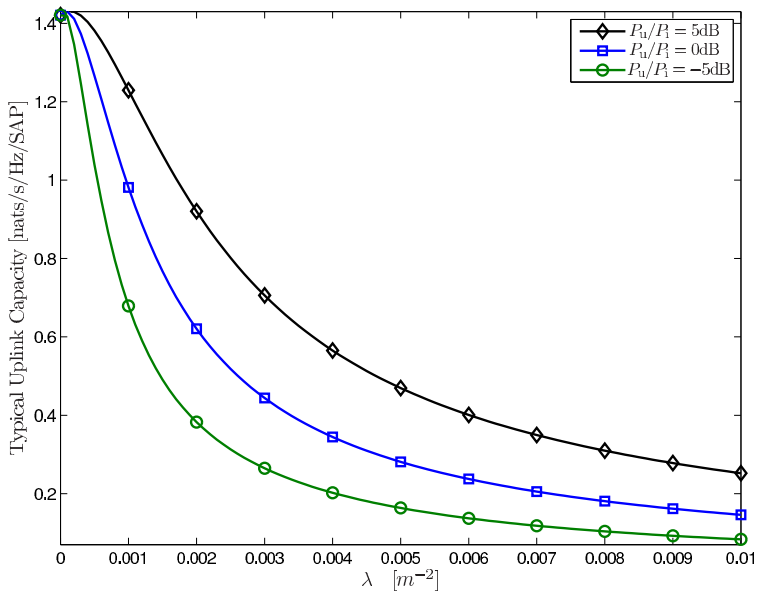

Figure 4.4: The average channel capacity corrected by the detection probability for different values of the power ratio between the SoI and the interferers.

4.7.2 SAP energy efficiency

Since this work focuses on the trade-off between the energy consumption and the aggregate offload throughput and capacity, it is meaningful to analyze how the energy consumption depends on the interferer density. In the following numerical examples, we consider that SNR = 3 dB defined for the UE at the edge of the SAP coverage $R = 20$, while the INR = 10 dB defined at a distance of 1 meter (far-field assumption). We consider the densities of MBSs, SAPs, and users to be $\lambda_{\mathrm{m}} = 10^{-6}$ m^{-2} , $\lambda_{\mathrm{s}} = 10^{-5}$ m^{-2}, and $\lambda_{\mathrm{u}} = 10^{-4}$ m^{-2}. From (4.2), we observe that the power consumption consists of three components Ξ_c, Ξ_{s}, and Ξ_t, which we assume to be constant and given by $\Xi_c = 6W$, $\Xi_{\mathrm{s}} = 4W$, and $\Xi_t = 5W$ [115]. Unless otherwise specified, we set the probabilities $p_{\mathrm{I}} = 0.1$, $p_{\mathrm{s}} = 1$, and $p_{\mathrm{UE}} = 0.1$. Furthermore, we let the frame length $T = 400/f_{\mathrm{s}}$ and the maximum duty cycle (DC) is 25 %.

Figure 4.5 shows the total energy consumption considering a constant target $\mathbb{P}_{\mathrm{d}}$ and a constant threshold, respectively. We observe that for all scenarios the energy consumption grows with increasing interfering node density. This can be ascribed to the fact that the energy consumption is linear in $\mathbb{P}_{\mathrm{d}}$ and $\mathbb{P}_{\mathrm{fa}}$. As more energy is provided to the ED with increasing interferer density, $\mathbb{P}_{\mathrm{d}}$ and $\mathbb{P}_{\mathrm{fa}}$ increase for the constant threshold scenario. In this numerical example, $p_{\mathrm{UE}} = 0.1$ and therefore, the increase of energy consumption is dominated by $\mathbb{P}_{\mathrm{fa}}$. If information is available about the interference environment, the threshold can be altered such that $\mathbb{P}_{\mathrm{d}} = \mathbb{P}_{\mathrm{d}}^*$. Raising the threshold with the interferer density, moderates the increase of $\mathbb{P}_{\mathrm{fa}}$ and the energy consumption, which is reflected in the figure. This means that the knowledge of the interference environment allows to improve the energy efficiency of small cell networks.

Figure 4.6 illustrates the effect of the SAP coverage range and the interferer node density on the energy consumption. The energy consumption increases with almost 50 % when R varies from 15 to 50 m. The sensing time is fixed to $N = 15$ samples and $\mathbb{P}_{\mathrm{d}} = \mathbb{P}_{\mathrm{d}}^* = 0.9$ for all values of the coverage. To satisfy the constraint on $\mathbb{P}_{\mathrm{d}}$, the detection threshold decreases for a larger coverage, and as a consequence $\mathbb{P}_{\mathrm{fa}}$ increases. This is reflected in the total energy consumption. From the numerical results presented in Fig. 4.6, we can conclude that the energy consumption is affected considerably by changing the SAP coverage due to the strong relation between the user detection performance and the coverage range.

In Section 4.5.1, we defined an optimization problem that minimizes the energy consumption subject to constraints on both the traffic offload and the detection probability. Figure 4.7 depicts the objective function (4.23) of the energy consumption optimization problem for different interferer densities. We ascertain the convexity of the energy consumption of all SAPs belonging to a macrocell Voronoi cell subject to constraints on $\mathbb{P}_{\mathrm{d}}$ and
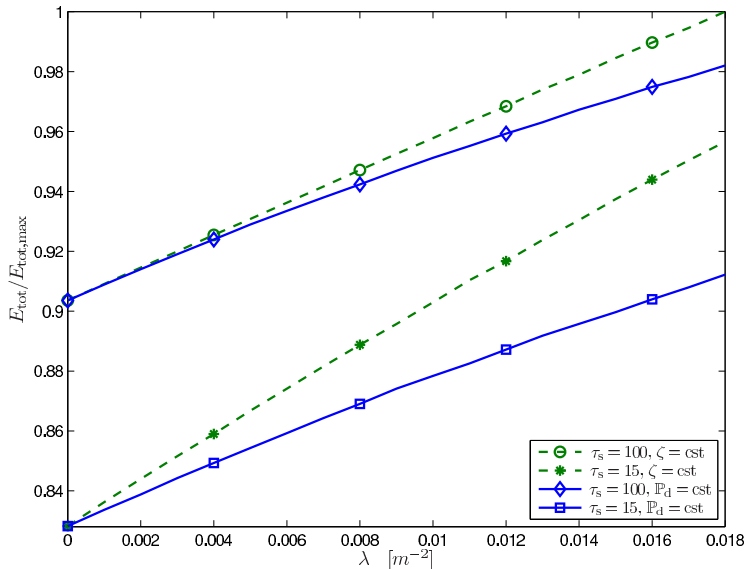
Figure 4.5: Total energy consumption for different values of the sensing time and with fix or variable detection threshold value.
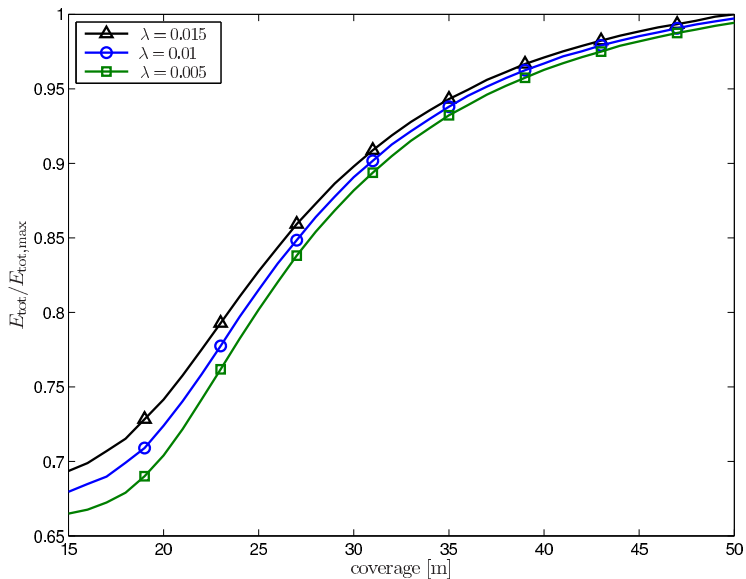
Figure 4.6: Total energy consumption for different values of the interferer density.

ζ_c. The initial decrease of the energy consumption is due to the decrease of $\mathbb{P}_{\mathrm{fa}}$ with the sensing time until $\mathbb{P}_{\mathrm{fa}}$ reaches a stationary value. Any further increase of the energy consumption is related to the sensing energy
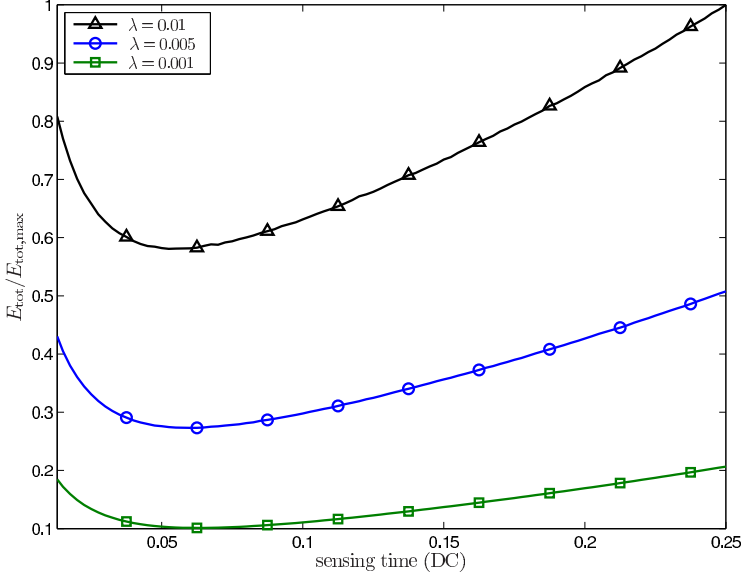
Figure 4.7: E_{tot} for different values of the interferer density and with $p_{UE} = 0.1$. The optimization is performed subject to $\mathbb{P}_d^* = 0.9$ and $\xi_c^* = 0.5$ nats/s/Hz/macrocell.

accruing with the sensing time. Furthermore, this example reveals that for increasing interferer density, the optimal sensing time decreases, which can be ascribed to a higher stationary $\mathbb{P}_{fa}$ with increasing λ. The impact of λ on the optimal sensing time is however negligible. This result highlights that the proposed framework can be used to find the optimal sensing time and sensing probability. Moreover, we observe that the energy consumption can be improved considerably and the energy consumption gain by joint optimization of τ_s and p_s increases with larger interferer density.

To elucidate the trade-off between the energy consumption and the traffic offload, we define the energy efficiency as $\varsigma = \xi_c / E_{tot}$. Figure 4.8 shows the effect of the sensing time and the interferer density on the energy efficiency. We observe that there exists an optimal value of the sensing time balancing the two opposing requirements. With respect to the optimization of the energy consumption subject to a constraint on $\mathbb{P}_d$, this figure shows that with increasing interferer density the optimal sensing time shifts to smaller values. This effect is related to the linear decrease of the traffic offload with increasing sensing time, as can be verified in (4.12) or (4.15).

Defining the load of a typical base station (SAP or MBS) as the number of active users within the coverage, we notice that the small cell load is related to the density of the active users and the small cell coverage. Owing to the major coverage differences between the tiers, the load of a typical SAP and
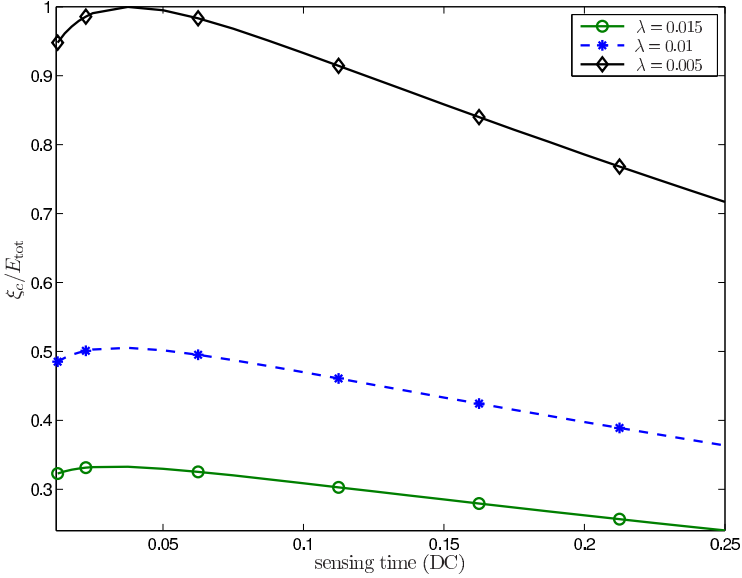
Figure 4.8: Energy efficiency for different values of λ as a function of the sensing duty cycle.

MBS differ considerably such that the aggregate offload capacity depends on λ_{m}, λ_{s}, and λ_{u}. Figure 4.9 illustrates how the energy consumption and the traffic offload of the SAPs within a macrocell vary as a function of λ_{u} and how they relate. The numerical results illustrate the impact of the quality of the cognitive capabilities on both the energy consumption and traffic offload. In this scenario, we assume λ_{u} to vary as $10^{-6} < \lambda_{\mathrm{u}} < 10^{-3}$ and that SIR $= 0$dB. For sensing DC $= 0.05$, the energy efficiency ς is clearly superior than for higher values of the duty cycle. In case of perfect sensing and low values of the load, the energy consumption is lower than the curves with realistic detection performance due to $\mathbb{P}_{\mathrm{fa}} = 0$, and this effect diminishes with increasing load.

4.7.3   Performance limits

Figure 4.10 shows the sample complexity to satisfy a target $\mathbb{P}_{\mathrm{fa}}$ and $\mathbb{P}_{\mathrm{d}}$ for increasing interferer density. This figure illustrates the fundamental limit of the interfering node density under which the SAP can robustly detect the macrocell user presence. Beyond the interference wall, the noise uncertainty becomes too big to distinguish between SoI or noise. The curves are drawn using the 87 percentile of the stable distribution, the truncated stable distribution and numerical simulations. For $d_{\min} = 1$ and $d_{\max} = 100$, the approaches with the stable and the truncated stable distribution are in
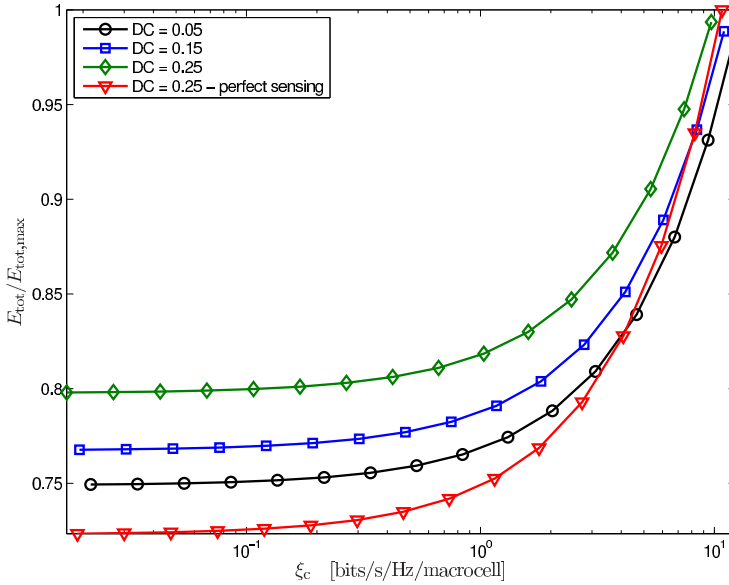
Figure 4.9: Energy consumption for different values of the sensing time and for the ideal case of perfect sensing as a function of the load.

good agreement and correspond well with the numerical simulation. Figure 4.11 shows the $\mathbb{P}_{\text{fa}}$ decay rate as expressed in (4.45) as a function of the threshold x for different values of the interference power and the interferer density. It can be observed that with increasing density and interference power the rate function decreases. Thus, the rate function can reveal more insight into the effect of λ and P_{i} on the SAP power consumption and reflects the achievable energy efficiency.
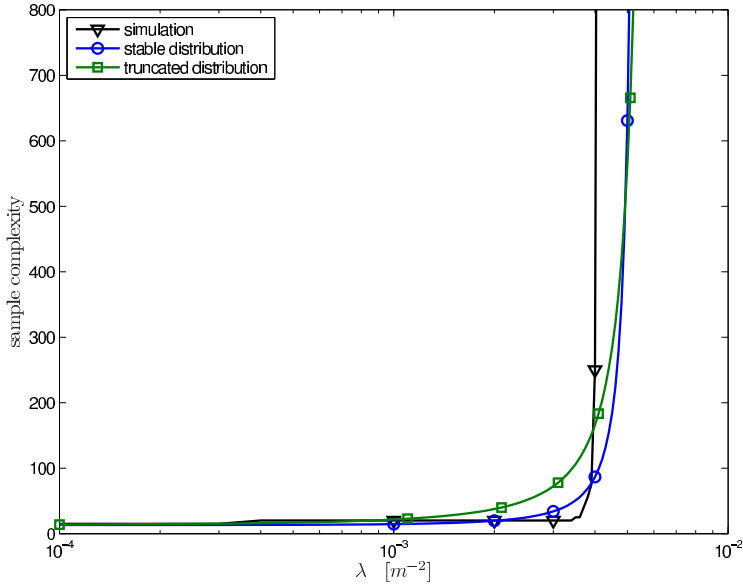
Figure 4.10: The interference wall using the approximation with the 87 percentile of the stable distribution, using the truncated stable distribution and using numerical simulations for $\mathbb{P}^*_{fa} = 0.1$ and $\mathbb{P}^*_{d} = 0.9$, SNR = 3 dB and INR = 20 dB.
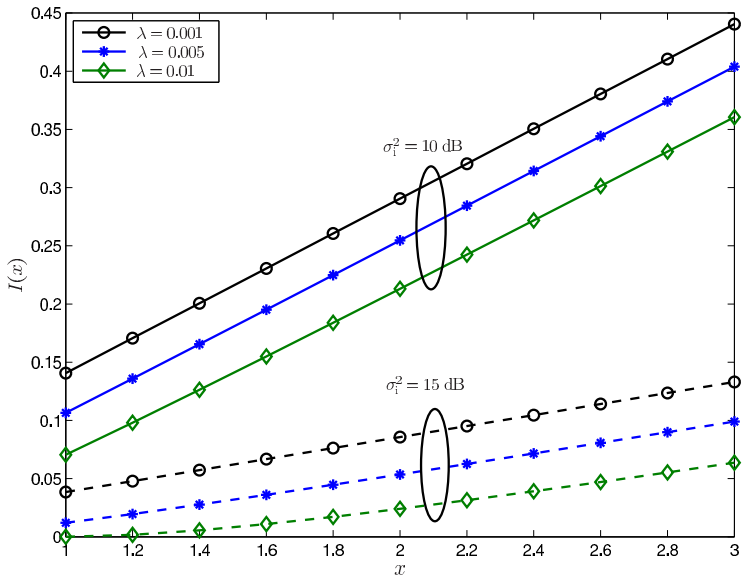
Figure 4.11: The rate function is given for different values of the interference power and density.

4.8   Conclusions

In this chapter, we proposed an analytical framework that allows to analyze the trade-off between the energy consumption and the traffic offload of cognitive SAPs located in an MBS Voronoi cell. In particular, we defined the detection performance of an energy detector for a typical user, as well as the aggregate capacity and throughput that can be offloaded from an MBS. The model accounts for channel fading, aggregate network interference, bursty activity, network topology, and load. The proposed model allows to quantify the effect of critical system parameters such as the interferer density and the SAP coverage on the detection performance, the aggregate offload capacity and throughput, and the total energy consumption. Numerical results reveal that the knowledge of the interference environment can lead to a substantial reduction of the SAP energy consumption. We defined several optimization problems and showed that the proposed framework can be used both for the design of the optimal sensing time and sensing probability, as for the evaluation of the energy efficiency with respect to network topology and load. Further, fundamental limits of the detection robustness are defined by introducing the interference wall and the speed of convergence of $\mathbb{P}_{fa}$. In conclusion, the framework can be used for the energy efficient design and operation of cognitive SAPs in heterogeneous networks. Possible future directions to extend this work are to consider the combined energy consumption of multiple tiers, include constraints on the user quality of service, and compare the effectiveness of the distributed sleep mode scheme with strategies such as random sleeping or centralized sleep mode schemes exploiting user location awareness.

Chapter 5

Successive interference cancellation in heterogeneous networks

[1]At present, operators address the explosive growth of mobile data demand by densification of the cellular network so as to reduce the transmitter-receiver distance and to achieve higher spectral efficiency. Due to such network densification and the intense proliferation of wireless devices, modern wireless networks are interference-limited, which motivates the use of interference mitigation and coordination techniques. In this chapter, we develop a statistical framework to evaluate the performance of multi-tier heterogeneous networks with SIC capabilities, accounting for the computational complexity of the cancellation scheme and relevant network related parameters such as random location of the access points (APs) and mobile users, and the characteristics of the wireless propagation channel. We explicitly model the consecutive events of canceling interferers and we derive the success probability to cancel the n-th strongest signal and to decode the signal of interest after n cancellations. When users are connected to the AP which provides the maximum average received signal power, the analysis indicates that the performance gains of SIC diminish quickly with n and the benefits are modest for realistic values of the SIR. We extend the statistical model to include several association policies where distinct gains of SIC are expected: (i) minimum load association, (ii) maximum instantaneous SIR association, and (iii) range expansion. Numerical results

---

[1]This chapter is under review at IEEE Transactions on Signal Processing [116]. Part of this chapter has been presented at the IEEE Workshop on Signal Processing Advances in Wireless Communications (SPAWC), Darmstadt, Germany, June 2013 [117] and has been submitted for the 2014 IEEE International Conference on Acoustics, Speech, and Signal Processing (ICASSP) [118] .

show the effectiveness of SIC for the considered association policies. This chapter deepens the understanding of SIC by defining the achievable gains for different association policies in multi-tier heterogeneous networks.

5.1 Background

Small cell networks are an important trend in current wireless networks, which increase the density of transmitters and result in interference-limited networks where the thermal noise is negligible with respect to the interference [75, 78]. The motivation of small cell networks stems from the idea to reduce the distance between transmitter and receiver by deploying additional base stations as to increase the spectral efficiency. Yet, as the network interference is the most important obstacle for successful communication, effective interference management schemes are essential to further enhance the performance of dense networks. These mechanisms impose the orthogonality between transmitted signals in frequency, time, or space, and include adaptive spectrum allocation policies [79, 84], MAC schemes, spatial interference mitigation by means of zero-forcing beamforming [119], and signal processing algorithms usually referred to as IC techniques [120–127].

Signal processing techniques such as joint detection (JD) [120] or SIC reduce the interference power by decoding and canceling interfering signals. In this work, we focus on the SIC receiver which decodes signals according to descending signal power and subtracts the decoded signal from the received multi-user signal, so as to improve the signal-to-interference ratio (SIR). The process is repeated until the signal of interest (SoI) is decoded. A common approach in literature is to consider an exclusion region around the receiver. In [7], a Gaussian approximation is proposed for the sum of interfering signals, while [12] performs an asymptotic analysis of the interference distribution in cognitive radio networks. The methodology based on the exclusion region leads to the definition of lower and upper bounds of the outage probability. For instance, in [121, 122], a stochastic geometric model is adopted to capture the spatial distribution of the interfering nodes, accounting for cancellation and decoding errors. The key idea of this work is the division into near field and far field interferers, where every near field interferer is able to cause outage at the reference receiver. Building on this work, [123, 124] propose bounds of the outage/success probability including the effects of the fading channel, while [126] includes accurately the consecutive steps of the SIC scheme. None of these works concerns a specific cancellation technique, since the order statistics of the received signal power are disregarded, which is an essential aspect in the analysis of SIC. The ordering of the received signal power depends on the transmission power

of the network nodes, the spatial distribution of the active transmitters, and the propagation channel conditions. Specifically, the inclusion of SIC in the network performance analysis requires the characterization of the fundamental information-theoretic metric, the SIR, and to model the network interference as a trimmed sum of order statistics. In [125], closed-form expressions are presented for the outage probability accounting for the order statistics, assuming that all interferers are at the same distance from the intended receiver, while [128] derives a lower bound of the outage probability based on the order statistics of the strongest uncanceled and partially canceled signals accounting for distance and fading. Very recently, some excellent contributions can be found that explicitly include both the topology and the fading effects in the description of sum of order statistics of the received signal power [129–132], yet, these models limit the analysis to single-tier networks.

A unified approach to describe the performance of SIC, which jointly accounts for the interference cancellation scheme, network topology, channel fading, and the specific aspects of multi-tier networks, is still evasive. In this work, we develop an analytical framework that describes the success probability for transmissions in multi-tier networks with SIC capabilities. The main contributions of this work are listed as follows.

- We derive the probability of successfully canceling the *n*-th interferer and show that the order statistics of the received signal power are dominated by path loss attenuation. We demonstrate how the effectiveness of the SIC scheme depends on the path loss exponent, the density of users and APs, and the maximum number of cancellations.

- We provide an analytic framework that accommodates for the heterogeneity that characterizes future wireless networks. To this end, we include different association policies for multi-tier networks for which SIC yields distinct performance gains. In particular, we include the minimum load association policy, maximum instantaneous SIR policy, and range expansion in the analysis.

The proposed framework accounts for all essential network parameters and provides insight in the achievable gains of SIC in multi-tier heterogeneous networks. The minimum load policy can be used to enhance the feasibility of load balancing [133], the maximum instantaneous SIR policy is relevant to define the achievable capacity in multi-tier networks [134], and range expansion with SIC capabilities can allow for efficient traffic offloading [135].

The remainder of the chapter is organized as follows. In Section 5.2, the system model is introduced. In Section 5.3, the success probability of transmissions in multi-tier heterogeneous networks with SIC capabilities is defined. In Section 5.4, several association policies different from

the maximum long-term SINR policy are introduced, where SIC yields a substantial increase of the coverage probability or the rate distribution. Numerical results are presented in Section 5.5 and conclusions are drawn in Section 5.6.

5.2 System Model

We consider a multi-tier heterogeneous network composed of K tiers. For every tier $k \in \mathcal{K} = \{1, ..., K\}$, the access points (APs) are distributed according to a homogeneous Poisson point process (PPP) Φ_k in the Euclidean plane with density λ_k such that $\Phi_k \sim \mathrm{PPP}(\lambda_k)$. While it is natural to use the Poisson model as the underlying spatial stochastic process for irregularly deployed APs such as picocells and femtocells, modeling the location of regularly deployed macrocell base stations (MBSs) by means of a PPP has been empirically validated and yields conservative bounds on the network performance [15]. More recently, also theoretical evidence has been given for modeling the deterministic locations of MBSs by means of a PPP, provided there is sufficiently strong log-normal shadowing [104]. All APs apply an open access (OA) policy, such that users can be served by each AP of each tier. The mobile users are spatially distributed as $\Psi \sim \mathrm{PPP}(\mu)$ over $\mathbb{R}^2$. Each AP of tier k transmits with power P_k over the total bandwidth W. The total available spectrum W is divided in subchannels by aggregating a fixed number of consecutive subcarriers of bandwidth B, such that the total number of available subchannels equals $\lfloor W/B \rfloor$.[2] We denote the subchannel index as j, where $j \in \mathcal{J} = \{1, 2, \ldots, \lfloor W/B \rfloor\}$. In order to maximize frequency reuse and throughput, each AP has access to the entire available spectrum. We represent the i-th AP of tier k as $x_{k,i}$. Hence, denoting the available channels of $x_{k,i}$ as $\mathcal{J}^{(x_{k,i})}$, we have $\mathcal{J}^{(x_{k,i})} = \mathcal{J}$, $\forall i, k$. A user receives a signal from $x_{k,i}$ with signal power $P_k h_u g_\alpha(u - x_{k,i})$, where h_u represents the power fading coefficient for the link between the user u and $x_{k,i}$, and $g_\alpha(x) = \|x\|^{-\alpha}$ is the power path loss function with path loss exponent α. For notational convenience, u and x will be used to denote network nodes as well as their location. The association of a user to $x_{k,i}$ is based on the following association metric

$$x_{k,i} = \arg \max_{k,i} A_k \|u - x_{k,i}\|^{-\alpha} \tag{5.1}$$

where A_k represents the association rule. For all $A_k = 1$, the user is associated to the nearest base station. For $A_k = P_k$, the association is based on the maximum average received signal power, where the averaging is done with

---

[2]Without loss of generality, we assume $B = 1$.
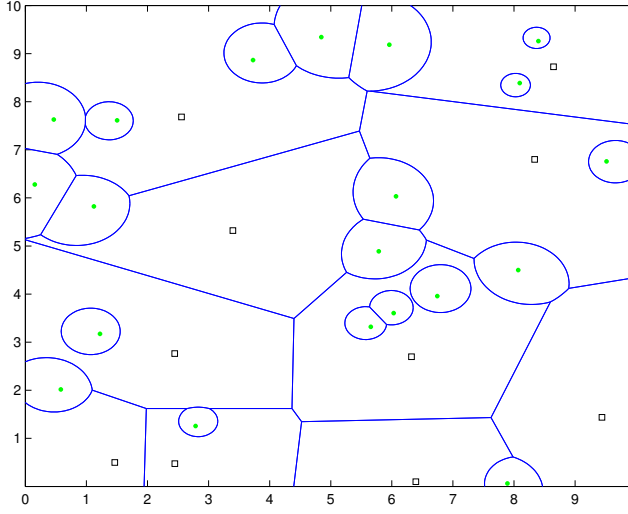
Figure 5.1: Multiplicatively weighted Voronoi tessellation for a two-tier network.

respect to the fading parameter h.[3] Using this association rule, the set of APs forms a multiplicatively weighted Voronoi tessellation on the two dimensional plane, where each cell $C_{k,i}$ consists of those points which have a higher average received signal power from $x_{k,i}$ than from any other AP, as depicted in Fig. 5.1. Formally, we define the cells as

$$C_{k,i} = \{y \in \mathbb{R}^2 \mid \|y - x_{k,i}\| \leq (A_k/A_l)^{1/\alpha}\|y - x\|, \ \forall x \in \Phi_l \backslash \{x_{k,i}\}, l \in \mathcal{K}\}. \tag{5.2}$$

According to the association rule in (5.1), users will connect to different tiers and the density of users connected to tier k is given by μ_k. Considering a K-tier network, each tier $k \in \mathcal{K}$ is characterized by the set consisting of the UL transmission power, DL transmission power, AP density, and associated user density $\{Q_k, P_k, \lambda_k, \mu_k\}$. The sets of transmission powers and densities are denoted as $\mathbf{Q} = \{Q_1, \ldots, Q_K\}$, $\mathbf{P} = \{P_1, \ldots, P_K\}$, $\boldsymbol{\lambda} = \{\lambda_1, \ldots, \lambda_K\}$, and $\boldsymbol{\mu} = \{\mu_1, \ldots, \mu_K\}$, respectively. Within a Voronoi cell, mobile users are independently and uniformly distributed over the cell area. Fairness between users is accomplished by proportional allocation of the time and frequency resources. We consider an orthogonal multiple access scheme which ensures that at any given time and channel, only a single user per cell is active. As the number of users per Voronoi cell active on channel j is restricted to one, the

---

[3]The association rule can further be adjusted to accommodate for cell range expansion by defining $A_k = b_k P_k$, where b_k represents an association bias for tier k.

multiple access scheme introduces coupling between the locations of mobile users and APs. It can be shown that this dependence has negligible effects on the performance analysis, and in the sequel we will therefore assume independent PPPs to maintain the tractability of the system model [136]. As interference dominates noise in modern cellular networks, we consider the network to be interference-limited. For the link between user u and base station $x_{k,i}$, we define the signal-to-interference ratio (SIR) on channel j in DL as

$$\mathrm{SIR}_j(x_{k,i} \to u) = \frac{P_k h_u g_\alpha(x_{k,i} - u)}{\sum_{k \in \mathcal{K}} \sum_{v \in \Phi_{k,j} \setminus \{x_{k,i}\}} P_k h_v g_\alpha(v - u)}. \tag{5.3}$$

Let $\Phi_{k,j}$ and $\Psi_{k,j}$ denote the network nodes active on channel j in tier k for the APs and mobile users, respectively. A transmission is successful if the SIR of the intended link exceeds a prescribed threshold η_t, which reflects the required quality-of-service (QoS) in terms of transmission rate. Hence, the success probability can be written as $\mathbb{P}_s(\eta_t) = \Pr\{\mathrm{SIR}_j(x_{k,i} \to u) \geq \eta_t\}$.

5.3 Successive Interference Cancellation

In this section, we study how SIC affects the success probability in multi-tier heterogeneous networks where the association policy is based on the maximum average received signal power. The analysis will be presented for UL transmissions but the results similarly apply for DL transmissions. This choice is motivated by the higher computational capabilities of APs in comparison with the mobile nodes, which is essential to successfully implement advanced signal processing techniques, as well as power consumption considerations which are less restrictive for APs. The concept of SIC is to decode the strongest signal and subtract it from the incoming signal which yields an increase of the SIR. In the analysis, we explicitly model the sequence of events in the cancellation process. We define the success probability as a function of the threshold, the number of canceled interferers, and all relevant system parameters such as the interferer density, transmission power, path loss exponent, and channel fading.

Owing to constraints on computational complexity and delay, the number of interferers that can be canceled is limited to $N \in \mathbb{N}$. The AP with SIC capabilities attempts first to decode the SoI without any interference cancellation. If an outage occurs, the AP seeks to decode the strongest signal, subtract it from the incoming signal, and performs a new attempt to decode the SoI [126]. The received signal power at the typical AP can be ordered as $\{X_{(1)}, X_{(2)}, ...\}$ such that $X_{(i)} \geq X_{(j)}$, with $i \leq j$ and $X_{(i)} = Q_i h_i v_i^{-\alpha}$. The same actions are repeated until the SoI is decoded while satisfying the constraint on the maximum number of cancellations. Hence, UL transmission is successful

as long as one of the following events is successful

$$0 : \left(\frac{Q_u h_u u^{-\alpha}}{I_{\Omega_j^0}} \geq \eta_{\text{t}} \right)$$

$$1 : \left(\frac{Q_u h_u u^{-\alpha}}{I_{\Omega_j^0}} < \eta_{\text{t}} \right) \cap \left(\frac{X_{(1)}}{I_{\Omega_j^1}} \geq \eta_{\text{t}} \right) \cap \left(\frac{Q_u h_u u^{-\alpha}}{I_{\Omega_j^1}} \geq \eta_{\text{t}} \right)$$

$$\vdots$$

$$N : \left(\bigcap_{n=0}^{N-1} \frac{Q_u h_u u^{-\alpha}}{I_{\Omega_j^n}} < \eta_{\text{t}} \right) \cap \left(\bigcap_{n=1}^{N} \frac{X_{(n)}}{I_{\Omega_j^n}} \geq \eta_{\text{t}} \right) \cap \left(\frac{Q_u h_u u^{-\alpha}}{I_{\Omega_j^N}} \geq \eta_{\text{t}} \right)$$

$$(5.4)$$

where the set of interferers on subchannel j after cancellation of the n strongest interferers is represented by $\Omega_j^n = \Omega_j \backslash \{X_{(1)}, \ldots, X_{(n)}\}$, and $\Omega_j = \cup_{k \in \mathcal{K}} \Psi_{k,j} \backslash \{u\}$. The aggregate interference after cancellation is given by

$$I_{\Omega_j^n} = \sum_{i=n+1}^{\infty} X_{(i)}. \tag{5.5}$$

The first and third factor in the n-th event of (5.4) represent outage and success for decoding the SoI when $n - 1$ and n interferers are canceled, respectively. The second factor in the n-th event of (5.4) represents the event of successfully canceling the n-th interferer.

The cancellation order is based on the received signal power and is independent of the tier to which the interferers belong. Since $X_{(i)}$ can originate from different tiers with different transmission power Q_i, (5.5) represents the sum of order statistics, where the transmission power, fading parameter, and path loss component are random variables (r.v.'s). Recent work shows that a generic heterogeneous multi-tier network can be represented by a single-tier network where all system parameters such as the transmission power, fading parameter, and path loss exponent are set to constants, while the determinative parameter is an isotropic (possibly non-homogeneous) AP density [137]. For a constant path loss exponent, the isotropic density of the equivalent network reduces to a homogeneous value, as such generalizing previous results where the dispersion of the aggregate interference depends on a single moment of the transmission power and the fading distribution [2]. The stochastic equivalence between multi-tier and single-tier networks allows for the comparison between apparently different networks in a simplified framework. For the performance evaluation of SIC, we will relax the system model to the stochastically equivalent single-tier network with density given by $\lambda_{\text{eq}} = \sum_{k \in \mathcal{K}} \lambda_k P_k^{2/\alpha}$, which follows from

Campbell's theorem [23], and where the transmission power is equal to one.[4] We indicate the density of the mobile users active on channel j by μ_j. In the following sections, different lemma's are formulated, which define the probability of successfully decoding the SoI after canceling n interferers and the success probability of canceling the n-th interferer.

5.3.1 Decoding after interference cancellation

We define the success probability of a link in an interference-limited network after successfully canceling n interferers as

$$\mathbb{P}_{\mathrm{s,IC}}(\eta_\mathrm{t}, n) = \Pr\left[\sum_{i=n+1}^{\infty} X_{(i)} < h_u u^{-\alpha}/\eta_\mathrm{t}\right] = \Pr\left[I_{\Omega_j^n} < h_u u^{-\alpha}/\eta_\mathrm{t}\right]. \quad (5.6)$$

Note that the calculation of the success probability for decoding the SoI is based on the distribution of the sum of order statistics, which requires the joint distribution of infinitely many r.v.'s. There are several possibilities to handle this problem, which have in common to limit the summation of order statistics to the M strongest interferers, generally denoted as a trimmed sum. Since order statistics are mutually dependent, the cumulative distribution function (CDF) of their sum is hard to characterize. The CDF of the sum of order statistics can be found by the inverse Laplace transform of the moment generating function (MGF). It can be shown that the transformation of the order statistics of a set of exponentially distributed r.v.'s to the spacing between the order statistics statistics results in independent r.v.'s, which alleviates the complexity to calculate the MGF [138]. Neglecting the topology and assuming that all interferers are at the same distance from the receiver, a closed form solution of the CDF can be found [125]. Likewise, the difference of the square of consecutive distances follows an exponential distribution, i.e. $R_{(i)}^2 - R_{(i-1)}^2 \sim \exp(\pi\lambda)$ with $R_{(i)}^2$ the ordered Euclidean distance in $\mathbb{R}^2$ of the interferers with respect to the receiver and λ the intensity of the Poisson process [139]. Hence, including the topology and neglecting fading effects, a closed form solution can be reached similarly. However, the computational complexity to calculate the CDF of a trimmed sum of order statistics including both topology and fading is prohibitive. An alternative promising approach to characterize the sum of order statistics is to consider the asymptotic distribution of the sum $T_M(m, k) = \sum_{i=m}^{M-k} X_{(i)}$, where a fixed number $k \geq 0$ of the smallest values and a fixed number $m \geq 0$ of the largest values is trimmed, denominated as lightly trimmed sums [138,140,141]. The main result of [140] is based on the quantile function $Q(s)$, defined as the inverse of the CDF of the considered r.v., but no closed form solution can be found for the considered scenario.

---

[4]Note that we assume in this work a constant path loss exponent α for all tiers.

In our model, we include the effects of both fading and topology, yet, we assume that the order statistics are dominated by the distance. As to the received signal power in the equivalent single-tier network, the order statistics of the distance outweigh the fading effects, which have an effect on a much shorter time scale. There is a more formal motivation why we assume that the order statistics are dominated by the distance rather than the fading distribution. In the following lemma, we define the distribution of the received signal power.

Lemma 1. *The distribution of* $Y = hX^{-\alpha}$ *where* $h \sim \exp(\lambda)$ *follows a Pareto distribution with CDF*

$$F_Y(y) = 1 - \Gamma\left(\frac{2}{\alpha} + 1\right)\frac{y^{-2/\alpha}}{R^2} \tag{5.7}$$

where R is the maximum considered range for the position of interferers.

Proof. See Appendix A.5. □

Note that $X^{-\alpha}$ follows a Pareto distribution, which belongs to the class of subexponential distributions. According to the theorem of Breiman, which states that the class of subexponential distributions is closed under the product convolution, the multiplication of $X^{-\alpha}$ with the exponential r.v. h does not change the distribution [142]. Same conclusions hold for other types of fading distributions.

Remark 1. *In the remainder, we will often make use of integrals of the form* $\int 1/(1 + w^{\alpha/2})dw$. *For the integration interval* $[b, \infty)$, *we define*

$$C(b, \alpha) = \int_b^\infty \frac{1}{1 + w^{\alpha/2}}dw = 2\pi/\alpha \csc(2\pi/\alpha) - b\, {}_2F_1(1, 2/\alpha; (2 + \alpha)/\alpha; -b^{\alpha/2}) \tag{5.8}$$

where ${}_2F_1(.)$ *is the Gaussian hypergeometric function. For special cases, we have* $C(0, \alpha) = 2\pi/\alpha \csc(2\pi/\alpha)$ *and* $C(b, 4) = \arctan(1/b)$.

Lemma 2. *A mobile user is connected to a typical AP, which has successfully canceled n interferers. The success probability of UL transmission in the presence of network interference is given by*

$$\mathbb{P}_{s,IC}(\eta_t, n) \approx \int_{R_{I,n}}^\infty \exp\left(-\pi\mu_j\eta_t^{2/\alpha}u^2 C(R_{I,n}^2/(\eta_t^{2/\alpha}u^2), \alpha)\right)$$

$$\times 2\pi\lambda_{eq}u \exp(-\lambda_{eq}\pi u^2)du \tag{5.9}$$

where $R_{I,n} = \sqrt{n/\mu_j\pi}$ *is the cancellation radius that defines the area around the victim receiver without interferers.*

Proof. Similar to the DL coverage probability derived in [15], we define the UL coverage probability conditioned on the distance of the intended link after successfully canceling n interferers as

$$\mathbb{P}_{\text{s,IC}}(\eta_{\text{t}}, n \mid u) = \mathbb{P}^{!u} \left\{ \frac{h_u u^{-\alpha}}{\sum_{v \in \Omega_j^n \setminus \{u\}} h_v v^{-\alpha}} \geq \eta_{\text{t}} \right\}$$

$$\overset{(a)}{=} \mathbb{E}_{I_{\Omega_j^n}} \left\{ \Pr\left[h_u > \eta_{\text{t}} u^{\alpha} I_{\Omega_j^n} \right] \right\}$$

$$\overset{(b)}{=} \mathbb{E}_{I_{\Omega_j^n}} \left\{ \exp(-\eta_{\text{t}} u^{\alpha} I_{\Omega_j^n}) \right\}$$

$$= \mathcal{L}_{I_{\Omega_j^n}}(\eta_{\text{t}} u^{\alpha}) \tag{5.10}$$

where (a) holds because of Slivnyak's theorem [3], and where (b) assumes a Rayleigh fading channel. The Laplace transform of $I_{\Omega_j^n}$ is denoted as $\mathcal{L}_{I_{\Omega_j^n}}(s)$.

Similar to [15], the Laplace transform of the partially canceled interference is obtained by applying the probability generating functional (PGFL) and the conditional coverage probability in (5.10) can be written as

$$\mathbb{P}_{\text{s,IC}}(\eta_{\text{t}}, n \mid u) = \exp\left(-2\pi\mu_j \int_{R_{\text{I}}(n)}^{\infty} \frac{v}{1 + \frac{v^{\alpha}}{\eta_{\text{t}} u^{\alpha}}} dv \right) \tag{5.11}$$

where $R_{\text{I}}(n)$ is the distance from the origin to the n-th interferer. By change of variable $w = v^2/(\eta_{\text{t}}^{2/\alpha} u^2)$, we can express (5.11) as

$$\mathbb{P}_{\text{s,IC}}(\eta_{\text{t}}, n \mid u)$$

$$= \exp\left(-\pi\mu_j \eta_{\text{t}}^{2/\alpha} u^2 \int_{b(u)}^{\infty} \frac{1}{1 + w^{\alpha/2}} dw \right)$$

$$= \exp\left(-\pi\mu_j \eta_{\text{t}}^{2/\alpha} C(b(u), \alpha) u^2 \right) \tag{5.12}$$

where $b(u) = R_{\text{I}}(n)^2/\eta_{\text{t}}^{2/\alpha} u^2$. The integration interval of the function $C(b(u), \alpha)$ depends on $R_{\text{I}}(n)$, and therefore, the expectation should be taken with respect to the distance to the n-th interferer. From [139], the probability density function (PDF) of $R_{\text{I}}(n)$ is given by

$$f_{R_{\text{I}}(n)}(r) = \exp(\mu_j \pi r^2) \frac{2(\mu_j \pi r^2)^n}{r \Gamma(n)} \qquad . \tag{5.13}$$

Since the expectation can only be solved by numerical integration, we will approximate $R_{\text{I}}(n)$ by the cancellation radius $R_{\text{I},n} = \sqrt{n/\mu_j \pi}$, which encloses on average n mobile users such that $b(u) \approx R_{\text{I},n}^2/(\eta_{\text{t}}^{2/\alpha} u^2)$. As the SIC procedure cancels at each step the signal with the strongest power, we will

have $u \in [R_{I,n}, \infty)$ on average. To guarantee the maximum average received signal power in the equivalent single-tier network, each user connects to the closest AP such that the distribution of the distance D with respect to the intended base station is given by $f_D(u) = 2\lambda_{eq}\pi u \exp(-\lambda_{eq}\pi u^2)$ [139].[5] To find the unconditional success probability, we take the expectation over u and find (5.9) which concludes the proof. $\qquad\square$

5.3.2 Interference cancellation

In the following, the success probability is derived to decode and cancel the n-th strongest signal, assuming that the interference from the $n - 1$ strongest signals has been previously canceled. This result can be achieved by (i) building on the PGFL and distance dominated order statistics, or (ii) using the truncated stable distribution (TSD). Both approaches lead to an elegant expression of the success probability. However, the approach based on the PGFL is more general, while the approach based on the TSD gives more insight in terms of the convergence of the interference distribution.

Probability generating functional approach

Lemma 3. *Considering a typical AP that successfully canceled the $n - 1$ strongest signals, the success probability to decode the n-th strongest signal is given by*

$$\mathbb{P}_{s,can}(\eta_t, n) = \frac{1}{(1 + \eta_t^{2/\alpha} C(1/\eta_t^{2/\alpha}, \alpha))^n} \quad . \tag{5.14}$$

Proof. In the SIC scheme, interferers are canceled according to descending received signal power. We consider the order statistics $X_{(i)}$ of the signal power to define the probability of successfully decoding the n-th strongest signal. After successfully decoding and subtracting $n - 1$ signals from the received signal, the success probability can be written as

$$\Pr\left[\frac{X_{(n)}}{\sum_{i \in \Omega_j^n} X_{(i)}} \geq \eta_t\right] = \Pr\left[\sum_{i=n+1}^{\infty} X_{(i)} \leq X_{(n)}/\eta_t\right]. \tag{5.15}$$

Since it is unwieldy to characterize the distribution of the sum of order statistics including both geometry and fading, we assume that the order statistics are dominated by the distance, such that $X_{(j)} \geq X_{(i)}$ with $i < j$ is equivalent to $v_j \leq v_i$. When the SoI is the strongest signal from the received multi-user signal corresponding to distance v_j, then the distance of the remaining interferers will be in the interval $[v_j, \infty)$. This approximation

---

[5]Note that this distance distribution is only exact when the point processes of users and base stations are independent.

leads to a remarkable simplification for the calculation of the probability of successfully decoding the n-th interferer conditioned on v_n, which can then be expressed as

$$\mathbb{P}_{\text{s,can}}(\eta_t, n \mid v_n) = \Pr\left(\frac{X_{(n)}}{I_{\Omega_j^n}} \geq \eta_t\right)$$

$$= \exp\left(-\pi\mu_j\eta_t^{2/\alpha}v_n^2 \int_{R_I(n)^2/(\eta^{2/\alpha}v_n^2)}^{\infty} \frac{1}{1+w^{\alpha/2}}dw\right)$$

$$= \exp\left(-\pi\mu_j\eta_t^{2/\alpha}v_n^2 C(1/\eta_t^{2/\alpha}, \alpha)\right) \quad . \tag{5.16}$$

Note that the residual interferers are located outside the circular area with radius v_n, where $R_I(n) = v_n$ and the function $C(1/\eta_t^{2/\alpha}, \alpha)$ is independent of v_n. Using (5.13) and (5.16), we get

$$\mathbb{P}_{\text{s,can}}(\eta_t, n)$$

$$= \int_0^{\infty} \exp\left(-\pi\mu_j\eta_t^{2/\alpha}C(1/\eta_t^{2/\alpha}, \alpha)v_n^2\right) \exp(-\pi\mu_j v_n^2)\frac{2(\pi\mu_j v_n^2)^n}{v_n\Gamma(n)}dv_n$$

$$= \frac{(\pi\mu_j)^n}{\Gamma(n)} \int_0^{\infty} \exp\left(-\pi\mu_j(1+\eta_t^{2/\alpha}C(1/\eta_t^{2/\alpha}, \alpha))v_n^2\right) v_n^{2n-2}dv_n^2$$

$$= \frac{(\pi\mu_j)^n}{\Gamma(n)} \int_0^{\infty} \exp\left(-\pi\mu_j(1+\eta_t^{2/\alpha}C(1/\eta_t^{2/\alpha}, \alpha))w\right) w^{n-1}dw$$

$$= \frac{(\pi\mu_j)^n}{\Gamma(n)}(\pi\mu_j(1+\eta_t^{2/\alpha}C(1/\eta_t^{2/\alpha}, \alpha)))^{-n}\Gamma(n)$$

$$= \frac{1}{(1+\eta_t^{2/\alpha}C(1/\eta_t^{2/\alpha}, \alpha))^n} \quad . \tag{5.17}$$

$$\square$$

It is worthwhile to note that (5.17) is independent of μ_j. This is in line with [129, 130] where the authors prove that the probability to successfully cancel at least n interferers is scale invariant with respect to the density as long as the analysis is restricted to the power-law density case.

Truncated stable distribution approach

In the unbounded path loss model $g_\alpha(x) = \|x\|^{-\alpha}$, the aggregate interference power generated by the interfering nodes scattered over $\mathbb{R}^2$ can be modeled by a skewed stable distribution $I_{\Omega_j} \sim \mathcal{S}(\alpha_I = 2/\alpha, \beta = 1, \gamma = \pi\lambda C_{2/\alpha}^{-1}\mathbb{E}\{P_i^{2/\alpha}\})$ [2]. Since the singularity at 0 in the unbounded path loss model can have significant effects on the interference distribution [143], a bounded path loss model based on the truncated stable distribution (TSD)

has been proposed to avoid the singularity for zero distance by restricting the interferers to a ring structure with a minimum range $d_{\min}$ and maximum range $d_{\max}$ [13]. The ring structure can be applied similarly to represent the guard zone around the victim receiver in the SIC scenario, where the inner radius corresponds to the interference cancellation radius and $d_{\max} = \infty$. In the bounded path loss model, the aggregate interference power is distributed according to a skewed TSD with CF given by [114]

$$\psi_{I_{\Omega_j^n}}(j\omega) = \exp\left(\gamma'\Gamma(-\alpha_I)\left[(g - j\omega)^{\alpha_I} - g^{\alpha_I}\right]\right) \tag{5.18}$$

where the parameters α_I, g, and γ' determine the shape of the TSD.

Lemma 4. *For $\alpha = 4$, the probability to decode and cancel the n-th strongest signal after $n - 1$ successful cancellations is given by*

$$\mathbb{P}_{\text{s,can}}(\eta_t, n | \alpha = 4) = \frac{1}{(\sqrt{9/4 + 3\eta_t} - 1/2)^n} \tag{5.19}$$

Proof. See Appendix A.6. $\qquad\square$

Note that (5.19) has the same structure as (5.17) and similarly shows that the probability of canceling the n-th interferer is independent of the interferer density. The use of the TSD approach is beneficial since it can provide insight how fast the aggregate network interference converges to a Gaussian distribution by calculating the kurtosis after canceling n interferers. Conditioned on the exclusion radius r, we have

$$\gamma_2 = \frac{\kappa(4)}{\kappa(2)^2} = \frac{6(\alpha - 1)^2}{(2\alpha - 1)} \frac{1}{\mu_j \pi r^2} \tag{5.20}$$

where $\gamma_2 = 0$ represents the case of a normal distribution. By averaging over r, the kurtosis after canceling n interferers is given by

$$\begin{aligned}
\gamma_2(\alpha, n) &= \frac{6(\alpha - 1)^2}{(2\alpha - 1)} \int_0^\infty \frac{1}{\mu_j \pi r^2} \exp(-\mu_j \pi r^2) \frac{2(\mu_j \pi r^2)^n}{r\Gamma(n)} \mathrm{d}r \\
&= \frac{6(\alpha - 1)^2}{(2\alpha - 1)} \frac{1}{\Gamma(n)} \int_0^\infty \exp(-\mu_j \pi r^2)(\mu_j \pi r^2)^{n-2} \mathrm{d}\mu_j \pi r^2 \\
&= \frac{6(\alpha - 1)^2}{(2\alpha - 1)} \frac{\Gamma(n - 1)}{\Gamma(n)} \\
&= \frac{6(\alpha - 1)^2}{(2\alpha - 1)} \frac{1}{n - 1}.
\end{aligned} \tag{5.21}$$

This expression yields useful insight in the convergence rate of the aggregate network interference to a Gaussian distribution as a function of the number of canceled interferers.

5.3.3 Success probability with SIC

Theorem 4. *The coverage probability $\mathbb{P}_{\text{s,SIC}}$ for a receiver that applies SIC with a maximum of n interferers being canceled is given by*

$$\mathbb{P}_{\text{s,SIC}}(\eta_{\text{t}}, n) \approx \mathbb{P}_{\text{s}}(\eta_{\text{t}}) + \sum_{i=1}^{N} \left(\prod_{n=0}^{i-1} (1 - \mathbb{P}_{\text{s,IC}}(\eta_{\text{t}}, R_{\text{I},n})) \right)$$
$$\times \left(\prod_{n=1}^{i} \mathbb{P}_{\text{s,can}}(\eta_{\text{t}}, n) \right) \mathbb{P}_{\text{s,IC}}(\eta_{\text{t}}, R_{\text{I},i}) \quad (5.22)$$

where $\mathbb{P}_{\text{s,IC}}(\eta_{\text{t}}, R_{\text{I},n})$ and $\mathbb{P}_{\text{s,can}}(\eta_{\text{t}}, n)$ are given in (5.9) and (5.14), respectively.

Proof. The proof follows directly from the definition of the sequence of events in (5.4) and the results of $\mathbb{P}_{\text{s,IC}}$ and $\mathbb{P}_{\text{s,can}}$ in Lemma 2 and 3. $\qquad\square$

We provide now some numerical results that illustrate the effectiveness of SIC for the association policy based on the maximum average received signal power. We consider a network of APs arranged over a two-dimensional plane with density $\lambda_{\text{m}} = 10^{-4}$ /m². We assume a fully loaded network, where each cell allocates at a given time every subchannel to an active user. Hence, the density of mobile users on subchannel j is given by $\mu_j = 10^{-4}$/m². In Fig. 5.2, $\mathbb{P}_{\text{s,can}}$ is depicted for different values of the threshold as a function of the order of the canceled interferer. The figure illustrates that the probability to cancel the n-th interferer decreases quickly with n and with increasing target SIR. Simulation results are added to validate the model. When the received signal power is ordered only with respect to the distance, the simulations coincide with the analytical results based on the PGFL approach and the TSD approach. Moreover, a good agreement between analysis and simulations is achieved even when the ordering is performed based on the joint effect of distance and fading. From the numerical results depicted in Fig. 5.2, we observe that the approximation deteriorates for lower values of the SIR threshold. As the SIR threshold decreases, we resort to values drawn from the central part of the PDF of the SINR, whereas the theorem of Breiman, necessary to assume that the order statistics are dominated by the distance, holds for the tail of the distribution.

Figure 5.3 illustrates the success probability including SIC as a function of the SINR target for different values of the maximum number of cancellations. To validate our analysis, we compare the results with bounds that have been proposed in [123] for the scenario of spectrum sharing between cellular and mobile ad hoc networks (MANET), which can be shaped to represent a single-tier cellular network. In this work, the authors present bounds based on the separation of interferers into groups of strong and weak interferers where each strong interferer alone can cause outage, accounting both for
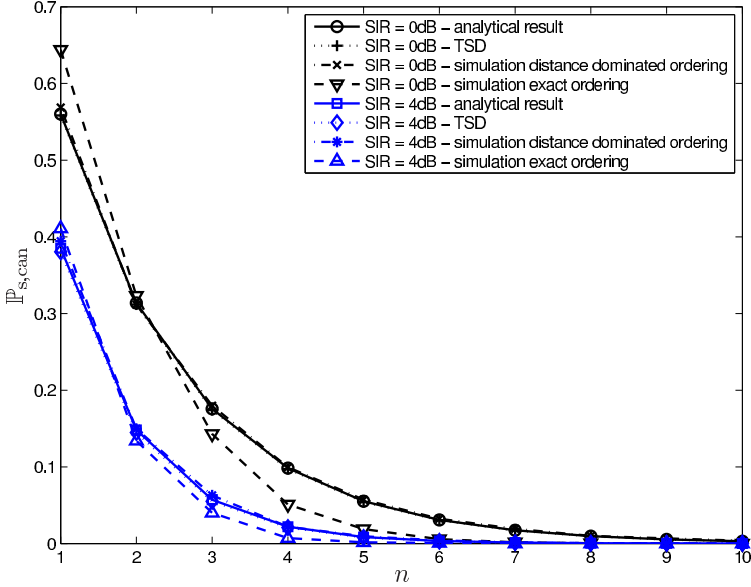
Figure 5.2: Comparison of $\mathbb{P}_{s,can}$ using analytical and simulation results.

the effects of the spatial distribution of the nodes and the fading affecting each link. Interference cancellation is performed in descending order or received signal power, and the received power of each interferer intended for cancellation must exceed the SoI signal power multiplied with a factor $\kappa > 1$. From Fig. 5.3, we observe that the curves derived by our analysis strictly fall within the bounds proposed in [123]. Furthermore, we observe a modest improvement in the success probability when SIC is applied for threshold values lower than 2 dB, whilst for higher threshold values this improvement is negligible. The numerical results illustrate that the cancellation of the first order interferer has a sensible effect on the receiver performance, while the cancellation of higher order interferers yields a marginal improvement of the success probability.

The results presented in this section provide a guideline for the SIC computational requirements by investigating the performance gain from the cancellation of n interferers. Although applicable for UL and DL transmissions, SIC is particularly attractive in UL since it harnesses the processing power of access points to cancel strong interfering signals from nearby transmitters. However, as only the first cancellation has a significant effect on the performance, the computational requirements related to SIC are limited and hence, SIC qualifies also for DL transmissions. Following the association policy where the nodes connect to the AP offering the highest average received signal power, the overall performance gain of SIC is however modest for realistic values of the target SINR. In the following
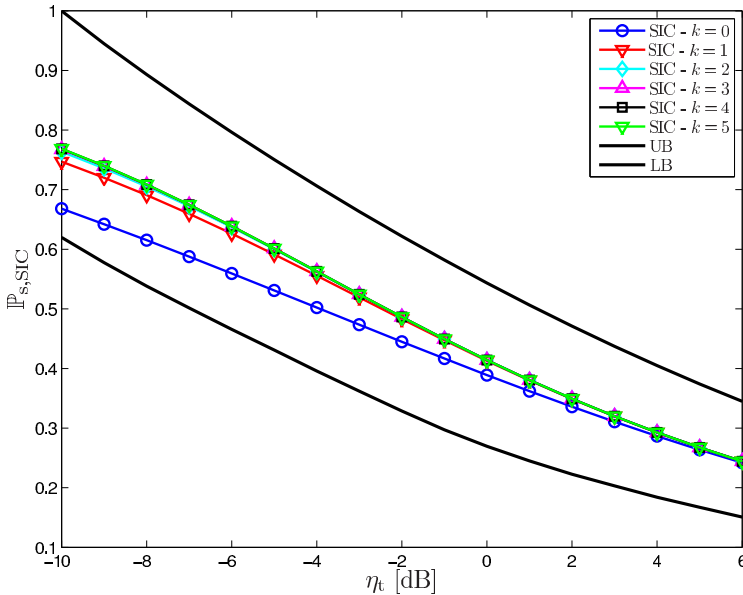
Figure 5.3: Coverage probability in the presence of SIC for different values of the maximum number of cancellations. The blue curve represents the success probability when no IC technique is used.

section, we present several association policies where the performance gain of SIC is far more appreciable.

5.4 Association policies and SIC gains

In this section, we analyze multi-tier networks with different association policies. Since we aim to deepen the understanding of heterogeneous networks using concepts such as coverage area and load, we will not resort to the single-tier stochastic equivalent of the network if this results in a loss of physical insight related to the differences between the tiers.

5.4.1 Minimum load association policy

Considering fairness between users, in case of data sensitive applications it can be preferential to connect to the AP with the lowest load, rather than to the AP that offers the highest SIR. The same observation holds for networks that apply a load balancing policy and where users are actively transferred to lightly loaded APs different from the AP of their own Voronoi cell [133]. In the following, we consider the association policy where a user connects to the AP with the lowest load for a given connectivity range R_{con} with respect

to the user. In this scenario, the performance metric of interest is the rate per user, which reflects the quality of service (QoS) and depends on the AP load, defined as the number of users M connected to the AP. This scenario leads to interesting trade-offs between APs where the loss of SIR can be compensated by the gain of available resource blocks per user. We consider a single tier network and we model explicitly the load of the APs by considering the marked PPP $\tilde{\Phi} = \{(X_i, L_i) \mid X_i \in \Phi(\lambda), L_i \sim F_L(l)\}$, with L_i the load of X_i and $F_L(l)$ the load distribution. We consider a typical user at the origin of the Euclidean plane and we compare the performance of the max-SIR association policy with the minimum load association policy for DL transmissions in terms of rate per user. Let $\mathcal{R}$ denote the rate per user and we define the coverage probability as the CCDF of the rate $\mathbb{P}_c(\rho) = \mathbb{P}[\mathcal{R} > \rho]$ [135], which is given by

$$\mathbb{P}_c(\rho) = \Pr\left[\frac{1}{M}\log(1 + \text{SIR}) > \rho\right]$$
$$= \Pr[\text{SIR} > 2^{M\rho} - 1] = \mathbb{E}_M[\mathbb{P}_s(2^{M\rho} - 1)] \quad . \tag{5.23}$$

To calculate the coverage probability, we need to characterize the distribution of M. The load of a cell depends on the area distribution of the Voronoi cell, for which an approximation has been proposed in [144]. Using this approximation, the probability mass function of M is given by [135]

$$f_M(m) = \Pr[M = m] = \frac{3.5^{3.5}}{m!} \frac{\Gamma(m + 4.5)}{\Gamma(3.5)} \left(\frac{\mu_j}{\lambda}\right)^m \left(3.5 + \frac{\mu_j}{\lambda}\right)^{-(m+4.5)}. \tag{5.24}$$

In case of the max-SIR policy, the coverage probability conditioned on the number of associated users is given by

$$\mathbb{P}_c^{(\text{MAX SIR})}(\rho|M) = \int_0^\infty 2\lambda\pi r \exp(-\pi\lambda r^2(1 + \varsigma^{2/\alpha}C(1/\varsigma^{2/\alpha}, \alpha)))\mathrm{d}r$$
$$= \frac{1}{1 + \varsigma^{2/\alpha}C(1/\varsigma^{2/\alpha}, \alpha)} \tag{5.25}$$

where $\varsigma = 2^{M\rho} - 1$. Deconditioning over M, the rate coverage can be written as

$$\mathbb{P}_c^{(\text{MAX SIR})}(\rho) = \sum_{m \geq 0} f_M(m)\mathbb{P}_c^{(\text{MAX SIR})}(\rho|m + 1) \tag{5.26}$$

where the load of the cell under consideration includes the admitted user.

Lemma 5. *For a typical user that connects to the AP with the lowest load within the range R_{con}, the coverage probability is given by*

$$\mathbb{P}_c^{(\text{MINLOAD})}(\rho) = \sum_{m \geq 0} f_{M_{(1)}}(m)\mathbb{P}_c^{(\text{MINLOAD})}(\rho|m + 1) \tag{5.27}$$

where $f_{M_{(i)}}(m)$ represents the probability mass function (PMF) of the i-th order statistic of the load.

Proof. For the minimum load association policy, the typical user is appointed to the AP with the lowest load which is uniformly distributed over $b(0, R_{\mathrm{con}})$ with distance distribution $f_R(r) = 2r/R_{\mathrm{con}}^2$. We assume that there are $N = \lfloor \lambda \pi R_{\mathrm{con}}^2 \rfloor$ APs within the connectivity range. The coverage probability for the minimum load scheme conditioned on the load is given by

$$
\begin{aligned}
\mathbb{P}_{\mathrm{c}}^{(\mathrm{MINLOAD})}(\rho | M) &= 1/R_{\mathrm{con}}^2 \int_0^{R_{\mathrm{con}}^2} \exp(\pi \lambda \varsigma^{2\alpha} C(0, \alpha) r^2) 2r \mathrm{d}r \\
&= \frac{1 - \exp(-\pi \lambda \varsigma^{2/\alpha} C(0, \alpha) R_{\mathrm{con}}^2)}{\pi \lambda \varsigma^{2/\alpha} C(0, \alpha) R_{\mathrm{con}}^2}.
\end{aligned}
\tag{5.28}
$$

The i-th order statistic of the load is given by [138]

$$
f_{M_{(i)}}(m) = \frac{1}{\mathcal{B}(i, M - i + 1)} \int_{F_M(m-1)}^{F_M(m)} w^{i-1}(1 - w)^{m-i} \mathrm{d}w
\tag{5.29}
$$

where $\mathcal{B}(a, b)$ represents the beta function. Deconditioning (5.28) with respect to the first order statistic of the load, the proof is concluded. $\qquad \square$

5.4.2 Maximum instantaneous received signal power

Connecting to the AP which yields instantaneously the highest SIR can be of interest for a mobile node to obtain the maximum data rate [134], or to reduce the local delay $\tau = \mathbb{E}\{1/\mathbb{P}_{\mathrm{s}}(\eta_{\mathrm{t}})\}$, which is defined as the mean time until a packet is successfully received [145]. In the following, we will evaluate how SIC can affect the UL success probability when the maximum instantaneous SIR policy is applied.

In this scenario, we assume that (i) the current network state and load per AP is based on mobile node connecting to the AP which provides the maximum DL average received signal power, (ii) all tiers have equal SIR target values, and (iii) the network operates in time division duplex (TDD) mode, such that we can assume channel reciprocity, i.e. the maximum SIR in DL is also the max SIR in UL. We first determine the node densities μ_k connected to tier k, based on the maximum DL average received signal power. This approach is realistic since it does not require extra signaling from the APs. The user density is given by $\mu_k = p_{\mathrm{a},k}\mu$, where $p_{\mathrm{a},k}$ is the association

probability to tier k given by

$$
\begin{aligned}
p_{\mathrm{a},k} &= \Pr\left\{\bigcap_{i\neq k}\left(\max_{\Phi_k}\mathrm{SIR}_j > \max_{\Phi_i}\mathrm{SIR}_j\right)\right\} \\
&= \prod_{i\neq k}\Pr\left\{P_k x_k^{-\alpha} > P_i x_i^{-\alpha}\right\} \\
&= \prod_{i\neq k}\Pr\left\{x_i > x_k(P_i/P_k)^{1/\alpha}\right\} \\
&= \int_0^{\infty}\exp\left(-\pi x_k^2\sum_{i\neq k}\lambda_i(P_i/P_k)^{2/\alpha}\right)2\pi\lambda_k x_k\exp(-\lambda_k\pi x_k^2)\mathrm{d}x_k \\
&= \frac{\lambda_k}{\sum_{i\in\mathcal{K}}\lambda_i\left(\frac{P_i}{P_k}\right)^{2/\alpha}}
\end{aligned}
\tag{5.30}
$$

where x_i represents the distance to the closest AP of tier i and we consider that the maximum SIR corresponds to the maximum received signal power. In the following lemma, we define the outage probability for UL transmissions in a multi-tier heterogeneous network without IC capabilities.

Lemma 6. *If a typical user connects to the AP which yields the maximum instantaneous SIR, then the outage probability is given by*

$$
\mathbb{P}_{\mathrm{out}}(\eta_{\mathrm{t}},\boldsymbol{\lambda},\boldsymbol{\mu},\mathbf{Q}) = \exp\left(\frac{-\sum_{j=1}^{K}\lambda_j Q_j^{2/\alpha}}{\eta_{\mathrm{t}}^{2/\alpha}C(0,\alpha)\sum_{i=1}^{K}\mu_i Q_i^{2/\alpha}}\right).
\tag{5.31}
$$

Proof. For mobile nodes applying the maximum instantaneous SIR association policy, the outage probability is given by

$$
\begin{aligned}
\mathbb{P}_{\mathrm{out}}(\eta_{\mathrm{t}},\boldsymbol{\lambda},\boldsymbol{\mu},\mathbf{Q}) &= \Pr\{\max_{k\in\mathcal{K},x_{k,i}\in\Phi_k}\mathrm{SIR}_j(u\to x_{k,i}) < \eta_{\mathrm{t}}\} \\
&= \bigcap_{k\in\mathcal{K},x_{k,i}\in\Phi_k}\Pr\{\mathrm{SIR}_j(u\to x_{k,i}) < \eta_{\mathrm{t}}\} \\
&\overset{(a)}{=} \bigcap_{k\in\mathcal{K}}\mathbb{E}_{\Phi_k}\left\{\prod_{x_{k,i}\in\Phi_k}\mathbb{P}^{!u}\left(\frac{Q_k h_u u^{-\alpha}}{I_{\Omega_j}} < \eta_{\mathrm{t}}\right)\right\} \\
&= \prod_{k\in\mathcal{K}}\mathbb{P}_{\mathrm{out}}^{(k)}(\eta_{\mathrm{t}})
\end{aligned}
\tag{5.32}
$$

where $\mathbb{P}_{\mathrm{out}}^{(k)}$ is the outage probability of a typical user connected to the AP of tier k that yields the maximum instantaneous SIR. Note that in (a) we assume

that all $\text{SIR}_j(u \to x_{k,i})$ are independent.[6] We can further develop $\mathbb{P}_{\text{out}}^{(k)}$ as

$$
\begin{aligned}
\mathbb{P}_{\text{out}}^{(k)}(\eta_t, \lambda_k, \boldsymbol{\mu}, \mathbf{Q}) &= \mathbb{E}_{\Phi_k} \left[\prod_{x_{k,i} \in \Phi_k} 1 - \mathbb{E}_{I_\Omega} \left[\exp\left(-\eta_t \frac{u^\alpha}{Q_k} I_{\Omega_j} \right) \right] \right] \\
&= \exp\left(-2\pi\lambda_k \int_0^\infty \mathbb{E}_{I_{\Omega_j}} \left[\exp\left(-\eta_t \frac{u^\alpha}{Q_k} I_{\Omega_j} \right) \right] u \mathrm{d}u \right) \\
&= \exp\left(-2\pi\lambda_k \int_0^\infty \exp\left(-\pi\eta_t^{2/\alpha} C(0,\alpha) u^2 \sum_{i=1}^{K} \mu_i \left(\frac{Q_i}{Q_k} \right)^{2/\alpha} \right) u \mathrm{d}u \right) \\
&= \exp\left(\frac{-\lambda_k}{\eta_t^{2/\alpha} C(0,\alpha) \sum_{i=1}^{K} \mu_i (Q_i/Q_k)^{2/\alpha}} \right).
\end{aligned}
\tag{5.33}
$$

Combining (5.32) and (5.33), the proof is concluded. □

From Lemma 6, we can conclude that the density of the superposition of network nodes with different transmit powers is equal to a weighted sum of the densities $\tilde{\mu}_k = \sum_{i=1}^{K} \mu_i (Q_i/Q_k)^{2/\alpha}$.

Lemma 7. *The success probability for UL transmissions with SIC is given by*

$$
\begin{aligned}
\mathbb{P}_s^{\text{SIC}}(\eta_t, \boldsymbol{\lambda}, \boldsymbol{\mu}, \mathbf{Q}) &= 1 - \mathbb{P}_{\text{out}}(\eta_t, \boldsymbol{\lambda}, \boldsymbol{\mu}, \mathbf{Q}) \\
&\quad \times \prod_{k \in \mathcal{K}} \left\{ \exp\left(-2\pi\lambda_k \int_0^\infty \mathbb{P}_{s,\text{SIC}}^{\text{gain}}(\eta_t, N|u) u \mathrm{d}u \right) \right\}
\end{aligned}
\tag{5.34}
$$

where

$$
\begin{aligned}
\mathbb{P}_{s,\text{SIC}}^{\text{gain}}(\eta_t, N|u) &= \sum_{i=1}^{N} \left(\prod_{n=0}^{i-1} \left[1 - \exp(-\pi\eta_t^{2/\alpha} C(R_{I,n}^2/\eta_t^{2/\alpha} u^2, \alpha) \tilde{\mu}_j u^2) \right] \right) \\
&\quad \times \left(\prod_{n=1}^{i} \mathbb{P}_{s,\text{can}}(\eta_t, n) \right) \exp(-\pi\eta_t^{2/\alpha} C(R_{I,i}^2/\eta_t^{2/\alpha} u^2, \alpha) \tilde{\mu}_j u^2)
\end{aligned}
\tag{5.35}
$$

Proof. When a typical user is associated to the AP corresponding to the highest instantaneous SIR, we can write

$$
\mathbb{P}_{\text{out}}^{\text{SIC}}(\eta_t, \boldsymbol{\lambda}, \boldsymbol{\mu}, \mathbf{Q}) = \bigcap_{k \in \mathcal{K}} \mathbb{E}_{\Phi_k} \left\{ \prod_{x_{k,i} \in \Phi_k} \mathbb{P}\left(\frac{Q_k h_u u^{-\alpha}}{I_{\Omega_j^n}} < \eta_t \right) \right\}
\tag{5.36}
$$

---

[6]In [134], the authors limit the range of the SIR threshold to $\eta_t > 1$ to avoid the dependence, while an exact approach is proposed in [146] where the joint SINR distribution is presented.

where $\mathbb{P}(Q_k h_u u^{-\alpha}/I_{\Omega_j^n} < \eta_t)$ is the outage probability conditioned on the distance u and n interferers being canceled. From (5.36), we can rewrite as

$$
\mathbb{P}_{\text{out}}^{\text{SIC}}(\eta_t, \boldsymbol{\lambda}, \boldsymbol{\mu}, \mathbf{Q}) = \prod_{k \in \mathcal{K}} \left\{ \exp \left(-2\pi\lambda_k \int_0^\infty \underbrace{\mathbb{E}_{I_{\Omega_j^n}}[\exp(-\eta_t u^{-\alpha} I_{\Omega_j^n}/Q_k)]}_{\mathbb{P}_{\text{s,SIC}}^{(k)}(\eta_t, n|u)} u\, du \right) \right\}
$$
(5.37)

where the typical user is assumed to be at the origin and the APs at a distance u from the origin. Still, the interference cancellation radius for each AP is considered with respect to the AP under consideration, which does not induce any problems since we consider motion-invariant point processes. Therefore, the success probability $\mathbb{P}_{\text{s,SIC}}^{(j)}(\eta_t, n|u)$ referenced to tier j is invariant under translation. The success probability including SIC conditioned on the distance can further be written as

$$
\begin{aligned}
\mathbb{P}_{\text{s,SIC}}^{(j)}(\eta_t, n|u) =& \mathbb{P}_s(\eta_t|u) + \sum_{i=1}^N \left(\prod_{n=0}^{i-1} (1 - \mathbb{P}_{\text{s, IC}}(\eta_t, R_{\text{I},n}|u)) \right) \\
& \times \left(\prod_{n=1}^i \mathbb{P}_{\text{s,can}}(\eta_t, n) \right) \mathbb{P}_{\text{s,IC}}(\eta_t, R_{\text{I},i}|u) \\
=& \exp(-\pi\eta_t^{2/\alpha} C(0, \alpha)\tilde{\mu}_j u^2) \\
& + \sum_{i=1}^N \left(\prod_{n=0}^{i-1} \left[1 - \exp(-\pi\eta_t^{2/\alpha} C(R_{\text{I},n}^2/\eta_t^{2/\alpha} u^2, \alpha)\tilde{\mu}_j u^2) \right] \right) \\
& \times \left(\prod_{n=1}^i \mathbb{P}_{\text{s,can}}(\eta_t, n) \right) \exp(-\pi\eta_t^{2/\alpha} C(R_{\text{I},i}^2/\eta_t^{2/\alpha} u^2, \alpha)\tilde{\mu}_j u^2).
\end{aligned}
$$
(5.38)

Note that in (5.38) the single-tier equivalent network referenced to the transmission power of tier j is used. Substituting (5.38) in (5.37), the proof is concluded. □

Considering network infrastructure with SIC capabilities, the typical user will connect to the AP that offers the highest instantaneous SIR after canceling n interferers. The maximum instantaneous SIR association policy that accommodates for SIC, does not necessarily connect the mobile node to the AP which yields the maximum average SIR nor to the closest one.

5.4.3 Range expansion

While the higher tiers in a multi-tier network are intended to offload data traffic from the macrocell network, this target is impeded considerably due

to the relatively small coverage area of the higher tiers, which are usually denoted as small cells. To encourage users to connect to the small cells, range expansion has been proposed which applies an association policy based on a biased received signal power [79]. Although range expansion mitigates the UL cross-tier interference, users in DL experience bad signal conditions in the range expanded areas since they are not connected to the base station that provides the highest average SIR. It is therefore meaningful to study the benefit of SIC in DL for those users located in the range expanded areas (REAs). To calculate the success probability of the users belonging to the REA, we need to define the distance distribution of these users with respect to the serving AP. The following lemma is an extension of [147] for a *K*-tier network.

Lemma 8. *Let $B = \{b_k\}$ be the set of biases corresponding to each tier. The distance distribution of users located in the REA to the serving AP is given by*

$$f_{X_k^{(\mathrm{RE})}}(x) = \frac{2\pi\lambda_k}{p_{\mathrm{a},k}^{(\mathrm{RE})}} x \left[\exp\left(-\pi \sum_{i\in\mathcal{K}} \lambda_i \left(\frac{P_i}{P_k} \frac{b_i}{b_k} \right)^{2/\alpha} x^2 \right) \right.$$
$$\left. - \exp\left(-\pi \sum_{i\in\mathcal{K}} \lambda_i \left(\frac{P_i}{P_k} \right)^{2/\alpha} x^2 \right) \right] \quad (5.39)$$

where the association probability to the REA of tier k is $p_{\mathrm{a},k}^{(\mathrm{RE})} = 1 - \sum_{i\neq k} p_{\mathrm{a},i}(b) - p_{\mathrm{a},k}(B \,|\, b_k = 1)$ and the association probability to the k-th tier is given by

$$p_{\mathrm{a},k}(B) = \frac{\lambda_k}{\sum_{i\in\mathcal{K}} \lambda_i \left(\frac{P_i}{P_k} \frac{b_i}{b_k} \right)^{2/\alpha}} \quad (5.40)$$

For the proof, we refer to [148] and [147]. Note that a user, which belongs without biasing to tier $i \neq k$, is located in the REA $C_k^{(\mathrm{RE})}$ of tier k if the relationship $P_k x_k^{-\alpha} < P_i x_i^{-\alpha} < b_k P_k x_k^{-\alpha}$ holds. In order to calculate the benefit of canceling the strongest interferer for the users located in the REA, we provide the following lemma.

Lemma 9. *After canceling the strongest AP, the success probability of the users*

located in $C_k^{(\text{RE})}$ is given by

$$\mathbb{P}_{\text{s,IC}}(\eta_{\text{t}}, 1 \mid x_k \in C_k^{(\text{RE})}) =$$

$$\frac{1}{p_{\text{a},k}^{(\text{RE})}} \left[\frac{1}{\sum_{i \in \mathcal{K}} \left(\frac{\lambda_i}{\lambda_k} \right) \left(\frac{P_i}{P_k} \right)^{2/\alpha} \left(\eta_{\text{t}}^{2/\alpha} C((1/\eta_{\text{t}})^{2/\alpha}, \alpha) + \left(\frac{b_i}{b_k} \right)^{2/\alpha} \right)} \right.$$

$$\left. - \frac{1}{\sum_{i \in \mathcal{K}} \left(\frac{\lambda_i}{\lambda_k} \right) \left(\frac{P_i}{P_k} \right)^{2/\alpha} \left(\eta_{\text{t}}^{2/\alpha} C((1/\eta_{\text{t}})^{2/\alpha}, \alpha) + 1 \right)} \right]. \quad (5.41)$$

Proof. See Appendix A.7 □

From Lemma 9, the bias factors of the different tiers can be determined to guarantee a given performance for the mobile users belonging to the REA.

5.5 Numerical Results

In this section, we present some numerical results that illustrate that SIC, although not very effective in networks applying the association policy based on the maximum average received signal power, can have distinct advantages in scenarios with other association policies. Figure 5.4 depicts the coverage probability and compares the max-SIR association policy with the minimum load association policy. From the numerical results, we see that the coverage probability decreases significantly for the minimum load policy when no SIC is applied. This means that the loss in SIR cannot be compensated by the lower load of the AP. However, when SIC is applied ($n = 1$), the coverage probability is comparable with that of the max-SIR policy. From this figure, we conclude that when SIC is applied, users can be offloaded to nearby APs without loss of capacity, which paves the way for more advanced load balancing techniques.

Figure 5.5 shows the success probability for a typical user that connects to the AP that provides the highest instantaneous SIR, with and without SIC. We considered a two-tier network with densities $\lambda_1 = 10^{-5}\text{m}^{-2}$ and $\lambda_2 = 10^{-4}\text{m}^{-2}$, respectively, while the user density is given by $\mu = 10^{-4}\text{m}^{-2}$. The ratio between transmission powers is given by $P_1/P_2 = 10$ and $Q_1/Q_2 = 10$. From the figure, we observe an increase of the success probability up to 20% in the range of interest, i.e. for values of the threshold above $0\,\text{dB}$. However, this scheme requires additional signaling between the APs to connect the user to the AP which provides instantaneously the highest SIR, which limits the practical feasibility.

Figure 5.6 depicts the success probability of a typical user in the REA in a two-tier network with densities $\lambda_1 = 10^{-5}\text{m}^{-2}$ and $\lambda_2 = 10^{-4}\text{m}^{-2}$
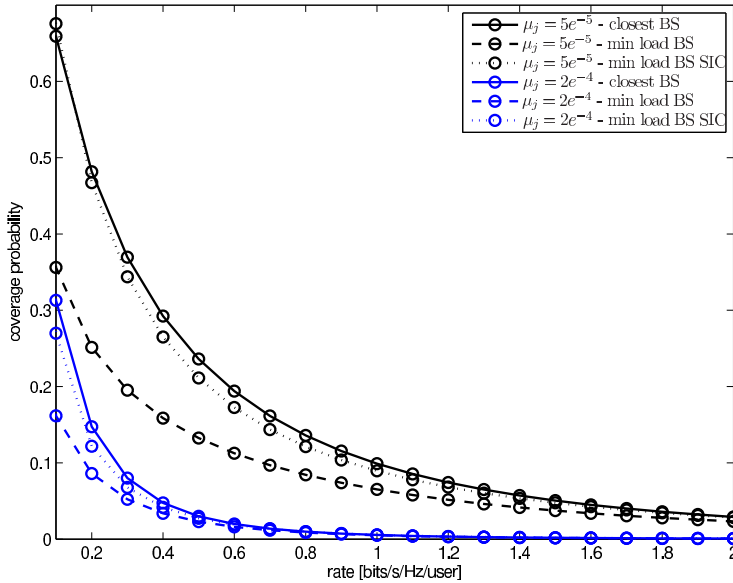
Figure 5.4: The coverage probability is depicted for the max-SIR association policy (solid lines), the minimum load association policy (dashed lines), and the minimum load policy with SIC (dotted lines) for $\lambda = 10^{-5}$ and $\alpha = 4$.
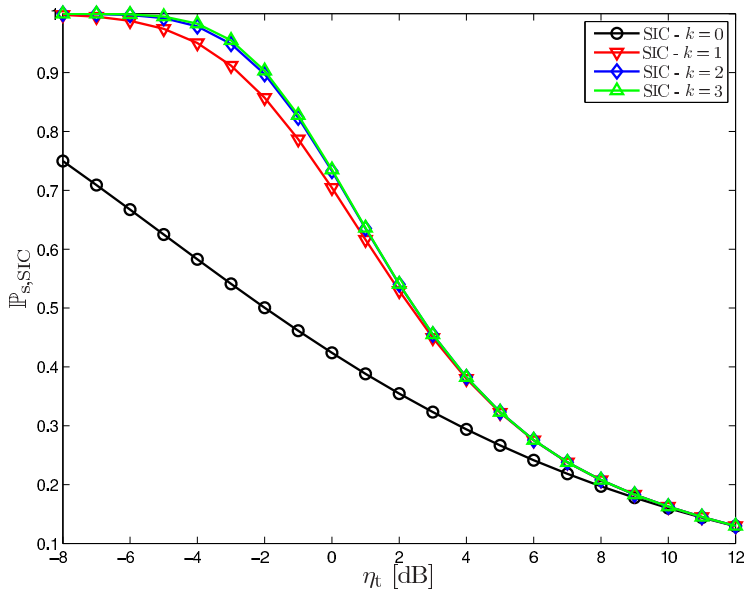
Figure 5.5: The gain in success probability that can be achieved by successively canceling interferers.
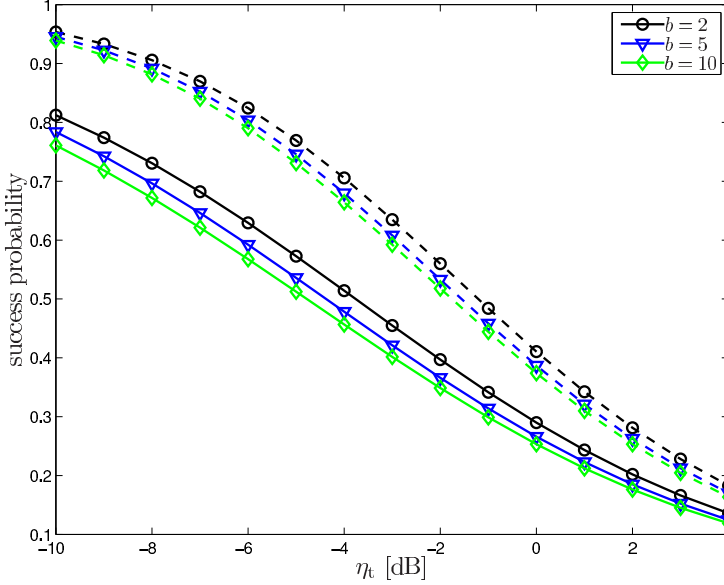
Figure 5.6: Success probability for users belonging to the range expansion region. Solid lines represent the success probability without interference cancellation, whereas the dashes lines represent the success probability when the closest AP is canceled. The power ratio $P_1/P_2 = 10$.

for different values of the range expansion factor b. The figure illustrates how the success probability decreases as the REA gets larger with increasing values of b. Moreover, from the numerical results we observe that the increase of success probability due to SIC is substantial. This scenario is a realistic example where SIC can provide high performance gain.

5.6   Conclusions

In this chapter, we developed a probabilistic framework for the performance analysis of multi-tier heterogeneous networks with SIC capabilities. The framework accounts for the consecutive steps of the IC scheme, network topology, propagation effects, and the association policy. For users connected to the AP that provides the maximum average received signal power, performance benefits diminish quickly with the number of cancellations n and are modest for realistic values of the SIR. Yet, we presented several deployment scenarios for future multi-tier networks where SIC yields distinct performance gains, such as for the minimum load association policy, the maximum instantaneous SIR policy, and range expansion. The proposed framework can be applied to define the achievable performance of

multi-tier networks with SIC capabilities. Future work to extend the current framework will include imperfect interference cancellation and will model the decreasing cost of APs of higher tiers considering for each tier a different maximum number of interferer cancellations.

Chapter 6

Conclusions and outlook

In this chapter, we summarize the contributions made in the dissertation and highlight possible extensions for future work.

6.1 Contributions

Owing to the proliferation of wireless technologies, network architectures go through drastic transformations that call for novel ways to model and evaluate system performance. The main objective of this dissertation is to include the spatial randomness of the network nodes into the performance evaluation of problems related to detection, communication, and energy efficiency. Stochastic geometry allows us to answer the research questions that were introduced in Chapter 1 and to develop an analytical toolset to assess the detection performance, energy efficiency, and interference management in networks with multiple concurrent transmissions. As this toolset incorporates the innate relationship between the network spatial statistics and several performance metrics, it can be used to refine the understanding of future network design.

The first set of research problems is related to detection theory. In Chapter 3, we applied a unified approach for single and multiple interferers to characterize the detection performance in terms of probability of detection and probability of false alarm. Focusing on the scenario of GNSS signal acquisition, the detection of CDMA signals has been considered starting from the single interferer case. Closed form expressions for the CF of the decision variable were presented, such that the detection performance can be calculated by means of integration. The analysis accounts for thermal noise, interference, channel fading, as well as two detection strategies. The developed framework is flexible enough to account for different fading distributions for the SoI and the interference, which is practical in case of GNSS. By addressing different detection schemes, we concluded that

the GLRT strategy outperforms the MRT strategy. Given the current proliferation of wireless devices, we extended the analysis to aggregate network interference. The framework is able to capture the deployment density, transmission power, and fading distribution of the interferers. In Chapter 4, we explored the potential of a distributed sleep mode strategy to reduce the energy consumption of the small cell tier. Given that the energy consumption is closely related to the correct sensing of user presence within the small cell, we characterized the detection performance for a typical user considering energy detection and the presence of multiple interferers. Furthermore, we established a fundamental limit of the interferer node density beyond which no robust detection is possible. For interfering node densities greater than this limit, which we called the interference wall, the uncertainty prohibits to distinguish between SoI and interference. Finally, using large deviations theory we presented a convergence analysis of the false alarm probability as a function of the sensing time. We showed how the $\mathbb{P}_{fa}$ decay rate is affected by the the interfering node density and transmission power. In conclusion, we systematically included the network geometry in the analysis of the detection performance, robustness, and convergence and we demonstrated the pivotal role of spatial randomness to evaluate signal detection.

The second set of research problems is related to energy efficiency. The need to respond to the exponential increase in mobile data demand is at odds with the requirement to decrease the network energy consumption. This apparent contradiction requires a unifying framework that accommodates for the novel features of future networks. In Chapter 4, we formulated an average network energy consumption model for the cognitive SAPs that are located within the Voronoi cell of an MBS. The energy consumption model accounts for the sleeping policy, detection performance, sensing strategy, uncoordinated network interference, and geometry of base stations and users. Furthermore, we derived tractable expressions for the aggregate throughput and capacity that can be offloaded by the small cells within an MBS Voronoi cell. We casted the trade-off between energy consumption and capacity as a set of optimization problems, which resulted in a tool to correctly set sensing time and sensing probability whilst guaranteeing user QoS. We illustrated how the proposed framework can be used in practice to trade-off the energy consumption and the aggregate traffic offload, taking into account the network load. Including the geometry of the network nodes in the evaluation of the energy efficiency, the numerical results demonstrated that a distributed sleep mode strategy can substantially reduce the small cell energy consumption.

The third set of research problems focuses on interference cancellation to increase the SINR. In Chapter 5, we developed a probabilistic framework

to predict the performance improvement related to SIC in multi-tier heterogeneous networks. To this end, we characterized the success probability to cancel the n-th strongest interferer, which can be represented as a surprisingly simple function of the SIR target value, path loss exponent, and the cancellation order n. This result was obtained considering the intrinsic connection between the IC scheme and the network geometry, in particular the order statistics of the received signal power. We described the performance of SIC for uplink communications when users are connected to the access point that provides the maximum average SIR, jointly accounting for the sequence of events in the SIC scheme, topology of the network nodes, and channel fading. For this association policy, our results indicate that SIC yields modest improvements of the SIR. Yet, as only the cancellation of the strongest interferer results in a significant performance gain, SIC qualifies also for DL communications. Subsequently, we demonstrated that for specific association policies in multi-tier networks SIC entails distinct benefits. For the association policy based on the maximum instantaneous SIR, we demonstrated that the performance gain due to SIC is significant. In addition, considering the heterogeneous load distribution in multi-tier networks, we developed an analytical framework for association policies based on minimum load or biased received power. For the minimum load policy, we provided a tool to calculate the rate distribution, while for the range expansion scenario, we developed a tool to compute the SIR distribution.

In addition to the theoretical significance to characterize how the spatial statistics of the network nodes affect the system performance in terms of detection, energy efficiency, and network capacity, the toolset developed in this dissertation is also of practical interest. The tool developed in Chapter 3 allows us to evaluate the detection performance in harsh urban environment and to determine in which urban areas the required detection performance cannot be guaranteed. As such, the framework can be applied to determine where localization alternatives are necessary in the network. The framework proposed in Chapter 4 gave rise to several guidelines for energy-efficient design. For instance, our results illustrated that the correct setting of the detection threshold can substantially reduce the energy consumption. Given the strong relation between the detection performance and the small cell coverage, we characterized how the coverage range of SAPs affects the energy consumption. The proposed optimization framework is an instrument to correctly set sensing time and sensing probability so as to reduce the energy consumption whilst guaranteeing the aggregate offload capacity. The tool developed in Chapter 5 characterizes the attainable performance improvement due to SIC. Although the benefits are modest for users that connect to the AP which provides the maximum average received

signal power, the numerical results reveal the substantial gain that can be obtained by SIC for practical deployment scenarios such as range expansion and minimum load association. Consequently, this dissertation identifies valuable applications of SIC accounting for the envisioned modifications in the design, operation, and evaluation of future wireless networks.

6.2   Outlook

The relentless increase in mobile data demand over the latest decennium urges wireless network engineers to develop new network architectures and to address a series of problems that emanate from these novel wireless network settings. Bearing in mind the ongoing drastic revision of the cellular network, there are many interesting extensions worth pursuing, which are listed as follows:

- In order to allow ubiquitous wireless connectivity, various wireless technologies and different types of links (ad-hoc and infrastructure-based) will converge and form complex, adaptive networks. Network nodes will be allowed to exploit the proximity between each other to establish a direct device-to-device (D2D) link. D2D communications differ from the well-understood cognitive radio devices by the possibility of central control by the infrastructure-based network. There has been considerable research attention on heterogeneous networks and D2D communications, yet fundamental understanding is still missing concerning the relation between network load, QoS, and access policies. As to the network load, current state of the art studies consider mostly a saturated resource model, where every transmitter is assumed to always have a full queue of data to transmit. This worst-case assumption results in a pessimistic performance assessment that hinders optimal network dimensioning. It is of major theoretical and practical relevance to characterize the network load and individual rate distribution accounting for the complex system interactions in adaptive multi-tier networks with D2D capabilities, considering complexity constraints.

- For D2D transmissions with spectrum underlay, the adoption of a medium access policy can be beneficial to guarantee the performance of those nodes that use the network infrastructure. In the context of D2D communications, a relevant path for future work is to carry out cross-layer optimization and develop a probabilistic framework to design medium access control (MAC) protocols. By the adoption of priority laws, the MAC layer design will accommodate for different groups of users with varying QoS requirements. For instance,

some nodes in the network are mainly concerned about delay, while other nodes running data-hungry applications have stringent traffic requirements.

- The channel reciprocity in time-division duplexing (TDD) networks can be exploited to estimate the downlink channel from uplink pilots, which is of particular interest for multi-antenna systems. An interesting extension of the work presented in this dissertation is to account for multiple antenna systems in the network performance evaluation, bringing together tools from stochastic geometry and random matrix theory.

- The ever-increasing demand for higher data rates in wireless communication networks together with the strong requirement to reduce the energy consumption of the network infrastructure, calls for structural changes in the network design, such as cognitive APs, cooperation schemes, and energy harvesting. Self-powered APs with energy harvesting capabilities have become realistic due to the low-power consumption of small cells compared with the traditional macrocell base stations. An interesting avenue for future research is to extend the energy consumption analysis of the small cell tier to the overall energy consumption of multi-tier networks. Specifically, as sleep mode strategies and energy constraints for self-powered APs can engender strong variations in the number of active APs, it is worthwhile to investigate how the network should be designed to guarantee user QoS.

- In order to bridge the gap between the statistical network performance and the actual real-time system performance, a fundamental ingredient is missing in this dissertation, which is multi-tier network dynamics. In future heterogeneous networks, user populations will have different association policies according to the required quality of the communication link, the amount of data to be sent, and the cost of the resources. The association to a given base station will cease to be optimal after a short time span due to users entering and leaving the network. Therefore, future networks will be self-organizing, complex systems with cognitive capabilities to adapt to the current network state. Each population will have an optimal transmission mode as a function of the network dynamics, which are defined by the mobility distribution of the users, the network topology, and the growth and death rate of the different populations. An ambitious direction for future research is the adoption of network dynamics in the performance analysis of heterogeneous wireless networks. Because of the network dynamics, several fundamental questions arise related to stability and

robustness. Control theory can be applied for the stability analysis and optimal control is a possible tool to study the energy efficiency under central control.

Appendix A

Proofs and derivations

A.1 Proof of Theorem 1

Let $S = s[k]/\sqrt{N}$, $I = i[k]/\sqrt{N}$ and $W = n[k]/\sqrt{N}$ with $\sigma_n^2/N = \sigma_W^2$, then the discrete decision statistic in (4.8) can be rewritten as

$$V_{\text{ED}|\mathcal{H}_1} = \sum_{k=1}^{N} \Big(\underbrace{\frac{h}{r_f^{\alpha/2}} S[k] + I[k]}_{K} + W[k] \Big)^2.$$

Conditioning on K, V_{ED} follows a non-central chi-square distribution and therefore, the CF of V_{ED} is given by

$$\psi_{V_{\text{ED}}|\mathcal{H}_1,K}(j\omega) = \frac{1}{\left(1 - 2j\omega\sigma_W^2\right)^{N/2}} \exp\left(\frac{j\omega N K^2}{1 - 2j\omega\sigma_W^2} \right). \qquad \text{(A.1)}$$

Since the network interference follows a symmetric stable distribution, the decomposition property can be applied and the interference can be represented as $I = \sqrt{U}G$, with $U \sim \mathcal{S}(2/\alpha, 1, \cos(\frac{\pi}{\alpha}))$ and $G \sim \mathcal{N}(0, 2\gamma^{\alpha/2}/N)$. If we assume that the SoI has a normal distribution, then K^2 in (A.1) stands for the power of a normally distributed r.v. with variance $h^2 P_u/(r_f^{\alpha} N) + 2\gamma^{\alpha/2}U/N$. Let $V = 2\gamma^{\alpha/2}U$, then we can write

$$\psi_{V_{\text{ED}}|\mathcal{H}_1,h,r_f,V}(j\omega) = \frac{1}{\left(1 - 2j\omega\sigma_W^2\right)^{N/2}} \exp\left(\frac{j\omega N(h^2 P_u/(r_f^{\alpha} N) + V/N)}{1 - 2j\omega\sigma_W^2} \right).$$

The exponential can be expanded as the product of two exponentials. Further deconditioning on h and V, we get

$$\psi_{V_{\text{ED}}|\mathcal{H}_1,r_{\text{f}}}(j\omega) = \frac{1}{\left(1 - 2j\omega\sigma_W^2\right)^{N/2-1}}$$
$$\times \frac{1}{1 - j\omega(P_{\text{u}}/(2r_{\text{f}}^\alpha) + \sigma_W^2)} \psi_V\left(\frac{j\omega}{1 - 2j\omega\sigma_W^2}\right).$$

Using the scaling property of a stable random variable, the CF of the decision variable can be written as

$$\psi_{V_{\text{ED}}|\mathcal{H}_1,r_{\text{f}}}(j\omega) = \frac{1}{\left(1 - 2j\omega\sigma_W^2\right)^{N/2-1}}$$
$$\times \frac{1}{1 - j\omega(P_{\text{u}}/(2r_{\text{f}}^\alpha) + \sigma_W^2)}$$
$$\times \exp\left\{-2^{2/\alpha}\gamma\cos(\pi/\alpha)\left|\frac{j\omega}{1 - 2j\omega\sigma_W^2}\right|^{2/\alpha}\right.$$
$$\times \left.\left[1 - \text{sign}\left(\frac{j\omega}{1 - 2j\omega\sigma_W^2}\right)\tan(\pi/\alpha)\right]\right\}.$$

We take the expectation with respect to r_{f} bearing in mind that the UE is within the range $[0, R]$ and that the probability density function (PDF) of r_{f} is given by $f_X(r_{\text{f}}) = 2r_{\text{f}}/R^2$. Solving the expectation, the proof is concluded.

A.2 Proof of Theorem 2

The average capacity of a typical user can be written as

$$\bar{C} = \mathbb{E}_{r_{\text{f}},\phi,h}[\ln(1 + \eta)]$$

where the expectation is taken over the distance r_{f} between the UE and the SAP, over the spatial PPP ϕ of the interferers and over the fading distribution h. For a positive r.v. X, $\mathbb{E}[X] = \int_0^\infty 1 - F_X(x)dx$ with $F_X(x)$ the cumulative distribution function. Following the approach of [15], the average throughput can be expressed as

$$\bar{C} = \int_0^R \int_0^\infty \exp\left(-\frac{\sigma_n^2}{P_{\text{u}}}(e^x - 1)r_{\text{f}}^\alpha\right) \mathcal{L}_I\left(\frac{e^x - 1}{P_{\text{u}}}r_{\text{f}}^\alpha\right) dx \frac{2r_{\text{f}}}{R^2} dr_{\text{f}} \qquad \text{(A.2)}$$

where $\mathcal{L}_I(s)$ is the Laplace transform of the network interference I. Applying the probability generating functional of the PPP and assuming that the

interfering signal is affected by Rayleigh fading, we can write

$$\mathcal{L}_I\left(\frac{e^x - 1}{P_u}r_f^\alpha\right) = \exp\left[-2\pi\lambda\int_0^\infty\left(1 - \frac{1}{1 + \frac{P_i}{P_u}(e^x - 1)(r_f/u)^\alpha}\right)u\,du\right]$$

which by a change of variables can further be simplified to

$$\mathcal{L}_I\left(\frac{e^x - 1}{P_u}r_f^\alpha\right) = \exp\left(-\frac{2\pi^2}{\alpha}\csc\left(\frac{2\pi}{\alpha}\right)\lambda\left(\frac{P_i}{P_u}\right)^{2/\alpha}(e^x - 1)^{2/\alpha}r_f^2\right). \quad \text{(A.3)}$$

Inserting (A.3) in (A.2), the proof is concluded.

A.3 Proof of Theorem 3

The success probability for a typical user in the coverage of the SAP is given by

$$\mathbb{P}_s(\eta_t) = \mathbb{E}_{r_f,\phi,h}\left\{\Pr\left[\frac{h^2 P_u r_f^{-\alpha}}{\sigma_n^2 + I} > \eta_t\right]\right\}.$$

For a typical user uniformly distributed over the coverage of the SAP and considering Rayleigh fading, we can write

$$\mathbb{P}_s(\eta_t) = \int_0^R\exp\left(-\frac{r_f^\alpha\eta_t\sigma_n^2}{P_u}\right)\mathbb{E}_\phi\left[\exp\left(-\frac{r_f^\alpha\eta_t I}{P_u}\right)\right]\frac{2r_f}{R^2}dr_f$$

where $\mathbb{E}_\phi\left[\exp\left(-r_f^\alpha\eta_t I/P_u\right)\right] = \mathcal{L}_I(r_f^\alpha\eta_t/P_u)$. Evaluating the Laplace transform of the network interference (A.3) at $r_f^\alpha\eta_t/P_u$, the proof is concluded.

A.4 Proof of Proposition 1

Let $\mathcal{G}(\tau_s)$ be the objective function in (4.20). If $\mathcal{G}(\tau_s)$ is differentiable over $[0, T]$, then $\mathcal{G}(\tau_s)$ is convex iff $\mathcal{G}'(\tau_s)$ is increasing over the considered interval. We write the derivative of $\mathcal{G}(\tau_s)$ with respect to τ_s as

$$\mathcal{G}'(\tau_s) = \lambda_s/\lambda_m[p_s\Xi_s - p_u p_s\mathbb{P}_d^*\Xi_t - (1 - p_u)p_s\mathbb{P}_{fa}(\zeta^*, \tau_s)\Xi_t \\ + (1 - p_u)p_s\Xi_t(T - \tau_s)\mathbb{P}'_{fa}(\zeta^*, \tau_s)]. \quad \text{(A.4)}$$

For $\zeta^* > \sigma_n^2$, $\mathbb{P}_{fa}$ is positive and decreasing with τ_s, while $\mathbb{P}'_{fa}$ is negative and increasing with τ_s. Therefore, the third and fourth term in (A.4) are increasing over $[0, T]$. Since the first two terms in the expression of $\mathcal{G}'(\tau_s)$ are constant, this concludes the proof.

A.5 Proof of Lemma 1

We calculate the distribution of $Y = hX^{-\alpha}$. For the uniformly distributed distance variable X, the distribution is given by $F_X(x) = x^2/R^2$ such that R is the maximum considered range where nodes still have a contribution to the aggregate interference. The distribution of $W = X^{-\alpha}$ is given by

$$
\begin{aligned}
F_W(w) &= \Pr[X^{-\alpha} < w] \\
&= \Pr[X \geq (1/w)^{1/\alpha}] \\
&= 1 - \frac{w^{-2/\alpha}}{R^2}
\end{aligned}
$$

which corresponds to the CDF of a Pareto distribution. The distribution of the product of W and the exponential r.v. h is now given by

$$
\begin{aligned}
F_Y(y) &= \mathbb{E}\left\{\Pr[W \leq y/h]\right\} \\
&= \int_0^\infty \left(1 - \frac{(y/h)^{-2/\alpha}}{R^2}\right) \exp(-h)dh \\
&= 1 - \Gamma\left(\frac{2}{\alpha} + 1\right)\frac{y^{-2/\alpha}}{R^2}
\end{aligned}
$$

which concludes the proof.

A.6 Proof of Lemma 4

In (5.18), α_{I} is chosen equal to the characteristic exponent of the skewed stable distribution in the unbounded path loss model. The parameters of the TSD can be found using the method of the cumulants. From (5.18), the cumulants of the truncated stable distribution can be expressed as

$$
\begin{aligned}
\kappa_I(k) &= \left.\frac{1}{j^k}\frac{d^k}{d\omega^k}\ln\psi_{I_{\Omega_j^n}}(j\omega)\right|_{\omega=0} \\
&= (-1)^k\gamma'\Gamma(-\alpha_{\mathrm{I}})g^{\alpha_{\mathrm{I}}-k}\Pi_{i=0}^{k-1}(\alpha_{\mathrm{I}} - i).
\end{aligned} \tag{A.5}
$$

Building on Cambell's theorem [13], the cumulants of the aggregate interference can be expressed as

$$
\kappa(k) = Q^k\frac{2\pi\mu_j}{k\alpha - 2}d_{\min}^{2-k\alpha}\mu_{h^2}(k). \tag{A.6}
$$

Using (A.5) and (A.6), the parameters γ' and g can be written as a function of the first two cumulants as follows

$$
\begin{aligned}
\gamma' &= \frac{-\kappa(1)}{\Gamma(-\alpha_I)\alpha_I \left(\frac{\kappa(1)(1-\alpha_I)}{\kappa(2)} \right)^{\alpha_I-1}} \\
g &= \frac{\kappa(1)(1-\alpha_I)}{\kappa(2)}.
\end{aligned}
\tag{A.7}
$$

The success probability of successfully canceling the strongest interferer can be written as

$$
\begin{aligned}
\mathbb{P}_{\text{s,can}}(\eta_t, n|r) &= \Pr\left(\frac{X_{(n)}}{I_{\Omega_j^n}} \geq \eta_t \right) \\
&= \mathcal{L}_{I_{\Omega_j^n}}(\eta_t r^\alpha) \\
&= \exp\left(\gamma'\Gamma(-\alpha_I)[(g + \eta_t r^\alpha)^{\alpha_I} - g^{\alpha_I}] \right).
\end{aligned}
\tag{A.8}
$$

For the special case where $\alpha = 4$, we get $\alpha_I = 2/\alpha = 1/2$, and $\mathbb{P}_{\text{s,can}}(\eta_t, n|r)$ conditioned on the distance of the strongest node is given by

$$
\begin{aligned}
\mathbb{P}_{\text{s,can}}(\eta_t, n|r, \alpha = 4) &= \exp\left(\gamma'\Gamma(-1/2)\sqrt{g} \left[\sqrt{1 + \frac{\eta_t}{g}r^4} - 1 \right] \right) \\
&= \exp\left(-2\kappa(1)\sqrt{\frac{\kappa(1)}{2\kappa(2)}} \sqrt{\frac{\kappa(1)}{2\kappa(2)}} \left[\sqrt{1 + \frac{2\eta_t r^4 \kappa(2)}{\kappa(1)}} - 1 \right] \right) \\
&= \exp\left(-\frac{\kappa(1)^2}{\kappa(2)} \left[\sqrt{1 + \frac{2\eta_t r^4 \kappa(2)}{\kappa(1)}} - 1 \right] \right) \\
&\overset{(a)}{=} \exp(-3/2\mu_j \pi r^2 [\sqrt{1 + 4\eta_t/3} - 1])
\end{aligned}
\tag{A.9}
$$

where (a) follows from the fact that $d_{\min}$ corresponds to the distance r of the nth interferer, and we assume Rayleigh fading such that $\mathbb{E}[h^k] = k!/\lambda^k$ with $\lambda = 1$ the intensity of the exponential distribution. The unconditional success

probability can now be written as

$$
\mathbb{P}_{s,\text{can}}(\eta_t, n | \alpha = 4)
$$

$$
= \int_0^\infty \exp(-3/2\mu_j\pi r^2[\sqrt{1+4\eta_t/3}-1])\exp(\mu_j\pi r^2)\frac{2(\mu_j\pi r^2)^n}{r\Gamma(n)}dr
$$

$$
= \int_0^\infty \exp(\mu_j\pi r^2[\sqrt{9/4+3\eta_t}-3/2+1])\frac{2(\mu_j\pi)^n r^{2n-1}}{\Gamma(n)}dr
$$

$$
= \int_0^\infty \exp(\mu_j\pi r^2[\sqrt{9/4+3\eta_t}-1/2])\frac{(\mu_j\pi)^{n-1}r^{2n-2}}{\Gamma(n)}d\mu_j\pi r^2
$$

$$
= \int_0^\infty \exp([\sqrt{9/4+3\eta_t}-1/2]w)\frac{w^{n-1}}{\Gamma(n)}dw
$$

$$
= \frac{1}{(\sqrt{9/4+3\eta_t}-1/2)^n} \tag{A.10}
$$

A.7 Proof of Lemma 9

The success probability of a mobile node belonging to $C_k^{(\text{RE})}$ and connected to the kth tier conditioned on the distance can be written as

$$
\mathbb{P}_s(\eta_t \mid x_k \in C_k^{(\text{RE})}, x_k) = \prod_{i\in\mathcal{K}} \mathcal{L}_{I_{\Phi_i}}\left(\frac{\eta_t x_k^\alpha}{P_k}\right)
$$

where

$$
\mathcal{L}_{I_{\Phi_i}}\left(\frac{\eta_t x_k^\alpha}{P_k}\right) = \exp\left(-\pi\lambda_i\eta_t^{2/\alpha}\left(\frac{P_i}{P_k}\right)^{2/\alpha}C((b_i/\eta_t b_k)^{2/\alpha},\alpha)x_k^2\right).
$$

The integration interval of the integral in $C(b,\alpha)$ is determined noting that the location of the user in the REA $P_i x_i^{-\alpha} < b_k P_k x_k^{-\alpha}$ yields the interferer exclusion region $x_i > (P_i/b_k P_k)^{1/\alpha}x_k$. Applying the change of variables $(P_k/\eta_t P_i)^{2/\alpha}(x_i/x_k)^2 \to u$ and deconditioning on x_k, we can write

$$
\mathbb{P}_s(\eta_t \mid x_k \in C_k^{(\text{RE})})
$$

$$
= \int_0^\infty \exp(-\pi\eta_t^{2/\alpha}\sum_{i\in\mathcal{K}}\lambda_i(P_i/P_k)^{2/\alpha}C((b_i/\eta_t b_k)^{2/\alpha},\alpha)x_k^2)f_{X_k^{(\text{RE})}}(x_k)dx_k
$$

$$
= \frac{1}{p_{a,k}^{(\text{RE})}}\left(\frac{1}{\sum_{i\in\mathcal{K}}\left(\frac{\lambda_i}{\lambda_k}\right)\left(\frac{P_i}{P_k}\right)^{2/\alpha}\left(\eta_t^{2/\alpha}C((b_i/\eta_t b_k)^{2/\alpha},\alpha)+\left(\frac{b_i}{b_k}\right)^{2/\alpha}\right)}\right.
$$

$$
\left. -\frac{1}{\sum_{i\in\mathcal{K}}\left(\frac{\lambda_i}{\lambda_k}\right)\left(\frac{P_i}{P_k}\right)^{2/\alpha}\left(\eta_t^{2/\alpha}C((b_i/\eta_t b_k)^{2/\alpha},\alpha)+1\right)}\right). \tag{A.11}
$$

Applying SIC to a user located in the REA, the highest unbiased received signal power of tier i is canceled. As a result the interference cancellation radius relative to the ith tier increases from $(P_i/b_k P_k)^{1/\alpha} x_k$ to $(P_i/P_k)^{1/\alpha} x_k$, and hence, the success probability after canceling the strongest AP can be written as (5.41).

Bibliography

[1] C. E. Shannon. A mathematical theory of communication. *Bell System Technical Journal*, 27:379–423, 623–656, Oct. 1948.

[2] M. Z. Win, P. C. Pinto, and L. A. Shepp. A mathematical theory of network interference and its applications. *Proc. IEEE*, 97(2):205–230, Feb. 2009.

[3] M. Haenggi and R. K. Ganti. *Interference in Large Wireless Networks*, volume 3. Now Publishers Inc., Hanover, MA, USA, 2009.

[4] F. Baccelli, M. Klein, M. Lebourges, and S. Zuyev. Stochastic geometry and architecture of communication networks. *Telecommunication Systems*, 7:209–227, 1997.

[5] F. Baccelli and S. Zuyev. Poisson-Voronoi spanning trees with applications to the optimization of communication networks. *Operations Research*, 47(4):619–631, 1999.

[6] M. Aljuaid and H. Yanikomeroglu. Investigating the Gaussian convergence of the distribution of the aggregate interference power in large wireless networks. *IEEE Trans. Veh. Technol.*, 59(9):4418–4424, Nov. 2010.

[7] H. Inaltekin. Gaussian approximation for the wireless multi-access interference distribution. *IEEE Trans. Signal Process.*, 60(11):6114–6120, Nov. 2012.

[8] G. Samorodnitsky and M.S. Taqqu. *Stable Non-Gaussian Random Processes*. Chapmann and Hall, 1994.

[9] J. Ilow and D. Hatzinakos. Analytic alpha-stable noise modeling in a Poisson field of interferers or scatterers. *IEEE Trans. Signal Process.*, 46(6):1601–1611, Jun. 1998.

[10] P. C. Pinto and M. Z. Win. Communication in a Poisson field of interferers–Part I: Interference distribution and error probability. *IEEE Trans. Wireless Commun.*, 9(7):2176–2186, Jul. 2010.

[11] A. Rabbachin, T. Q. S. Quek, P. C. Pinto, I. Oppermann, and M. Z. Win. Non-coherent UWB Communication in the Presence of Multiple Narrowband Interferers. *IEEE Trans. Wireless Commun.*, 9(11):3365–3379, Nov. 2010.

[12] Y. Wen, S. Loyka, and A. Yongacoglu. Asymptotic analysis of interference in cognitive radio networks. *IEEE J. Sel. Areas Commun.*, 30(10):2040–2052, Nov. 2012.

[13] A. Rabbachin, T. Q. S. Quek, H. Shin, and M. Z. Win. Cognitive network interference. *IEEE J. Sel. Areas Commun.*, 29(2):480–493, Feb. 2011.

[14] T. V. Nguyen and F. Baccelli. A stochastic geometry model for cognitive radio networks. *The Computer Journal*, 55(5):534–552, 2012.

[15] J. G. Andrews, F. Baccelli, and R. K. Ganti. A tractable approach to coverage and rate in cellular networks. *IEEE Trans. Commun.*, 59(11):3122–3134, Nov. 2011.

[16] B. V. Gnedenko and A. N. Kolmogorov. *Limit distributions for sums of independent random variables*. Addison-Wesley, 1954.

[17] W. Feller. *Introduction to Probability Theory and Its Applications*, volume 2. Wiley, New York, 2nd edition, 1974.

[18] N. Campbell. The study of discontinuous phenomena. In *Mathematical Proceedings of the Cambridge Philosophy Society*, volume 15, pages 117–136, 1909.

[19] W. Schottky. Über spontane stromschwankungen in verschiedenen elektrizitätsleitern. *Annalen der Physik*, 57:541–567, 1918.

[20] D. Stoyan, W. S. Kendall, and J. Mecke. *Stochastic Geometry and its Applications*. John Wiley and Sons, second edition, 2008.

[21] F. Baccelli and B. Blaszczyszyn. *Stochastic geometry and wireless networks: Volume I theory*. Now Publishers Inc., 2010.

[22] F. Baccelli and B. Blaszczyszyn. *Stochastic geometry and wireless networks: Volume II applications*. Now Publishers Inc., 2010.

[23] J. F. C. Kingman. *Poisson processes*. Oxford University Press, 1993.

[24] M. Wildemeersch, C. H. Slump, and A. Rabbachin. Acquisition of GNSS signals in a realistic signal environment. *IEEE Trans. Aerosp. Electron. Syst.*, 2013. to appear.

[25] M. Wildemeersch, A. Rabbachin, E. Cano, and J. Fortuny. Interference assessment of DVB-T within the GPS L1 and Galileo E1 band. In *5th ESA Workshop on Satellite Navigation Technologies and European Workshop on GNSS Signals and Signal Processing (NAVITEC)*, pages 1–8, Noordwijk, The Netherlands, Dec. 2010.

[26] M. Wildemeersch, A. Rabbachin, T. Q. S. Quek, and C. H. Slump. GNSS signal acquisition in harsh urban environments. In *Proc. IEEE Int. Conf. on Commun.*, pages 62–67, Budapest, Hungary, Jun. 2013.

[27] A. Goldsmith. *Wireless Communications*. Cambridge University Press, 2005.

[28] H. L. Van Trees. *Detection, Estimation, and Modulation Theory - Part 1*. Wiley, 2001.

[29] D. Borio. *A Statistical Theory for GNSS Signal Acquisition*. PhD thesis, Politecnico di Torino, Mar. 2008.

[30] A. Polydoros and C. L. Weber. A Unified Approach to Serial Search Spread-Spectrum Code Acquisition - Part I: General Theory. *IEEE Trans. Commun.*, 32(5):542–549, May 1984.

[31] G. E. Corazza. On the MAX/TC Criterion for Code Acquisition and its Application to DS-SSMA Systems. *IEEE Trans. Commun.*, 44(9):1173–1182, Sep. 1996.

[32] J. H. J. Iinatti. On the Threshold Setting Principles in Code Acquisition of DS-SS Signals. *IEEE J. Sel. Areas Commun.*, 18(1):62–72, Jan. 2000.

[33] M. D. Katz, J. H. J. Iinatti, and S. Glisic. Two-Dimensional Code Acquisition in Time and Angular Domains. *IEEE J. Sel. Areas Commun.*, 19(12):2441–2451, Dec. 2001.

[34] M. Chiani and M. G. Martini. Analysis of Optimum Frame Synchronization Based on Periodically Embedded Sync Words. *IEEE Trans. Commun.*, 55(11):2056–2060, Nov. 2007.

[35] D. M. Akos, P.-L. Normark, J.-T. Lee, and K. G. Gromov. Low Power Global Navigation Satellite System (GNSS) Signal Detection and Processing. In *Proc. of the ION GPS conf.*, pages 784–791, Salt Lake City, United States, Sep. 2000.

[36] D. Borio. GNSS Acquisition in the Presence of Continuous Wave Interference. *IEEE Trans. Aerosp. Electron. Syst.*, 46(1):47–60, Jan. 2010.

[37] A. T. Balaei, A. G. Dempster, and L. Lo Presti. Characterization of the Effects of CW and Pulse CW Interference on the GPS Signal Quality. *IEEE Transactions on Aerospace and Electronic Systems*, 45(4):1418–1431, Oct. 2009.

[38] F. Bastide, E. Chatre, C. Macabiau, and B. Roturier. GPS L5 and Galileo E5a/E5b Signal-to-Noise Density Ratio Degradation due to DME/TACAN Signals: Simulations and Theoretical Derivation. In *Proc. of the 2004 National Technical Meeting of The Institute of Navigation*, pages 1049–1062, San Diego, Jan. 2004.

[39] D. Borio, S. Savasta, and L. Lo Presti. On the DVB-T Coexistence with Galileo and GPS system. In *Proc. of the 3rd ESA Workshop on Satellite Navigation User Equipment Technologies (NAVITEC)*, Noordwijk, the Netherlands, Dec. 2006. ESA.

[40] E. A. Sourour and S. C. Gupta. Direct-Sequence Spread-Spectrum Parallel Acquisition in a Fading Mobile Channel. *IEEE Trans. Commun.*, 38(7):992–998, Jul. 1990.

[41] G. E. Corazza, C. Caini, A. Vanelli-Coralli, and A. Polydoros. DS-CDMA Code Acquisition in the Presence of Correlated Fading - Part I: Theoretical Aspects. *IEEE Trans. Commun.*, 52(7):1160–1168, Jul. 2004.

[42] C. Caini, G. E. Corazza, and A. Vanelli-Coralli. DS-CDMA Code Acquisition in the Presence of Correlated FadingÑPart II: Application to Cellular Networks. *IEEE Trans. Commun.*, 52(8):1397–1407, Aug. 2004.

[43] R. R. Rick and L. B. Milstein. Parallel Acquisition in Mobile DS-CDMA Systems. *IEEE Trans. Commun.*, 45(11):1466–1476, Nov. 1997.

[44] R. R. Rick and L. B. Milstein. Optimal Decision Strategies for Acquisition of Spread-Spectrum Signals in Frequency-Selective Fading Channels. *IEEE Trans. Commun.*, 46(5):686–694, May 1998.

[45] W. Suwansantisuk, M. Z. Win, and L. A. Shepp. On the Performance of Wide-Bandwidth Signal Acquisition in Dense Multipath Channels. *IEEE Trans. Veh. Technol.*, 54(5):1584–1594, Sep. 2005.

[46] W. Suwansantisuk and M. Z. Win. Multipath Aided Rapid Acquisition: Optimal Search Strategies. *IEEE Trans. Inf. Theory*, 53(1):174–193, Jan. 2007.

[47] W. Suwansantisuk, M. Chiani, and M. Z. Win. Frame Synchronization for Variable-Length Packets. *IEEE J. Sel. Areas Commun.*, 26(1):52–69, Jan. 2008.

[48] B. Motella, S. Savasta, D. Margaria, and F. Dovis. Method for Assessing the Interference Impact on GNSS Receivers. *IEEE Trans. Aerosp. Electron. Syst.*, 47(2):1416–1432, Apr. 2011.

[49] D. Lopez-Perez, I. Guvenc, G. De La Roche, M. Kountouris, T. Q. S. Quek, and J. Zhang. Enhanced intercell interference coordination challenges in heterogeneous networks. *IEEE Wireless Commun. Mag.*, 18(3):22–30, Jun. 2011.

[50] J. W. Betz and B. M. Titus. Intersystem and intrasystem interference with signal imperfections. In *Proc. IEEE Position Location and Navigation Symp. (PLANS)*, pages 558–565, San Diego, United States, Apr. 2006.

[51] S. Martin, H. Kuhlen, and T. Abt. Interference and Regulatory Aspects of GNSS Pseudolites. *J. of Global Positioning Systems*, 6(2):98–107, 2007.

[52] Regulatory framework for indoor GNSS pseudolites. Technical Report ECC Report 168, ECC-CEPT, 2011.

[53] D. Borio, C. O'Driscoll, and J. Fortuny-Guasch. Pulsed pseudolite signal effects on non-participating GNSS receivers. In *IEEE Int. Conf. on Indoor Positioning and Indoor Navigation (IPIN)*, pages 1–6, Guimarães, Portugal, Sep. 2011.

[54] D. S. Anderson, E. F. Drocella, Jones S. K., and M. A. Settle. Assessment of compatibility between ultrawideband (UWB) systems and global positioning system (GPS) receivers. Technical Report 01–45, NTIA, 2001.

[55] T. Van Slyke, W. B. Kuhn, and B. Natarajan. Measuring interference from a UWB transmitter in the GPS L1 band. In *IEEE Radio and Wireless Symposium (RWS)*, pages 887–890, Orlando, United States, Jan. 2008.

[56] K. M. Peterson and R. J. Erlandson. Analytic statistical model for aggregate radio frequency interference to airborne GPS receivers from ground-based emitters. *Navigation*, 59(1):25–35, Spring 2012.

[57] L. P. Goh, Z. Lei, and F. Chin. DVB detector for cognitive radio. In *Proc. IEEE Int. Conf. on Commun.*, pages 6460–6465, Glasgow, Scotland, Jun. 2007.

[58] B. Motella, M. Pini, and F. Dovis. Investigation on the effect of strong out-of-band signals on global navigation satellite systems receivers. *GPS Solut.*, 12(2):77–86, 2008.

[59] A. Giorgetti and M. Chiani. Influence of fading on the gaussian approximation for BPSK and QPSK with asynchronous cochannel interference. *IEEE Trans. Wireless Commun.*, 4(2):384–389, Mar. 2005.

[60] A. Giorgetti, M. Chiani, and M. Z. Win. The effect of narrowband interference on wideband wireless communication systems. *IEEE Trans. Commun.*, 53(12):2139–2149, Dec. 2005.

[61] D. Dardari and G. Pasolini. Simple and accurate models for error probability evaluation of IEEE802. 11 DS-SS physical interface in the presence of Bluetooth interference. In *Proc. IEEE Global Telecomm. Conf.*, pages 201–206, Taipei, Taiwan, Nov. 2002.

[62] J. W. Betz. Effect of Narrowband Interference on GPS Code Tracking Accuracy. In *Proc. of ION 2000 National Technical Meeting*, Anaheim, United States, Jan. 2000. ION.

[63] D. Borio, C. O'Driscoll, and G. Lachapelle. Coherent, noncoherent, and differentially coherent combining techniques for acquisition of new composite GNSS signals. *IEEE Trans. Aerosp. Electron. Syst.*, 45(3):1227–1240, Jul. 2009.

[64] G. E. Corazza and R. Pedone. Generalized and Average Likelihood Ratio Testing for Post Detection Integration. *IEEE Trans. Commun.*, 55(11):2159–2171, Nov. 2007.

[65] J. Jung. Implementation of Correlation Power Peak Ratio Based Signal Detection Method. In *Proc. of the 2004 ION GNSS conference*, pages 486–490, Long Beach, United States, Sep. 2004.

[66] J. Gil-Pelaez. Note on the Inversion Theorem. *Biometrika*, 38(3/4):481–482, Dec. 1951.

[67] A. Lehner, A. Steingaß, and F. Schubert. A Location and Movement Dependent GNSS Multipath Error Model for Pedestrian Applications. In *Proc. of the 13th European Navigation Conference (NAVITEC), Naples, Italy*, 2009.

[68] A. Broumandan, J. Nielsen, and G. Lachapelle. Indoor GNSS Signal Acquisition Performance Using a Synthetic Antenna Array. *IEEE Trans. Aerosp. Electron. Syst.*, 47(2):1337–1350, Apr. 2011.

[69] R. D. Gupta and D. Kundu. Generalized Exponential Distribution: Existing Results and Some Recent Developments. *J. Statist. Plann. Inference*, 137:3537 Ð 3547, Mar. 2007.

[70] M. Fantino, M. Pini, P. Mulassano, G. Girau, M. Nicola, and A. Nordio. Signal Compression for an Efficient and Simplified GNSS Signal Parallel Acquisition. In *Proc. of the 21st International Technical Meeting of the Satellite Division of The Institute of Navigation (ION GNSS)*, Savannah, United States, Sep. 2008. ION.

[71] R. D. Gupta and D. Kundu. Closeness of Gamma and Generalized Exponential Distribution. *Commun. Stat. - Theor. M.*, 32(4):705–722, 2003.

[72] B. C. Geiger, M. Soudan, and C. Vogel. On the Detection Probability of Parallel Code Phase Search Algorithms in GPS Receivers. In *Proc. IEEE Int. Symp. on Personal, Indoor and Mobile Radio Commun.*, pages 865–870, Istanbul, Turkey, Sep. 2010. IEEE.

[73] M. Z. Win. A mathematical model for network interference. In *IEEE Communication Theory Workshop*, Sedona, AZ, May 2007.

[74] J. Kingsman. *Poisson Processes*. Oxford University Press, 1993.

[75] M. Wildemeersch, T. Q. S. Quek, C. H. Slump, and A. Rabbachin. Cognitive small cell networks: Energy efficiency and trade-offs. *IEEE Trans. Commun.*, 61(9):4016–4029, Sep. 2013.

[76] M. Wildemeersch, T. Q. S. Quek, A. Rabbachin, C. H. Slump, and A. Huang. Performance limits for cognitive small cells. In *Proc. IEEE Wireless Commun. and Networking Conf.*, pages 2832–2836, Shanghai, China, Apr. 2013.

[77] M. Wildemeersch, T. Q. S. Quek, A. Rabbachin, C. H. Slump, and A. Huang. Energy efficient design of cognitive small cells. In *Proc. IEEE Int. Conf. on Commun.*, pages 1294–1299, Budapest, Hungary, Jun. 2013.

[78] T. Q. S. Quek, G. de la Roche, I. Guvenc, and M. Kountouris. *Small Cell Networks: Deployment, PHY Techniques, and Resource Allocation*. Cambridge University Press, 2013.

[79] D. Lopez-Perez, I. Guvenc, G. de la Roche, M. Kountouris, T. Q. S. Quek, and J. Zhang. Enhanced intercell interference coordination challenges in heterogeneous networks. *IEEE Wireless Commun. Mag.*, 18(3):22–30, Jun. 2011.

[80] J. G. Andrews, H. Claussen, M. Dohler, S. Rangan, and M. C. Reed. Femtocells: Past, present, and future. *IEEE J. Sel. Areas Commun.*, 30(3):497–508, Apr. 2012.

[81] H. Bogucka and A. Conti. Degrees of freedom for energy savings in practical adaptive wireless systems. *IEEE Commun. Mag.*, 49(6):38–45, Jun. 2011.

[82] Y. S. Soh, T. Q. S. Quek, M. Kountouris, and H. Shin. Energy efficient heterogeneous cellular networks. *IEEE J. Sel. Areas Commun.*, 31(5):840–850, May 2013.

[83] Y. Chen, S. Zhang, S. Xu, and G.Y. Li. Fundamental trade-offs on green wireless networks. *IEEE Commun. Mag.*, 49(6):30–37, Jun. 2011.

[84] W. C. Cheung, T. Q. S. Quek, and M. Kountouris. Throughput optimization, spectrum allocation, and access control in two-tier femtocell networks. *IEEE J. Sel. Areas Commun.*, 30(3):561–574, Apr. 2012.

[85] A.-H. Tsai, L.-C. Wang, J.-H. Huang, and R.-B. Hwang. High-capacity OFDMA femtocells by directional antennas and location awareness. *IEEE Systems J.*, 6(2):329–340, Jun. 2012.

[86] S.H. Wu, C.M. Chen, and M.S. Chen. Collaborative wakeup in clustered ad hoc networks. *IEEE J. Sel. Areas Commun.*, 29(8):1585–1594, Sep. 2011.

[87] A.P. Azad, S. Alouf, E. Altman, V. Borkar, and G.S. Paschos. Optimal control of sleep periods for wireless terminals. *IEEE J. Sel. Areas Commun.*, 29(8):1605–1617, Sep. 2011.

[88] W. Guo and T. O'Farrell. Green cellular network: Deployment solutions, sensitivity and tradeoffs. In *Wireless Advanced (WiAd)*, pages 42–47, London, UK, 2011.

[89] I. Ashraf, F. Boccardi, and L. Ho. Sleep mode techniques for small cell deployments. *IEEE Commun. Mag.*, 49(8):72–79, Aug. 2011.

[90] I. Haratcherev, M. Fiorito, and C. Balageas. Low-power sleep mode and out-of-band wake-up for indoor access points. In *Proc. IEEE Global Telecomm. Conf.*, pages 1–6, Honolulu, HA, Nov. 2009.

[91] L. Saker, S. E. Elayoubi, R. Combes, and T. Chahed. Optimal control of wake up mechanisms of femtocells in heterogeneous networks. *IEEE J. Sel. Areas Commun.*, 30(3):664–672, Apr. 2012.

[92] H. El Sawy and E. Hossain. Two-tier hetnets with cognitive femtocells: Downlink performance modeling and analysis in a multi-channel environment. *IEEE Trans. Mobile Comput.*, 2013. accepted for publication.

[93] Y. C. Liang, Y. Zeng, E. C. Y. Peh, and A. T. Hoang. Sensing-throughput tradeoff for cognitive radio networks. *IEEE Trans. Wireless Commun.*, 7(4):1326–1337, Apr. 2008.

[94] F. Moghimi, A. Nasri, and R. Schober. Adaptive L_p-norm spectrum sensing for cognitive radio networks. *IEEE Trans. Commun.*, 59(7):1934–1945, Jul. 2011.

[95] S. M. Cheng, W. C. Ao, and K. C. Chen. Efficiency of a cognitive radio link with opportunistic interference mitigation. *IEEE Trans. Wireless Commun.*, 10(6):1715–1720, Jun. 2011.

[96] E. Axell, G. Leus, E. G. Larsson, and H. V. Poor. Spectrum sensing for cognitive radio. *IEEE Signal Process. Mag.*, 29(3):101–116, May 2012.

[97] Q. Zhao and B. M. Sadler. A survey of dynamic spectrum access. *IEEE Signal Process. Mag.*, 24(3):79–89, May 2007.

[98] K. C. Chen and R. Prasad. *Cognitive Radio Networks*. Wiley, Hoboken, NJ, 2009.

[99] T. V. Nguyen, H. Shin, T. Q. S. Quek, and M. Z. Win. Sensing and probing cardinalities for active cognitive radios. *IEEE Trans. Signal Process.*, 60(4):1833–1848, Apr. 2012.

[100] L. Saker, S. E. Elayoubi, L. Rong, and T. Chahed. Capacity and energy efficiency of picocell deployment in LTE-A networks. In *Proc. 73rd Annual Int. Veh. Technol. Conf.*, pages 1–5. IEEE, 2011.

[101] S. M. Cheng, S. Y. Lien, F. S. Chu, and K. C. Chen. On exploiting cognitive radio to mitigate interference in macro/femto heterogeneous networks. *IEEE Wireless Commun. Mag.*, 18(3):40–47, Jun. 2011.

[102] C. H. M. de Lima, M. Bennis, and M. Latva-aho. Coordination mechanisms for self-organizing femtocells in two-tier coexistence scenarios. *IEEE Trans. Wireless Commun.*, 11(6):2212–2223, Jun. 2012.

[103] Y. S. Soh, T. Q. S. Quek, M. Kountouris, and G. Caire. Cognitive hybrid division duplex for two-tier femtocell networks. *IEEE Trans. Wireless Commun.*, 2013. accepted for publication.

[104] B. Blaszczyszyn, M. K. Karray, and H.-P. Keeler. Using Poisson processes to model lattice cellular networks. In *Proc. IEEE Joint Conf. of the IEEE Computer and Commun. Societies*, pages 797–805, Turin, Italy, Apr. 2013.

[105] S. G. Foss and S. A. Zuyev. On a Voronoi aggregative process related to a bivariate Poisson process. *Advances in Applied Probability*, pages 965–981, 1996.

[106] T. Yucek and H. Arslan. A survey of spectrum sensing algorithms for cognitive radio applications. *IEEE Commun. Surveys Tuts.*, 11(1):116–130, first quarter 2009.

[107] D. Bhargavi and C. R. Murthy. Performance comparison of energy, matched-filter and cyclostationarity-based spectrum sensing. In *Proc. IEEE Workshop on Signal Proc. Advances in Wireless Commun.*, pages 1–5, Marrakech, Morocco, Jun. 2010.

[108] R. Tandra and A. Sahai. SNR walls for signal detection. *IEEE J. Sel. Topics Signal Process.*, 2(1):4–17, Feb. 2008.

[109] I. Ashraf, L.T.W. Ho, and H. Claussen. Improving energy efficiency of femtocell base stations via user activity detection. In *Proc. IEEE Wireless Commun. and Networking Conf.*, Sydney, Australia, Apr. 2010.

[110] J. S. Ferenc and Z. Néda. On the size distribution of Poisson Voronoi cells. *Physica A: Statistical Mechanics and its Applications*, 385(2):518–526, Nov. 2007.

[111] T. D. Novlan, H. S. Dhillon, and J. G. Andrews. Analytical modeling of uplink cellular networks. *IEEE Trans. Wireless Commun.*, 2013. accepted for publication.

[112] A. Sahai, S. M. Mishra, and R. Tandra. *Cognitive Radios: System Design Perspective*, chapter Spectrum Sensing: Fundamental Limits. Springer, 2009.

[113] A. Mariani, A. Giorgetti, and M. Chiani. Effects of noise power estimation on energy detection for cognitive radio applications. *IEEE Trans. Commun.*, 59(12):3410–3420, Dec. 2011.

[114] A. Rabbachin, A. Conti, and M. Z. Win. Intentional network interference for denial of wireless eavesdropping. In *Proc. IEEE Global Telecomm. Conf.*, pages 4268–4273, Houston, Texas, Dec. 2011.

[115] G. Auer, V. Giannini, C. Desset, I. Godor, P. Skillermark, M. Olsson, M.A. Imran, D. Sabella, M.J. Gonzalez, O. Blume, and A. Fehske. How much energy is needed to run a wireless network? *IEEE Wireless Commun. Mag.*, 18(5):40–49, Oct. 2011.

[116] M. Wildemeersch, T. Q. S. Quek, M. Kountouris, A. Rabbachin, and C. H. Slump. Successive interference cancellation in heterogeneous cellular networks. *IEEE Trans. Signal Process.*, 2013. submitted.

[117] M. Wildemeersch, T. Q. S. Quek, M. Kountouris, and C. H. Slump. Successive interference cancellation in uplink cellular networks. In *Proc. IEEE Workshop on Signal Proc. Advances in Wireless Commun.*, pages 315–319, Darmstadt, Germany, Jun. 2013. Best Student Paper Award.

[118] M. Wildemeersch, T. Q. S. Quek, M. Kountouris, and C. H. Slump. Effectiveness of successive interference cancellation and association policies for heterogeneous wireless networks. In *Proc. IEEE Int. Conf. Acoustics, Speech, and Signal Processing*, Florence, Italy, May 2014. submitted.

[119] M. Kountouris and J. G. Andrews. Downlink SDMA with limited feedback in interference-limited wireless networks. *IEEE Trans. Wireless Commun.*, 11(8):2730–2741, Aug. 2012.

[120] S. Verdu. *Multiuser Detection*. Cambridge University Press, 1998.

[121] S. P. Weber, J. G. Andrews, X. Yang, and G. De Veciana. Transmission capacity of wireless ad hoc networks with successive interference cancellation. *IEEE Trans. Inf. Theory*, 53(8):2799–2814, Aug. 2007.

[122] S. Weber and J. G. Andrews. *Transmission capacity of wireless networks*. Foundations and Trends in Networking, 2012.

[123] K. Huang, V. K. N. Lau, and Y. Chen. Spectrum sharing between cellular and mobile ad hoc networks: transmission-capacity trade-off. *IEEE J. Sel. Areas Commun.*, 27(7):1256–1267, Sep. 2009.

[124] V. Mordachev and S. Loyka. On node density-outage probability tradeoff in wireless networks. *IEEE J. Sel. Areas Commun.*, 27(7):1120–1131, Sep. 2009.

[125] M. O. Hasna, M. S. Alouini, A. Bastami, and E. S. Ebbini. Performance analysis of cellular mobile systems with successive co-channel interference cancellation. *IEEE Trans. Wireless Commun.*, 2(1):29–40, Jan. 2003.

[126] J. Blomer and N. Jindal. Transmission capacity of wireless ad hoc networks: Successive interference cancellation vs. joint detection. In *Proc. IEEE Int. Conf. on Commun.*, pages 1–5, Dresden, Germany, Jun. 2009.

[127] T. M. Nguyen, Y. Jeong, T. Q. S. Quek, W. P. Tay, and H. Shin. Interference alignment in a Poisson field of MIMO femtocells. *IEEE Trans. Wireless Commun.*, 12(6):2633–2645, Jun. 2013.

[128] O. Ben Sik Ali, C. Cardinal, and F. Gagnon. On the performance of interference cancellation in wireless ad hoc networks. *IEEE Trans. Commun.*, 58(2):433–437, Feb. 2010.

[129] X. Zhang and M. Haenggi. The performance of successive interference cancellation in random wireless networks. In *Proc. IEEE Global Telecomm. Conf.*, pages 2317–2321, Anaheim, CA, Dec. 2012.

[130] X. Zhang and M. Haenggi. On decoding the kth strongest user in Poisson networks with arbitrary fading distribution. In *Proc. Asilomar Conf. on Signals, Systems and Computers*, pages 1–5, Pacific Grove, CA, Nov. 2013.

[131] X. Zhang and M. Haenggi. The aggregate throughput in random wireless networks with successive interference cancellation. In *Proc. IEEE Int. Symp. on Inform. Theory*, pages 1–5, Istanbul, Turkey, Jul. 2013.

[132] H. P. Keeler, B. Blaszczyszyn, and M. K. Karray. SINR-based k-coverage probability in cellular networks with arbitrary shadowing. In *Proc. IEEE Int. Symp. on Inform. Theory*, pages 1–5, Istanbul, Turkey, Jul. 2013.

[133] Q. Ye, B. Rong, Y. Chen, M. Al-Shalash, C. Caramanis, and J. G. Andrews. User association for load balancing in heterogeneous cellular networks. *IEEE Trans. Wireless Commun.*, 12(6):2706–2716, Jun. 2013.

[134] H. S. Dhillon, R. K. Ganti, F. Baccelli, and J. G. Andrews. Modeling and analysis of K-tier downlink heterogeneous cellular networks. *IEEE J. Sel. Areas Commun.*, 30(3):550–560, Apr. 2012.

[135] S. Singh, H. S. Dhillon, and J. G. Andrews. Offloading in heterogeneous networks: Modeling, analysis, and design insights. *IEEE Trans. Wireless Commun.*, 12(5):2484–2497, May 2013.

[136] H. S. Dhillon, T. D. Novlan, and J. G. Andrews. Coverage probability of uplink cellular networks. In *Proc. IEEE Global Telecomm. Conf.*, pages 1–6, Anaheim, USA, Dec. 2012.

[137] B. Blaszczyszyn and H. P. Keeler. Equivalence and comparison of heterogeneous cellular networks. In *Proc. IEEE Int. Symp. on Personal, Indoor and Mobile Radio Commun.*, London, UK, Sep. 2013.

[138] H. A. David and H. N. Nagaraja. *Order statistics*. Wiley Online Library, 2003.

[139] M. Haenggi. On distances in uniformly random networks. *IEEE Trans. Inf. Theory*, 51(10):3584–3586, Oct. 2005.

[140] S. Csorgo, E. Haeusler, and D. M. Mason. A probabilistic approach to the asymptotic distribution of sums of independent, identically distributed random variables. *Advances in applied mathematics*, 9(3):259–333, 1988.

[141] S. Csorgo. Limit theorems for sums of order statistics. In *Sixth International Summer School in Probability Theory and Mathematical Statistics*, pages 5–37, Varna, Bulgaria, 1988.

[142] D. B. H. Cline and G. Samorodnitsky. Subexponentiality of the product of independent random variables. *Stochastic Processes and their Applications*, 49(1):75–98, 1994.

[143] H. Inaltekin, M. Chiang, H. V. Poor, and S. B. Wicker. On unbounded path-loss models: effects of singularity on wireless network performance. *IEEE J. Sel. Areas Commun.*, 27(7):1078–1092, Sep. 2009.

[144] J.-S. Ferenc and Z. Néda. On the size distribution of Poisson Voronoi cells. *Physica A: Statistical Mechanics and its Applications*, 385(2):518–526, Apr. 2007.

[145] M. Haenggi. The local delay in Poisson networks. *IEEE Trans. Inf. Theory*, 59(3):1788–1802, Mar. 2013.

[146] S. Mukherjee. Distribution of downlink SINR in heterogeneous cellular networks. *IEEE J. Sel. Areas Commun.*, 30(3):575–585, Apr. 2012.

[147] H. Tang, J. Peng, P. Hong, and K. Xue. Offloading performance of range expansion in picocell networks: A stochastic geometry analysis. *IEEE Wireless Commun. Lett.*, pages 1–4, 2013. accepted for publication.

[148] H.-S. Jo, Y. J. Sang, P. Xia, and J. G. Andrews. Heterogeneous cellular networks with flexible cell association: A comprehensive downlink SINR analysis. *IEEE Trans. Wireless Commun.*, 11(10):3484–3495, Oct. 2012.

List of publications

Journals

[J1] **M. Wildemeersch**, T. Q. S. Quek, M. Kountouris, A. Rabbachin, and C. H. Slump, Successive interference cancellation in heterogeneous cellular networks, *IEEE Trans. Signal Process.*, 2013, submitted.

[J2] **M. Wildemeersch**, T. Q. S. Quek, C. H. Slump, and A. Rabbachin, Cognitive small cell networks: Energy efficiency and trade-offs, *IEEE Trans. Commun.*, vol. 61, no. 9, pp. 4016-4029, Sep. 2013.

[J3] **M. Wildemeersch**, C. H. Slump, and A. Rabbachin, Acquisition of GNSS signals in a realistic signal environment, *IEEE Trans. Aerosp. Electron. Syst.*, 2013, to appear.

Conferences

[C1] **M. Wildemeersch**, T. Q. S. Quek, M. Kountouris, and C. H. Slump, Effectiveness of successive interference cancellation and association policies for heterogeneous wireless networks, in *Proc. IEEE Int. Conf. Acoustics, Speech, and Signal Processing*, Florence, Italy, May 2014, submitted.

[C2] **M. Wildemeersch**, T. Q. S. Quek, M. Kountouris, and C. H. Slump, Successive interference cancellation in uplink cellular networks, in *Proc. IEEE Workshop on Signal Proc. Advances in Wireless Commun.*, Darmstadt, Germany, Jun. 2013, pp. 315-319, **Best Student Paper Award**.

[C3] **M. Wildemeersch**, T. Q. S. Quek, A. Rabbachin, C. H. Slump, and A. Huang, Energy efficient design of cognitive small cells, in *Proc. IEEE Int. Conf. on Commun.*, Budapest, Hungary, Jun. 2013, pp. 1294-1299.

[C4] **M. Wildemeersch**, A. Rabbachin, T. Q. S. Quek, and C. H. Slump, GNSS signal acquisition in harsh urban environments, in *Proc. IEEE Int. Conf. on Commun.*, Budapest, Hungary, Jun. 2013, pp. 62-67.

[C5] **M. Wildemeersch**, T. Q. S. Quek, A. Rabbachin, C. H. Slump, and A. Huang, Performance limits for cognitive small cells, in *Proc. IEEE Wireless Commun. and Networking Conf.*, Shanghai, China, Apr. 2013, pp. 2832-2836.

[C6] J. Fortuny-Guasch, **M. Wildemeersch**, and D. Borio, Assessment of DVB-T impact on GNSS acquisition and tracking performance, in *International Technical Meeting of The Institute of Navigation*, San Diego, California, Jan. 2011, pp. 347-356.

[C7] **M. Wildemeersch**, A. Rabbachin, E. Cano, and J. Fortuny, Interference assessment of DVB-T within the GPS L1 and Galileo E1 band, in *5th ESA Workshop on Satellite Navigation Technologies and European Workshop on GNSS Signals and Signal Processing (NAVITEC)*, Noordwijk, The Netherlands, Dec. 2010, pp. 1-8.

[C8] B. Motella, M. Pini, M. Fantino, P. Mulassano, M. Nicola, J. Fortuny-Guasch, **M. Wildemeersch**, and D. Symeonidis, Performance assessment of low cost GPS receivers under civilian spoofing attacks, in *5th ESA Workshop on Satellite Navigation Technologies and European Workshop on GNSS Signals and Signal Processing (NAVITEC)*, Noordwijk, The Netherlands, Dec. 2010.

[C9] **M. Wildemeersch** and J. Fortuny-Guasch, A laboratory testbed for GNSS interference impact assessment, in *Proceedings of the 22nd International Technical Meeting of The Satellite Division of the Institute of Navigation (ION GNSS)*, Savannah, GA, Sep. 2009, pp. 49-54.

Technical reports

[TR1] **M. Wildemeersch**, E. Cano Pons, A. Rabbachin, and J. Fortuny-Guasch, Impact study of unintentional interference on GNSS receivers, Publications Office of the European Union, EUR - Scientific and Technical Research Reports JRC62607, ISSN 1018-5593, ISBN 978-92-79-19523-5, 2010.

[TR2] **M. Wildemeersch** and J. Fortuny-Guasch, Radio frequency interference impact assessment on global navigation satellite systems, Publications Office of the European Union, EUR - Scientific and Technical Research Reports JRC55767, ISSN 1018-5593, ISBN 978-92-79-14989-4, 2010.

Acronyms

ASE	area spectral efficiency
AWGN	additive white Gaussian noise
AP	access point
BS	base station
CCDF	complementary cumulative distribution function
CDF	cumulative distribution function
CDMA	code division multiple access
CF	characteristic function
CLT	central limit theorem
CR	cognitive radio
CRN	cognitive radio network
CS	circular symmetric
DC	duty cycle
DL	downlink
DS-CDMA	direct sequence - code division multiple access
DSSS	direct sequence spread spectrum
DTV	digital television
DVB-T	digital video broadcasting - terrestrial
ED	energy detector
GLRT	generalized likelihood ratio test

GNSS	global navigation satellite system
IC	interference cancellation
i.i.d.	independent and identically distributed
INR	interference-to-noise ratio
JD	joint detection
LOS	line-of-sight
MAC	medium access control
MANET	mobile ad-hoc network
MBS	macrocell base station
MGF	moment generating function
MRT	maximum ratio test
OA	open access
OFDMA	orthogonal frequency-division multiple access
OSA	opportunistic spectrum access
PDF	probability density function
PGFL	probability generating functional
PMF	probability mass function
PPP	Poisson point process
PU	primary users
QoS	quality of service
REA	range expanded area
ROC	receiver operating curve
r.v.	random variable
SAP	small cell access point
SS	spread spectrum
SSC	spectral separation coefficient

SIC	successive interference cancellation
SINR	signal-to-interference-and-noise ratio
SIR	signal-to-interference ratio
SNR	signal-to-noise ratio
SoI	signal of interest
SU	secondary users
TDD	time division duplex
TDMA	time-division multiple access
TSD	truncated stable distribution
UE	user equipment
UL	uplink
UWB	ultra wideband

List of Notations

α	path loss exponent
α_{I}	characteristic exponent of stable distribution
β	skewness stable distribution
$\mathcal{B}$	$\mathcal{B}$-function
γ	dispersion stable distribution
Γ	Γ-function
$C_{k,i}$	Voronoi cell of $x_{k,i}$
$\mathbb{E}\{.\}$	expected value
E_{tot}	expected energy consumption of small cell access point
ζ	detection threshold
η_{t}	SINR threshold
$\mathcal{H}_0$	null hypothesis
$\mathcal{H}_1$	alternative hypothesis
$\mathcal{J}^{(x_{k,i})}$	available subchannels of $x_{k,i}$
$\mathcal{J}$	set of available subchannels
λ_k	access point density for tier k
$\mathcal{L}_X(.)$	Laplace transform of random variable X
μ_k	set of user density for tier k
ν	amplitude path loss exponent
$\mathcal{N}(\mu, \sigma^2)$	normal distribution with mean μ and variance σ^2

$\mathcal{N}_c(0, \sigma^2)$	circularly symmetric complex Gaussian distribution
$\xi_c(\tau_s)$	aggregate offload capacity
$\xi_t(\tau_s, \eta_t)$	aggregate offload throughput
$p_{a,k}$	association probability to tier k
p_s	sensing probability
p_{UE}	probability that at least one user equipment resides in coverage of small cell access point
$\psi_X(j\omega)$	characteristic function of X
$\mathbf{P}$	set of downlink transmission powers
$\Pr\{.\}$	probability
$\mathbb{P}^{!x}$	reduced Palm distribution
$\mathbb{P}_d$	probability of detection
$\mathbb{P}_{fa}$	probability of false alarm
$\mathbb{P}_c$	coverage probability
Poi	Poisson distribution
$\mathbb{P}_{out}$	outage probabilty
$\mathbb{P}_{out}^{(k)}$	outage probability of user connected to tier k
$\mathbb{P}_{s,can}$	success probability of decoding nth strongest signal
$\mathbb{P}_{s,IC}$	success probability of transmission with interference cancellation
$\mathbb{P}_{s,SIC}$	coverage probability with successive interference cancellation
$\mathbf{Q}$	set of uplink transmission powers
$\mathcal{Q}$	$\mathcal{Q}$-function
$\mathbb{R}^d$	d-dimensional space
$\mathbb{R}^+$	positive real numbers
$\mathcal{S}(\alpha_I, \beta, \gamma)$	stable distribution with parameters α_I, β, and γ

τ_s	sensing time
V	decision variable
$x_{k,i}$	ith AP of tier k

Acknowledgment

A journey of a thousand miles begins with a single step. – Laozi

The final period of this journey is a natural moment to look back and thank all those people who contributed in some way to this dissertation. It was late autumn 2008 when I was searching for a promotor. I sent out several mails with a description of my work, gently asking for some time to have a talk. Kees, you took me by surprise when you called me, setting that first essential step on this journey. Your dynamics were contagious and shortly after, we met in Enschede. I didn't have any clear idea what to do, but you put me on track introducing me in the field of signal processing, presenting me the Dutch no-nonsense style. It was refreshing and the beginning of a very pleasant collaboration.

I want to express my sincere gratefulness to you, Tony, for the last two years in Singapore. Every day, you create a highly motivating and enriching environment for your group. The exposure to many bright scientists, the sessions at the blackboard, the weekly group meetings were irrefutably inspiring, but I am especially indebted to you for never letting me settle down and for the continuous stimulus to reach further and grow. The financial support of the A*STAR Research Attachment Programme is also gratefully acknowledged.

Alberto, a plethora of reasons. Throughout this dissertation, you have been an advisor, a mentor, and a friend. My gratitude goes beyond the obvious thanks for launching me in the rich field of stochastic geometry, for passing on a rigorous methodology, for transforming my prose in scientific writing, for suggesting opportunities. You added an essential component to producing high quality work, the element of genuine passion and joy, such that we could discuss over an ice cream at San Gabriele, a dinner, or driving towards the mountains. Hard work gets truly easy when you like it. I will not forget some of the aperitivos around the lake, nor the descent of the Marmolada, which legitimately bears its epithet 'legendary'.

Marios, a sincere thanks for your insightful comments, the pleasant discussions, your advice, and the fruitful collaboration.

It was the best of times, it was the worst of times, it was the age of wisdom, it was the age of foolishness, it was the epoch of belief, it was the epoch of incredulity, it was the season of Light, it was the season of Darkness, it was the spring of hope, it was the winter of despair.
– Charles Dickens, A Tale of Two Cities

The beauty of research is related to the intensity and swift change of big emotions, oscillating back and forth, between delight and frustration. As the relation between effort and result is delusive, it is important to create a correct mindset, to acquire the ability to go slow and deeply understand, to take a step forward, often unfortunately also a step backward. On this path, I had the pleasure to meet so many interesting and inspiring people. Julien, we met just before the onset of this travel, but you were a great motivation. Yong Sheng and Niangjun, the lunch sessions with both of you were always very entertaining, thanks a lot for guiding me into the Singaporean and Chinese culture. A special thanks to Hamed – real pleasure to share the office with you – and for a diversity of reasons I want to thank Shi Jing, Yufei, Chen Sai, Michal, Subhash, Jemin, and Marco. A sincere thanks to Estefanía and Luca: with the cineforum and some parmigiano, Singapore tasted sometimes like Europe.

Far away from home, you need some reference points. Greg and Sam, dear friends, wherever I go, it never takes a long time before I can spot the two of you. We meet at the most random places, but there is that single, magic law of attraction that we faithfully respect when we gather on the banks of the river Gard and celebrate since more than a decade our summer version of new year. Giovanna and Alessandro, almost ten years since I left Rome, but we still share a profound friendship. Carved in stone, Jean-Jacques and Ignace, whenever possible we keep on strolling down the magnificent streets of Ghent, the most beautiful. Great source of inspiration, comfort, and glee, I thank you, Jochen, for the countless discussions we had in the shadow of the Sint-Baafskathedraal, staring over the Lago Maggiore, or plowing on the ciaspole, for the complicity, and your presence as if you were sneering at the distance.

Unquestionable and unshakable was the support that I got from you, my dearest parents. The choices I made must have asked plenty of comprehension, but you have always been so selfless and generous. That is why this dissertation is dedicated to you. Also a special thanks to Sofie, Olivier, and Julien, for many laughs and the beautiful family moments.

Then, my path crossed yours and for the most intense part of this journey we walked together. I owe you my deepest gratefulness and admiration, Mónica, for your involvement and encouragement to make this work the best possible, for your curiosity to embark on this journey, your radiant cheerfulness, and your ease to exchange uncertainty for opportunity. I spend my final thought to you, little one, as your captivating presence, although you're still not there, made the last months so exceptional.

Matthias Wildemeersch
October, 2013
Singapore

Curriculum Vitae

Matthias Wildemeersch received the MSc degree in electromechanical engineering from the University of Ghent (Belgium) in 2003. In 2009, he started working towards the PhD degree in Electrical Engineering at the University of Twente (the Netherlands). From 2008 to 2011 he was at the Joint Research Centre of the European Commission (Ispra, Italy), where he worked on the impact assessment of interference related to GNSS. Since 2012, he is with the Institute for Infocomm Research (Singapore) where his work broadly covers the analysis of heterogeneous networks. His research interests span various aspects of wireless communications and signal processing and focus on the application of probability theory and stochastic geometry to green communications, cognitive radio, and interference mitigation. He received the IEEE SPAWC 2013 Best Student Paper Award and is an awardee of the A*STAR Research Attachment Programme (2012-2013).